Informed Segmentation Approaches for Studying Time-Varying Functional Connectivity in Resting State fMRI

by

Marlena Duda

A dissertation submitted in partial fulfillment
of the requirements for the degree of
Doctor of Philosophy
(Bioinformatics)
in the University of Michigan
2021

Doctoral Committee:

Professor Danai Koutra, Co-Chair
Associate Professor Chandra Sripada, Co-Chair
Professor Elizaveta Levina
Professor Kayvan Najarian
Associate Professor Arvind Rao

Marlena Duda

mduda@umich.edu

ORCID iD: 0000-0003-2369-2225

Dedication

To all the little girls whose curiosity and capability knows no bounds. My dream is that when you picture a scientist, you picture someone who looks like you.

Acknowledgements

This work was made possible by the support and contributions of many incredible people I have had the pleasure of knowing and working with over the years. My interest in STEM was sparked under the instruction of Mr. John Girard and Mr. Timothy Rankin at Plainville High School. I thank them for making AP Biology and AP Calculus the two most memorable classes of my high school career, and for inspiring me to major in Biology at Northeastern University. I owe my trajectory into Bioinformatics to Dr. Dennis Wall, previously of Harvard Medical School and currently of Stanford University, for taking a chance on a student who had never written a line of code and teaching her the power and possibility of computational research. I express my deepest gratitude to all the members and collaborators of the Wall Lab during my five years there, namely Jena Daniels, Todd Deluca, Tristan Nelson, Dr. Jae-Yoon Jung, Dr. Vince Fusaro, Dr. Jack Kosmicki, Dr. Leticia Díaz Beltrán, Dr. Maude David, Dr. Nick Haber, Catalin Voss, and Aaron Kline, for all their support, mentorship, and friendship as I began my journey as a young researcher. I would not be the scientist I am today without the many hours of debugging help, poster feedback, lab meetings and happy hours we shared in Boston and Palo Alto.

I have been extremely fortunate to be co-mentored by Dr. Danai Koutra and Dr. Chandra Sripada during my PhD work at the University of Michigan. I could not have completed this

dissertation without their continuous support and encouragement. Dr. Koutra's commitment to conducting innovative, multidisciplinary research in data mining and network science has taught me to view neuroscience problems through an innovative lens and has equipped me to solve them with a state-of-the-art computational toolkit. Dr. Sripada's air of thoughtfulness and keen skills of expression have consistently inspired me to improve as a researcher, writer, and communicator, and to continuously reach for the highest level of scientific rigor. I thank them both for allowing me to spin my creative webs of research directions, and especially for pruning the branches when the webs inevitably grew too large. I look forward to continuing to benefit from their wisdom and mentorship as I move forward in my scientific career. I also thank my dissertation committee members, Dr. Arvind Rao, Dr. Kayvan Najarian and Dr. Liza Levina, for their valuable feedback throughout my doctoral research.

The Department of Computational Medicine and Bioinformatics and the Bioinformatics Graduate Program at the University of Michigan has provided me with exceptional support and training opportunities throughout my time as a graduate student. Thank you to graduate program chairs, Dr. Margit Burmeister and Dr. Maureen Sartor, for advising me through my coursework and beyond. Thank you to the many faculty members who have served as mentors and provided me with words of wisdom during my graduate studies, including Dr. Brian Athey, Dr. Gil Omenn, and Dr. Ryan Mills. Thank you to the many staff that ensure things run smoothly and help make our research and studies possible, namely Julia Eussen, Mary Freer and Jane Weisner.

The best outcome of my time in Ann Arbor has been the friendships I have forged with some of the funniest, smartest and overall most exceptional people I have ever known. I am grateful for my OG cohort mates turned ride-or-die crew, Kevin Hu, Louis Joslyn and Alex Weber, and for the many friendships that have developed along the way, including Ricardo D'Oliveira Albanus, Esra Ascigil, Christopher Castro, Ben Chandler, Brad Crone, Danny Geiszler, Ben Hillebrand, Alex Kalinin, Zena Lapp, Cathy Smith, Kelly Sovacool, and Brooke Wolford. In addition to your endless camaraderie and support, I will always cherish our lunch table debates, happy hours at Bill's Beer Garden and Ashley's (and Zoom, thanks to the pandemic), late nights at Garage Bar and Alley Bar, summertime grilling and tubing adventures, and much more—thank you for rarely leaving me with the opportunity to do work on nights and weekends. Thank you to Max Egan for being there for me in all ways through the years. Thank you to my dog, Lilah, and my cat, Evie, for being the best pandemic co-workers any doctoral candidate could ask for, and for making even the heaviest of days feel lighter. I also feel compelled to thank George Lucas and Stan Lee for the creation of their respective cinematic universes, which served as the soundtrack for the majority of my dissertation writing.

Finally, I thank my family, without whom this dissertation would surely not have been possible. Thank you to my parents, Janusz and Alina, who have supported me in every sense of the word and sacrificed so much to get me to where I am today. Words cannot express how grateful I am for the beautiful life you have given me. Thank you to my sister Emily, who has served many roles in my life over the years, including sounding board, roadtrip co-pilot, confidant, therapist, figure critic,

voice of reason, movie buddy, proofreader, teacher, comic relief, cheerleader, and most importantly, best friend. I am grateful for FaceTime and unlimited data plans so we are never far apart.

Table of Contents

Dedication **ii**

Acknowledgements **iii**

Table of Contents **vii**

List of Tables **xiii**

List of Figures **xiv**

Abstract **xvi**

Chapter 1 - Introduction **1**

1.1 Towards Decoding Human Thought 1

1.2 Dissertation Outline 5

1.3 Figures 6

Chapter 2 - Background **7**

2.0 Terminology 8

2.1 fMRI and Functional Connectivity 9

2.2 Time-Varying Functional Connectivity (TVFC) 12

2.3 Clinical and Behavioral Correlates of TVFC 13

2.3.1 Cognitive and Behavioral Traits 13

2.3.2 Demographic Phenotypes 15

2.3.3 Clinical Phenotypes 15

2.4 TVFC Methodologies 17

2.4.1 Sliding Window Methods 17

2.4.2 Instantaneous FC Estimators 19

2.4.3 Instantaneous Brain State Estimators 23

2.5 Doubts about TVFC 26

2.6 Current Gaps in Knowledge 27

2.7 Figures and Tables 28

Chapter 3 - Validating Dynamicity in Resting State fMRI with Activation-Informed Temporal Segmentation 29

3.1 Abstract 29

3.2 Introduction 30

3.3 Methods 35

3.3.1 Data Description 35

3.3.1.1 HCP Data 35

3.3.1.2 Data Preprocessing 37

3.3.2 The Activation-Informed Segmentation Framework 38

3.3.2.1 Activation-informed time series segmentation 39

3.3.2.2 Functional Connectivity Estimation 41

3.3.2.3 State Clustering 42

3.3.3 Evaluation against ground truth 45

3.3.4 Comparison to Sliding Window 46

3.4 Results 48

3.4.1. The GTD Method Accurately Identified Known Transitions During a Working Memory Task 48

3.4.2. In the Working Memory Task, Activation-informed Segmentation Performance Was Superior to Sliding Window 49

3.4.3. The Activation-informed Segmentation Method Identified Five Connectivity States During Rest 50

3.4.4. Connectivity States During Rest Exhibit Excellent Test-Retest Reliability 50

3.4.5. Activation Peaks Observed During Rest Closely Resemble Peaks Found When Transitioning In and Out of Cognitively Demanding Task States 51

3.4.6. Connectivity States Involve Brain-Wide Connectivity Patterns and Prominently Involve Prefrontal/Sensory-Motor Coupling 51

3.4.7. Resting Connectivity States Exhibit Complex Patterns of Transitioning 52

3.4.8. Resting Connectivity States are Predictive of Behavioral Phenotypes Including Cognition, Personality, and Psychopathology 53

3.4.9. Resting Connectivity States are Unrelated to Head Motion 53

3.5 Discussion 54

3.6 Figures and Tables 61

3.7 Publication and Acknowledgements 71

3.8 Supplementary Information 71

Chapter 4 - Data-driven Segmentation of Instantaneous Connectivity Estimates Reveals a Highly Stable Set of Time-Varying States in Resting fMRI 76

4.1 Abstract 76

4.2 Introduction 77

4.3 Methods 81

4.3.1 Data Description 81

4.3.1.1 HCP Data 81

4.3.1.2 Data Preprocessing 82

4.3.2 Instantaneous FC Estimators 83

4.3.2.1 Edge Co-fluctuations (ECF) 84

4.3.2.2 Multiplication of Temporal Derivatives (MTD) 85

4.3.2.3 Dynamic Conditional Correlation (DCC) 86

4.3.3 Post-processing Strategies 89

4.3.4 Experimental Design 93

4.3.5 Baseline Measures 95

4.3.4.1 Sliding Window Pearson Correlation 95

4.3.4.2 Activation Informed Segmentation 96

4.3.6 Application in Resting State fMRI 96

4.3.7 Connection to Phenotypes 96

4.4 Results 97

4.4.1 Informed Segmentation Offers Improved Noise Reduction Over Sliding Window Smoothing 97

4.4.2 ECF-Derived Estimates Best Summarize Changing FC Patterns 98

4.4.3 ECF + Connectivity-Informed Segmentation Framework Best Recovers Ground Truth Task Structure 100

4.4.4 Comparison to Baseline Approaches 101

4.4.5 ECF + Connectivity-Informed Segmentation Framework Detects Five High-Fidelity Resting States 102

4.4.6 Discovered Resting States are Predictive of Personality Traits 103

4.5 Discussion 104

4.6 Figures and Tables 114

4.7 Acknowledgements 124

4.8 Supplementary Material 125

Chapter 5 - Comparative Analysis Between Data-Driven and Model-Based Instantaneous State Estimation Approaches in Activation and Connectivity Domains 127

5.1 Abstract 127

5.2 Introduction 128

5.3 Methods 132

5.3.1 Data Description 132

5.3.1.1 HCP Data 132

5.3.1.2 Data Preprocessing 133

5.3.2 Instantaneous State Estimators 134

5.3.2.1 Co-activation Patterns (CAPs) 134

5.3.2.2 Hidden Markov Models (HMMs) 135

5.3.3 Instantaneous FC Time Series 136

5.3.4. Experimental Design 138

5.3.5 Application in Resting State 140

5.3.6 Connection to Phenotypes 141

5.4 Results 141

5.4.1 Instantaneous Co-Activation Patterns are More Informative Than Co-Connectivity Patterns in CAP analysis 141

5.4.2 Connectivity Time Series Improve HMM State Estimation 142

5.4.3 CAP Analysis Reliably Detects Four Distinct Brain States 143

5.4.4 Discovered Resting States are Predictive of Cognitive, Behavioral, and Personality Traits 145

5.5 Discussion 146

5.6 Figures and Tables 152

5.7 Acknowledgments 159

5.8 Supplementary Material 160

Chapter 6 - Exploration of Spatiotemporal Informed Segmentation with Deep Learning 162

6.1 Abstract 162

6.2 Introduction 163

6.3 Methods 165

6.4 Preliminary Results 166

6.5 Discussion and Future Directions 167

6.6 Figures and Tables 169

6.7 Acknowledgments 170

Chapter 7 - Discussion **172**

7.1 Summary of Main Findings 172

7.2 Emerging Themes 174

7.2.1 Converging Evidence Across Diverse Methodologies Supports the Existence of TVFC During Rest 174

7.2.2 Block-Design Task Data Can Serve as a Natural Ground Truth for Testing TVFC Performance 176

7.3.3 Data-Driven Informed Segmentation Approaches Outperform Purely Instantaneous and Rigid Windowing Approaches 178

7.3.4 Activation-Centric Methods Prevail Over Analogous Connectivity-Based Approaches 180

7.3.4 ECF Shows Promise for Instantaneous FC Estimation 181

7.3 Broader Limitations 182

7.3 Impacts 183

7.4 Future Directions 184

7.4.1 Methodological Directions 184

7.4.2 Experimental Directions 185

7.5 Conclusions 187

Bibliography **188**

List of Tables

Table 2.1. A glossary of common terms and abbreviations. 28

Table 3.1. Symbols and abbreviations**.** 68

Table 3.2. Performance of activation-informed segmentation method and the standard sliding window method in recovering ground truth dynamic state changes in WM task data. 69

Table 3.3. Ordinary least squares regression results for significantly predicted phenotypes. 70

Supplementary Table 3.1. Clustering performance of traditional FC summarization methods in our activation-informed segments. 71

Supplementary Table 3.2. Relation to head motion. 75

Table 4.1 Percent variance explained (PVE) by the top 100 PCs across all treatments of ECF and MTD instantaneous FC estimates. 119

Table 4.2. Clustering accuracy for all combinations of instantaneous FC estimation and state extraction applied in data from WM Session 1 (WM1) and Session 2 (WM2). 120

Table 4.3. Precision and recall of informed segmentation approaches across the ECF, MTD and DCC time series. 121

Table 4.4. Performance of the baseline activation-domain frameworks in recovering ground truth dynamic state changes in WM task data. 122

Table 4.5. Ordinary least squares regression results for significantly predicted phenotypes. 123

Table 5.1 Clustering accuracy for CAP and HMM instantaneous state estimation approaches across all baseline time series applied in data from WM Session 1 (WM1) and Session 2 (WM2). 157

Table 5.2. Ordinary least squares regression results for significantly predicted phenotypes. 159

List of Figures

Figure 1.1. Schematic representation of experimental pipelines used in Chapters 3-6. 6

Figure 3.1. Experimental pipeline. 38

Figure 3.2. Preprocessing Effects. 61

Figure 3.3. Results of the activation-informed segmentation for all subjects in structured WM task data. 62

Figure 3.4: Results of GIFT toolbox-based sliding window framework for all subjects in structured WM task data. 63

Figure 3.5: Temporal alignment of activation-informed segments and their corresponding state labels given by k-means in all four resting state fMRI sessions. 64

Figure 3.6. Histograms of GTD magnitudes at discovered peaks. 65

Figure 3.7. Connectivity signatures for each of the five discovered resting FC states. 66

Figure 3.8. Group average TVFC features. 67

Figure 4.1. Experimental pipeline. 89

Figure 4.2. Temporal alignment of states discovered in WM via pointwise clustering of FC estimates derived by the ECF, MTD and DCC methods. 114

Figure 4.3. Temporal alignment of states discovered via sliding window clustering applied to pointwise FC estimates derived by the ECF, MTD and DCC methods. 115

Figure 4.4. Temporal alignment of states discovered via informed segmentation applied to pointwise FC estimates derived by the ECF, MTD and DCC methods. 116

Figure 4.5. Connectivity signatures for each of the five resting states discovered by the ECF + connectivity-informed segmentation framework. 117

Figure 4.6. Temporal decomposition of resting state fMRI data with respect to states discovered by the ECF + connectivity-informed segmentation framework across four resting state scanning sessions. 118

Figure 4.7. TVFC features extracted from resting states discovered by the ECF + connectivity-informed segmentation framework. 118

Supplementary Figure 4.1. Cluster validity index (CVI) as a function of k in k-means clustering of ECF + connectivity-informed segmentation-derived states across four replicate resting fMRI scanning sessions. 125

Supplementary Figure 4.2. Replication of resting states discovered by the ECF + connectivity-informed segmentation framework across four sessions of resting state fMRI. 126

Figure 5.1. Experimental pipeline. 138

Figure 5.2. Temporal alignment of states discovered via CAP analysis applied to fMRI BOLD activation time series and pointwise FC estimates derived by the ECF, MTD and DCC methods. 152

Figure 5.3. Temporal alignment of states discovered via HMMs applied to fMRI BOLD activation time series and pointwise FC estimates derived by the ECF, MTD and DCC methods. 153

Figure 5.4. Activation signatures for each of the four resting states discovered by the CAP approach. 154

Figure 5.5. Connectivity signatures for each of the four resting states discovered by the CAP approach. 155

Figure 5.6. Temporal decomposition of resting state fMRI data with respect to states discovered by the CAP framework across four resting state scanning sessions. 155

Figure 5.7. TVFC features extracted from resting states discovered by the CAP framework. 156

Supplementary Figure 5.1. Replication of resting states discovered by the CAP framework across four sessions of resting state fMRI. 160

Supplementary Figure 5.2. Replication of connectivity signatures across resting states discovered by the CAP framework across four sessions of resting state fMRI. 161

Figure 6.1. Proposed experimental pipeline. 165

Figure 6.2. Patterns of next-frame prediction accuracies in dynamic video data. 169

Figure 6.3. PredNet prediction accuracies on windowed connectome frames. 170

Figure 6.4. True and predicted brain activity. 170

Abstract

The brain is a complex dynamical system that is never truly "at rest". Even in the absence of explicit task demands, the brain still manifests a stream of conscious thought, varying levels of vigilance and arousal, as well as a number of postulated ongoing "under the hood" functions such as memory consolidation. Over the past decade, the field of time-varying functional connectivity (TVFC) has emerged as a means of detecting dynamic reconfigurations of the network structure in the resting brain, as well as uncovering the relevance of these changing connectivity patterns with respect to cognition, behavior, and psychopathology. Since the nature and timescales of the underlying resting dynamics are unknown, methodologies that can detect changing temporal patterns in connectivity without imposing arbitrary timescales are required. Moreover, as the study of TVFC is still in its infancy, rigorous evaluation of new and existing methodologies is critical to better understand their behavior when applied in resting data, which lacks ground truth temporal landmarks against which accuracy can be assessed.

In this dissertation, I contribute to the methodological component of the TVFC discourse. I propose two distinct, yet related, approaches for identifying TVFC using an informed segmentation framework. This data-driven framework bridges instantaneous and windowed approaches for studying TVFC, in an attempt to mitigate the limitations of each while simultaneously leveraging the advantages of both. I also present a comprehensive, head-to-head comparative analysis of several of the

most promising TVFC methodologies proposed to date, which does not exist in the current body of literature.

Chapter 1 - Introduction

1.1 Towards Decoding Human Thought

One of the most ambitious and complex scientific goals of today is understanding the connection between the brain and the mind. Towards this goal, a necessary component is uncovering the mapping between brain activity, namely localized or regional activations within the brain, and individual cognitive processes. Reaching a sufficiently detailed mapping of this sort could enable the decoding of a person's spontaneous thoughts. In fact, in the recent book "The New Mind Readers" Dr. Russell Poldrack discusses the potential for this form of "mind reading" to become a scientific reality in the not-so-distant future largely due to the innovations in modern neuroimaging techniques, specifically functional magnetic resonance imaging (fMRI) (Poldrack, 2018). But is it truly possible to draw a direct biological map between patterns of brain activity and the full spectrum of human consciousness?

The study of the functional underpinnings of human cognition using neuroimaging began with the observation of brain activity during specialized tasks designed to probe specific cognitive processes. From these task-evoked studies, it quickly became clear that there does not exist a perfect one-to-one mapping of thoughts, emotions, or cognitive processes to singular brain regions—engagement in a single cognitive process often involves activation across several brain regions, and

conversely, activation of a particular brain region often occurs across multiple cognitive processes. This lack of selectivity between cognition and regional activation poses a problem for the reverse inference required for cognitive decoding, i.e., inferring the engagement of a certain cognitive process based on the activation of a particular brain region (Poldrack, 2006). To gain further insight into the neural basis of cognition, researchers have focused on studying the co-fluctuation, or temporal coupling, of activation patterns between brain regions, known as functional connectivity (FC). The study of task-based FC has uncovered a great deal about the functional organization of the human brain, and of particular importance among these discoveries has been the formalization of several connectivity networks in the brain that have been shown to reliably synchronize (either through strong coupling or anti-coupling) in certain cognitive contexts.

Beyond the study of task-evoked FC, there has been rising interest in studying the intrinsic patterns of brain activity in the absence of task stimulus, known as the "resting state". Studies of resting state fMRI were initially performed to capture baseline neural activity against which task activations could be compared, but it was quickly discovered that resting state FC actually captured important individual variation across several phenotypes, including fluid intelligence (Finn et al., 2015), working memory (Hampson et al., 2006), and a variety of neurological and psychiatric diseases such as Alzheimer's (Greicius et al., 2004) and schizophrenia (Bluhm et al., 2007). Importantly, these early studies of resting state FC operated on the critical assumption that FC patterns during rest are static, or unchanging, throughout the entire period of the fMRI scan. But how does this assumption of static FC reconcile with what we know about human cognition, specifically during the mind-

wandering resting state? If FC truly encodes neural patterns of thought and cognitive processes, which we know from experience are not static during the stream of spontaneous thought that occurs throughout the wakeful rest condition, then the assumption of static resting state FC indeed seems too strict.

Accordingly, there has been a shift in focus from studying static FC to time-varying FC (TVFC) in the context of resting state fMRI. Generally, the TVFC paradigm aims to decompose resting brain activity into a set of discrete FC states that are common across individuals. It is hypothesized that these time-varying states may correspond to distinct cognitive processes, and that the patterns in which individuals transition between these brain states can be predictive of a variety of neurally relevant phenotypes. In fact, when reviewing the burgeoning literature regarding resting state TVFC, one can come away with a few major conclusions. First, an overwhelming majority of TVFC studies find evidence of temporally changing FC patterns within the course of a single resting state scanning session. Second, the convergence of evidence in favor of the TVFC view of the resting state was arrived at using a number of statistically distinct methodologies. Third, evidence of TVFC is reproduced across several populations, including healthy adult, pediatric, and clinical populations. Fourth, features derived from TVFC analyses have been shown to capture important individual variation across a spectrum of phenotypes, as well as utility for tracking spontaneous thought (Kucyi & Davis, 2014). Taken together, these findings suggest that viewing resting state FC through a time-varying lens will be an integral component for innovation and progress in cognitive neuroscience, in particular for uncovering the mapping between brain and mind.

As one of the newest frontiers in the field of neuroimaging, the study of TVFC is met with nearly as much criticism as enthusiasm. Doubts have been cast about the origins of the dynamic FC patterns observed in resting state fMRI, with suggestion that these apparent dynamics could be by-products of non-neural noise such as head motion (Laumann et al., 2017) or confounding physiological signals like heart beats or respiration (Cordes et al., 2001; Nguyen et al., 2016). Moreover, there has been a great deal of speculation as to whether the observed temporal changes in FC patterns are artificially produced as an artifact of the statistical TVFC methods themselves (Laumann et al., 2017). The natural difficulty in studying resting state FC is the absence of a "ground truth", in which the time-resolved changes in cognitive states are known and against which the accuracy of various TVFC methods could be tested. For these reasons, development of methodologies capable of uncovering these "hidden" resting brain states is currently an active area of research.

In this dissertation, I contribute to the methodological component of the TVFC discourse. I propose two distinct yet related approaches for identifying TVFC using an informed segmentation framework. This data-driven framework bridges instantaneous and windowed approaches for studying TVFC, in an attempt to mitigate the limitations of each while simultaneously leveraging the advantages of both. I also present a comprehensive, head-to-head comparative analysis of several of the most promising TVFC methodologies proposed to date, which does not exist in the current body of literature.

1.2 Dissertation Outline

In Chapter 2, I provide the necessary background information and a review of the state of the field of TVFC. In Chapter 3, I propose the activation-informed segmentation method, a hybrid TVFC approach that leverages moment-to-moment changes in whole brain functional activity to generate discrete, data-driven segments of stable FC, and identify significant relationships between the resultant discovered dynamic states and phenotypes of interest. In Chapter 4, I perform a comparative analysis of three popular instantaneous connectivity estimation methods: multiplication of temporal derivatives (MTD), edge co-fluctuation (ECF) and dynamic conditional correlation (DCC). Using block design task data as a natural ground truth, I compare the performance of each instantaneous connectivity estimator alone, as well as a base signal for the sliding window and informed segmentation frameworks in identifying known boundaries between functional brain states. In Chapter 5, I explore the use of the instantaneous state estimation approaches of co-activation pattern (CAP) analysis and hidden Markov models (HMMs) across both the activation and connectivity domains. In Chapter 6, I present a proof-of-concept experiment utilizing recurrent neural network architectures to learn instantaneous FC patterns and identify anomalous frames of functional activation. A discussion of the results as a whole and proposed future directions is presented in Chapter 7. A schematic representation of the methodologies used in each of Chapters 3-6 is presented in Figure 1.1.

1.3 Figures

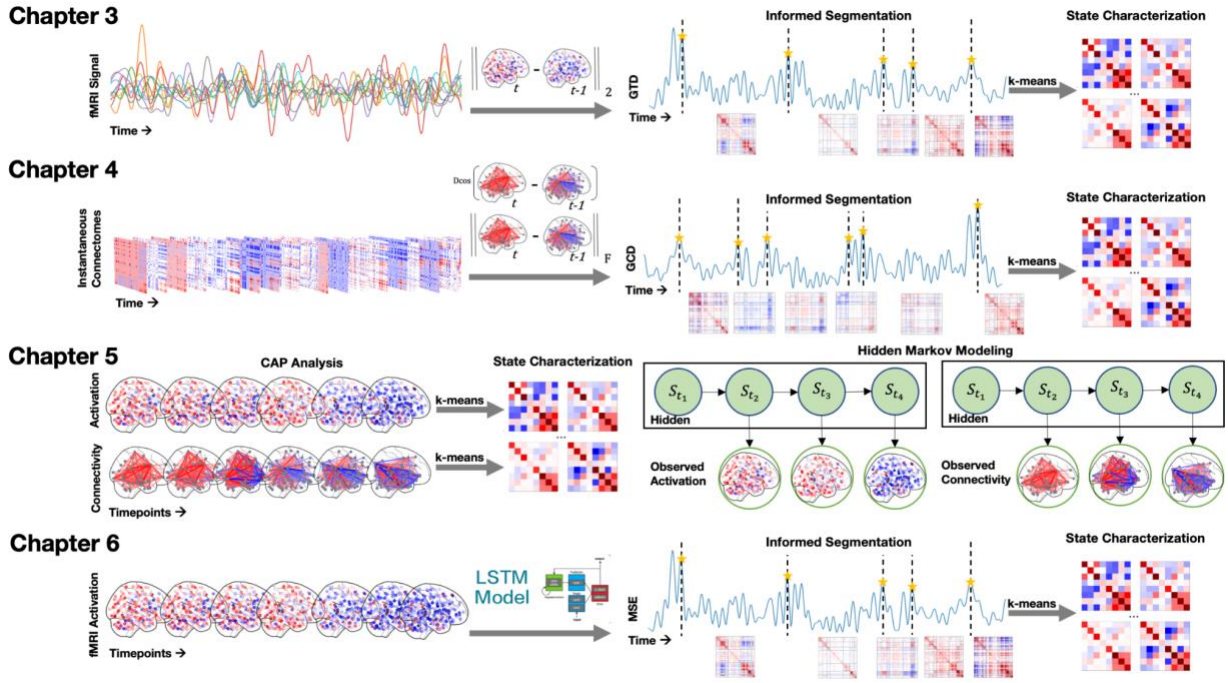

Figure 1.1. Schematic representation of experimental pipelines used in Chapters 3-6.

Chapter 2 - Background

The brain is a complex dynamical system that is never truly "at rest". Even in the absence of explicit task demands, the brain still manifests a stream of conscious thought, varying levels of vigilance and arousal, as well as a number of postulated ongoing "under the hood" functions such as memory consolidation. This "resting state", once regarded as a baseline or even a nuisance measurement, is now known to be rather cognitively rich. Considering task-unrelated thought and behavior accounts for nearly 50% of our waking time (Killingsworth & Gilbert, 2010) and may explain a much larger portion of individual neural variability than that of task-evoked cognition (Musall et al., 2019), gaining a more complete understanding of the functional underpinnings of resting cognition is of paramount importance to the field of cognitive neuroscience.

To this end, one specific area of interest lies in uncovering temporal changes in resting state functional connectivity patterns, with hopes that they may serve to illuminate the mechanistic underpinnings of mind wandering and other processes operating in the "resting" brain. While important, this study of spontaneous intrinsic changes in functional connectivity is challenging from both a methodological and biological perspective. Methodologically, techniques capable of capturing dynamic functional relationships between brain regions without imposing arbitrary timescales or artificially inducing the appearance of changing connectivity structure are required to obtain an unbiased understanding of time-varying functional connectivity (TVFC) at rest. Biologically, the

challenge lies in disentangling the neurophysiological basis of TVFC observed from the BOLD fMRI signal to understand the contribution of sleep/arousal state, neuromodulatory effects and true interregional neural interactions. As the latter biological challenges cannot be studied before the former methodological considerations are sufficiently resolved, this dissertation primarily aims to contribute to the methodological discussion for uncovering TVFC from resting state BOLD fMRI data.

2.0 Terminology

I begin by defining some key terminology used throughout this dissertation, to avoid confusion or ambiguity. Firstly, based on the suggestion in a recent work by Lurie and colleagues (Lurie et al., 2020), I refer to the study of changing functional connectivity patterns on the order of seconds as "time-varying functional connectivity" (TVFC). This phenomenon has often been referred to as "dynamic functional connectivity", or dFC, but ambiguity across disciplines in the definition of the term "dynamic" has led to the proposed standard nomenclature of TVFC. In contrast to TVFC, I refer to studies of functional connectivity (FC) that operate under the assumption that FC does not spontaneously change as a function of time as "static FC".

Secondly, throughout this dissertation I discuss different methodologies of parsing time series into smaller slices for TVFC analysis. To avoid confusion, I use the term "window" to describe *fixed-length* and often *overlapping* slices of the time series, usually in the context of the sliding window paradigm. Conversely, I use the term "segment" to refer to *tailored* or *variable-length* slices of the time

series that are *discrete* (i.e., *non-overlapping*). The term "segment" is often used in the context of my newly proposed informed segmentation TVFC paradigm.

Thirdly, I often refer to "instantaneous" methodologies of estimating functional connectomes or functional brain states. In the context of fMRI research, it is important to discuss the meaning of such a term precisely. Any "instantaneous" estimate derived from fMRI is dependent on the temporal resolution (TR) of the fMRI scanner, i.e., the interval between each functional brain "snapshot" or "frame". It is also critical to consider that fMRI is an indirect measure of functional brain activity, rather than a direct measure of electrical impulses generated by firing neurons, so any activity captured by fMRI is subject to hemodynamic lag. With this in mind, the term "instantaneous" in the context of FC or brain state estimates is synonymous with "pointwise" or "framewise", meaning an estimate is generated at each time point or frame within the fMRI time series.

A list of commonly used terms and abbreviations can be found in Table 2.1.

2.1 fMRI and Functional Connectivity

The intricate neural interactions that give rise to human cognition have been the subject of curiosity and study for centuries, but in-depth observation and investigation of these functional connections have only become a possibility in recent decades through the advancement of modern neuroimaging modalities. Though several functional neuroimaging techniques are available today, perhaps the most commonly used is functional magnetic resonance imaging (fMRI). fMRI is a method of non-invasively observing brain function using blood flow as a marker for functional

activation, resulting in what is known as the blood oxygen level dependent (BOLD) signal. In addition to its non-invasive nature, BOLD fMRI has the benefit of relatively high spatial resolution, enabling simultaneous imaging of activation in regions across the entire brain. This, however, comes at the expense of noisiness as an indirect measure of functional activation, as well as temporal resolution, owing to the intrinsically slow nature of the hemodynamic response. Despite its limitations, BOLD fMRI has become the leading modality for the study of functional connectivity (FC), defined as the statistical dependency of neurophysiological time series derived from individual regions or networks in the brain (Lurie et al., 2020).

In its infancy, the field of FC research focused on mapping the functional networks involved in specific cognitive processes, achieved through the use of meticulously designed task paradigms (Medaglia et al., 2015). However, following the seminal study by Biswal et al. (Biswal et al., 1995), which showed evidence of synchrony between voxels in the primary motor cortex and other seed regions across the brain in the absence of explicit task demands, there has been considerable interest in studying FC in the resting state. The collection of resting state fMRI data is usually conducted under a quiet "wakeful rest" condition, where subjects are asked to either visually focus on a crosshair within the MRI scanner or keep their eyes closed. While the absence of a predefined task structure precludes temporal alignment between subjects, the freeform mind-wandering nature of resting state fMRI affords a certain flexibility in analytical choices and naturally imposes fewer demands on subjects—a substantial benefit for collecting data from populations with cognitive or neurological impairments that may be unable to perform certain tasks in a standardized way in the scanner.

Traditionally, resting state functional connectivity (rsFC) has been viewed as a static phenomenon, meaning the statistical dependencies between distinct brain regions are considered constant and are thereby computed as an average across the entire available time series. Even under this somewhat stringent assumption, individual variation in static rsFC patterns have been associated with a variety of phenotypes. A majority of this research has focused on uncovering clinical correlates of static rsFC (Fox & Greicius, 2010), beginning with identification of group-level differences in resting FC patterns between individuals with neurological or psychiatric disorders and healthy controls (Fox & Raichle, 2007; Greicius, 2008; Hull et al., 2017; Lynall et al., 2010; D. Zhang & Raichle, 2010), to prediction of disease state (Greicius et al., 2004; Hedden et al., 2009; S.-J. Li et al., 2002; Zeng et al., 2018) and severity (Bluhm et al., 2007; Greicius et al., 2007; B. J. He et al., 2007) on an individual basis. Though static rsFC has been studied across the spectrum of clinically relevant phenotypes, the consistency and strength of disease-specific rsFC signatures vary from highly consistent, as in the case of Alzheimer's (Greicius et al., 2004; Hedden et al., 2009; S.-J. Li et al., 2002), to somewhat inconsistent, as seen with schizophrenia (Bluhm et al., 2009; Jafri et al., 2008; Liang et al., 2006). Beyond clinical diagnoses, static rsFC has also been studied in the context of broader cognitive phenotypes, showing the ability to predict measures of cognitive control (Cole et al., 2012), working memory (Hampson et al., 2006), and even fluid intelligence (Finn et al., 2015). Static rsFC has even exhibited utility for encoding behavioral performance, such as measures of attention (Rosenberg et al., 2016). As evidenced by this existing body of research, the average landscape of spontaneous brain

activity estimated by static measures of FC at rest captures both group-level and individual variability across several phenotypes of interest.

2.2 Time-Varying Functional Connectivity (TVFC)

Motivated by the mind-wandering nature of spontaneous thought in rest, researchers began studying the time-varying nature of rsFC. Researchers hypothesized that patterns of FC would be modulated by the changing cognitive processes associated with the undirected resting state and may also be temporally affected by changing levels of arousal or attention. The study of TVFC was born of two seminal works that were published in short succession, which presented the first evidence for meaningful variation in temporal patterns of rsFC (Chang & Glover, 2010; Sakoğlu et al., 2010). Importantly, though these studies differed in methodological design (time-frequency analysis between selected seed regions and whole brain sliding window analysis), as well as population (healthy adults only vs. a case-control schizophrenia cohort), both showed strong evidence that patterns of rsFC changed as a function of time. These studies opened the door for a broad array of work aimed at uncovering the nature and significance of TVFC in a variety of contexts and populations, which will be discussed in the following sections.

When we discuss the notion of TVFC, it is important that we specify the timescale of the dynamics of interest. Individual changes in FC have been demonstrated across several timescales, ranging from changes in FC that occur on the scale of hours (Bassett et al., 2011; Sami et al., 2014) to changes that occur across weeks, months, and even years (Choe et al., 2015; Poldrack et al., 2015).

These long-range changes in FC have been attributed to factors such as learning, gene expression and concentrations of metabolites. While such changes are of independent interest and importance, the study of TVFC as discussed in this dissertation focuses on changes that occur within the timescale of a single fMRI scan, usually on the order of seconds to a few minutes.

In the decade since such short-range temporal dynamics of rsFC were first described, TVFC has evolved into a burgeoning field of research. The number of papers published in the field of TVFC has grown rapidly and exponentially, increasing from just two publications in 2010 to 105 publications in 2018 (Lurie et al., 2020). In the following subsections, we aim to highlight key findings from studies of TVFC (Section 2.3), popular TVFC methodologies (Section 2.4), and concerns that have arisen about the nature of TVFC work (Section 2.5).

2.3 Clinical and Behavioral Correlates of TVFC

2.3.1 Cognitive and Behavioral Traits

One of the larger questions surrounding TVFC is the relevance of the time-varying patterns of FC with regard to cognition and behavior. Several studies have probed this link between neural dynamics and behavior, identifying several connections between the two. Broad connections have been identified between patterns of resting TVFC and general cognitive task performance (Jia et al., 2014), as well as specific relationships between the temporal contribution of dorsal attention network-dominant states and performance in attention tasks (Madhyastha et al., 2015). Studies of TVFC with respect to specific subnetworks have also elucidated meaningful cognitive correlates of connectivity

dynamics. Temporal flexibility within both the salience network (T. Chen et al., 2016) and posteromedial cortex (Yang et al., 2014) showed significant correlations with measures of cognitive flexibility and executive function.

Another point of interest has been in connecting features of TVFC with intelligence and processing speed (Vidaurre et al., 2017). A common approach in this arena is comparing the performance of time-varying measures of FC with those of static measures of FC in their ability to predict or capture the individual variation in measures of fluid intelligence (Liégeois et al., 2019; Vidaurre et al., 2021). The consensus of these recent works is that time-varying representations of FC are better predictors of fluid intelligence. This is in contrast to results from the same works that indicate TVFC does not provide any advantage over static FC in predicting certain facets of personality or self-reported measures of well-being.

Finally, studies of TVFC have also shown links to more abstract or subjective components of cognition and behavior. For example, larger variability in regional FC was connected to lowered frequency of positive thought (Schaefer et al., 2014) and increased connectivity strength and variability between the default mode network and periaqueductal gray was associated with individual ability to divert focus from pain (Kucyi et al., 2013). Finally, and perhaps most interestingly, time varying patterns of FC within and between the default mode network and other subregions was shown to track mind-wandering events in time (Kucyi & Davis, 2014), indicating that measures of TVFC do have the ability to localize spontaneous recruitment of cognitive processes within the resting state.

2.3.2 Demographic Phenotypes

In addition to the cognitive and behavioral relevance of TVFC, changing patterns of functional connectivity have also been associated with demographic features such as age and biological sex. TVFC correlates to age have been demonstrated in youth (Marusak et al., 2016), aging (Madhyastha & Grabowski, 2014), and throughout the lifespan (Hutchison & Morton, 2015). A common thread across these studies shows that increase in FC variability is associated with increased age. Sex-based differences in TVFC have also been reported, suggesting that males and females exhibit differing patterns of state occupancy in rest (Yaesoubi, Allen, et al., 2015; Yaesoubi, Miller, et al., 2015).

2.3.3 Clinical Phenotypes

Since measures of TVFC have been shown to be associated with individual variation in cognition and behavior, it is logical that work would build upon these associations and use TVFC to study brain disorders in which these processes are altered or disrupted. Moreover, conditions which are marked by increased variability (or stability) of thought are ideally suited for study with TVFC methods, as static approaches cannot capture these relevant alterations. Based on this, it is unsurprising that schizophrenia—characterized by highly disorganized thought, delusions, and hallucinations—was the first (Sakoğlu et al., 2010), and is among the most widely studied brain disorders in the context of TVFC. Interestingly, there is a strong concordance in the results across this wide range of schizophrenia TVFC studies. These works find that schizophrenia is marked by weakened cross-network connectivity (Damaraju et al., 2014), specifically in connections both across (Rashid et al.,

2014; Su et al., 2016) and within (Du et al., 2016) the default mode network compared to healthy controls. Individuals with schizophrenia also exhibited reduced dynamic flexibility, occupying a narrower set of meta-states (Miller et al., 2016; Yu et al., 2015), and spending more time in states characterized by lower connectivity overall (Damaraju et al., 2014; Du et al., 2016; Rashid et al., 2016). Taken together, these results provide an enhanced understanding of the functional underpinnings of schizophrenia that would not have been possible without studying this disorder through a time-varying framework.

In contrast to the increased variability in thought associated with schizophrenia, autism spectrum disorder (ASD) is characterized by unusual stability of thoughts, often manifesting as repeated, restricted interests and hyperfixations. The results of TVFC studies in ASD show dynamic signatures of FC that largely oppose the characteristics found for schizophrenia (de Lacy et al., 2017). Namely, ASD is shown to be characterized by decreased variability in connectivity between the default mode network and the posterior cingulate gyrus (PCC) (C. He et al., 2018), increased within-network connectivity of the PCC (Y. Li et al., 2020), and increased variability in time-varying FC overall (Harlalka et al., 2019; Y. Li et al., 2020). Recent work in ADHD suggests that children with ADHD exhibit similar patterns, particularly extended dwell time in hyperconnected network states (Shappell et al., 2021). This similarity in TVFC characteristics between ADHD and ASD is underscored by the large behavioral overlap between the two conditions.

Other works have shown that time-varying measures of FC are more informative than analogous static descriptions of FC in detecting disease-specific characteristics in the context of

Parkinson's disease (Díez-Cirarda et al., 2018), PTSD (Jin et al., 2017), Alzheimer's disease (Jones et al., 2012), and depression (Kaiser et al., 2016). Overall, this large body of work studying TVFC in various brain disorders has enabled a more thorough characterization of disease and will continue to do so as our understanding of TVFC in healthy rest is refined. Beyond the use of TVFC for enhancing our understanding of underlying functional processes that give rise to brain disorders, if the time-varying connectivity signatures become sufficiently disease-specific, there is great potential for TVFC signatures to serve as biomarkers for clinical diagnoses or as prognostic indicators for measuring disease progression or treatment response.

2.4 TVFC Methodologies

2.4.1 Sliding Window Methods

The sliding window paradigm is undoubtedly the most popular methodology used to study TVFC (Allen et al., 2014; Kucyi & Davis, 2014; Madhyastha et al., 2015; Marusak et al., 2016, 2018; Nomi et al., 2017; Sakoğlu et al., 2010; Yaesoubi, Allen, et al., 2015). In the basic sliding window method, a window of fixed length is slid across the entire time series, shifted by a predefined number of time points (step size) each time. Within each window, the functional connectivity is computed across all pairs of nodes, resulting in a set of time-evolving (and often heavily overlapping) windowed estimates of FC.

Importantly, there are two distinct elements of the sliding window paradigm—windowing and connectome estimation. These two components present several methodological choices that can be

mixed-and-matched to create numerous potential sliding window workflows. For example, the windowing step involves the definition of the size and shape of the window (Mokhtari et al., 2019; Shakil et al., 2016, 2018, 2015), the optimal choice of which still constitutes an active area of research. There are also several choices of connectivity estimators, including Pearson correlation (Allen et al., 2014), Spearman correlation (Savva et al., 2019), instantaneous shared trajectory (Faghiri et al., 2020), and instantaneous phase synchrony (Pedersen et al., 2018). Each of these methods presents its own benefits, but Pearson correlation is generally the most commonly used connectivity estimator in sliding window paradigms.

The use of the sliding window method can vary depending on the study design and goals of the analysis. For example, statistics that capture the temporal variability of the FC (i.e., standard deviation, variance) can be computed directly across all windowed connectomes and related to cognitive and behavioral correlates of interest (Kucyi et al., 2016; Kucyi & Davis, 2014; Patanaik et al., 2018). The sliding window method can also be combined with *k*-means clustering to segregate the temporal windows into a set of *k* discrete connectivity states (Allen et al., 2014). Each state can be defined by its corresponding cluster centroid and various dynamic features can be extracted on the individual or group level, including dwell times (i.e., the contiguous length of time spent in a single state) and state-to-state transition probabilities.

While the sliding window paradigm has proven useful for discovery of the time-varying nature of FC and insights into several cognitive and clinical correlates of TVFC (discussed in Section 2.3), it also suffers from several important limitations. First, the sliding window method relies heavily on the

somewhat arbitrary choice of window size, and results can differ substantially across various window widths (Hindriks et al., 2016; Shakil et al., 2016). Second, simulations suggest that sliding window methods can introduce artifactual connectivity variation even under conditions when such variation is known to be absent (Laumann et al., 2017; Lindquist et al., 2014a). Third, perhaps due to one or more of the preceding issues, the sliding window method has been found to have poor test-retest reliability (Choe et al., 2017). Fourth, the overlapping nature of the sliding windows precludes definitive segmentation of the fMRI time series into states, making interpretation of the state dynamics difficult. Finally, the sliding window approach requires constructing a sizable number of overlapping windowed connectivity matrices: with 400 timepoints and a 30 TR window, 370 distinct connectivity matrices are required (at a step = 1 TR = 1s). This poses serious scalability issues for relatively long or more temporally granular fMRI datasets.

2.4.2 Instantaneous FC Estimators

Due to the limitations associated with sliding window TVFC frameworks, there has been increased interest in the development of "windowless" methodologies, specifically those capable of estimating instantaneous, or frame-wise, FC. In this section, I provide a brief overview of popular or promising instantaneous FC estimation methods.

The Multiplication of Temporal Derivatives (MTD) method (Shine et al., 2015) was introduced as a way to estimate functional connectivity at a higher temporal resolution than what was available via windowed methods. The MTD is calculated by first computing the temporal derivative for each region of interest (ROI) time series by applying first-order differencing, and then calculating

the pairwise products of all ROI temporal derivatives at each time point. For an fMRI time series composed of n ROIs and T time points, the MTD method will result in a series of $T - 1$ connectome estimates of size $n \times n$. Intuitively, the magnitude of the MTD metric captures the degree of functional coupling between each pair of ROIs at each time point, whereas the sign captures the direction of the relationship—a positive MTD value indicates functional change in the same direction (either both increasing or both decreasing in fMRI amplitude), whereas a negative MTD value indicates anti-coupling. The MTD was shown to outperform the standard sliding window method in identifying changes in FC states in both simulated and real-world data (Shine et al., 2015).

Very recently, another approach that is formulaically related to the MTD method has been proposed for estimating instantaneous FC. This approach, here referred to as the edge co-fluctuation (ECF) metric (Esfahlani et al., 2020), is described as a "temporal unwrapping" of the Pearson correlation coefficient. The ECF is computed by first z-scoring each ROI time series and then calculating the element-wise product of the z-scored time series for all pairs of ROIs, resulting in a series of T connectome estimates of size $n \times n$. The formulation of the ECF metric is equivalent to the Pearson correlation across the entire time series without the averaging step, and so it follows that the temporal average of the ECF series is equivalent to the static FC estimated with pairwise Pearson correlation. In this way, each time-resolved connectivity matrix generated by the ECF can be interpreted as an instantaneous component of static Pearson correlation across the full time series. Furthermore, the MTD can be thought of as the ECF applied on the temporal derivative, rather than directly on the time series (more on this in Section. 4.3). The authors show that the ECF metric shows

inter-subject synchrony during a passive movie watching task, indicating the changing FC patterns captured by the ECF metric in this context may be associated with perception and processing of sensory information, and supporting the hypothesis that the ECF can potentially be used to track an individual's changing cognitive state over time, even in the absence of task.

Building on the ECF, the authors also propose an edge-centric approach for estimating static FC, aptly named edge functional connectivity (eFC) (Faskowitz et al., 2020). The eFC metric computes the statistical dependency (i.e., Pearson correlation) of all pairs of edges in the ECF (also referred to by the authors as the nodal functional connectivity [nFC]) series, resulting in a $m \times m$ edge-centric connectivity matrix, where $m = \frac{n(n-1)}{2}$. The resultant edge-by-edge connectivity matrix can be utilized to uncover overlapping communities of edges that co-fluctuate with one another and probe the differences in the organization of these communities under various cognitive conditions. While the eFC "super-connectome" is technically a measure of static FC, it cannot be computed without first generating an instantaneous connectivity series such as the ECF, making it a relevant post-processing procedure. Furthermore, the eFC has potential for use in a sliding window paradigm to capture time-varying edge functional connectivity and the changing underlying edge community structure, combining a unique perspective on FC with a familiar time-varying FC paradigm.

While the MTD and ECF are both non-parametric methods, parametric models are also available for estimating time-varying statistical dependencies between time series, namely those classically used for financial analysis. Of these the most well studied is the dynamic conditional

correlation (DCC) model (Engle, 2000), which is a form of a multivariate generalized autoregressive conditional heteroscedastic (GARCH) model. A general univariate GARCH(p,q) model estimates the conditional variance of a univariate time series at time t as a linear combination of q prior estimates of the conditional variance and p prior values of the time series itself. The DCC model generates a multivariate GARCH estimate using a two-step process: first, univariate GARCH models are fit to each of the ROI time series to estimate the time-varying variance of each ROI signal individually, and second, pairwise time-varying correlations are estimated using an exponentially weighted moving average (EWMA) scheme on the standardized residuals from the estimates in the first step. From the first application of DCC models to estimate TVFC in BOLD fMRI data, the authors report superior performance in identifying the true time-varying correlation structure across several simulated and real-world datasets as compared to the standard sliding window approach (Lindquist et al., 2014b).

Overall, instantaneous estimation of functional connectivity is a fairly new and promising methodological direction in the study of TVFC. The major benefit of this family of methods is the ability to mark changes in FC at the highest temporal granularity offered via fMRI, from one frame to the next. While this property can be advantageous towards the goal of precise temporal localization of changing FC, it is also naturally more susceptible to "noisy" time frames which are an inevitable outcome of fMRI acquisition. Furthermore, the generation of a connectivity matrix at each time point leads to an increase in dimensionality compared to the sliding window, which can potentially lead to issues with computational complexity in downstream analyses. However, this increase is usually negligible, less than or equal to the size of the window itself, and the benefits from the increased

temporal resolution of the connectivity estimates often outweigh the slight increase in dimensionality. Finally, it is important to note that instantaneous FC estimators cannot directly provide estimates of discrete connectivity states without the recruitment of further post-processing techniques, such as the *k*-means clustering approach commonly used in windowing methods, or other state estimation approaches introduced in Section 2.4.3.

2.4.3 Instantaneous Brain State Estimators

In addition to instantaneous FC estimators, there exists another class of methods that aim to estimate the time-varying connectivity states directly, without the need for estimation of FC at each time point. Three popular methods in this class are co-activation patterns (CAP), temporal independent component analysis (tICA), and hidden Markov models (HMM).

The simplest of these instantaneous state estimation methods is CAP analysis (Liang et al., 2006). The standard CAP approach involves the choice of a seed region and the selection of an activation threshold for defining "high-activity" frames. For all timepoints in which activation in the seed region exceeds the selected threshold, activation values across all voxels or ROIs are extracted and aggregated across all subjects. Finally, *k*-means clustering is applied to this aggregated set of activation patterns to identify a set of *k* distinct CAPs, or brain states. Each distinct CAP is defined by the average activation signature of each timepoint in the cluster. Based on this formulation, the standard CAP approach is not fully instantaneous, as only a subset of high activity timepoints are considered. However, the CAP paradigm can be extended by applying the clustering learned from the high-activity frames to all time points, or by omitting the framewise thresholding of the time series and

simply applying *k*-means clustering to all time points. The CAP approach has been applied in a variety of contexts (J. E. Chen et al., 2015; Liu et al., 2018), and certain variations on this method have been proposed, such as the iCAP method that includes a deconvolution step in attempts to distinguish between temporally overlapping CAPs (Karahanoğlu & Van De Ville, 2015). Recently, CAP analysis has been utilized to gain insights into the altered functional dynamics associated with ASD (Marshall et al., 2020).

While cluster analysis has been a popular method for decomposing activation or connectivity time series into a set of distinct FC states, it imposes a somewhat rigid requirement that each timepoint (or window in the case of sliding window analysis) be assigned to a single cluster, or in other words, it only allows for the existence of single connectivity state at any given moment. Such inflexibility could mistake instances of transitioning cognitive processes as a distinct state rather than a mixture of two existing states. For this reason, methods of instantaneous state estimation that enable the expression of FC at a single time point as a combination of multiple underlying connectivity states have been studied. One such method is tICA, which seeks to decompose the fMRI time series into a set of connectivity patterns that are maximally mutually temporally independent. These resultant connectivity patterns (i.e., states) are common across all subjects, and an individual subject connectivity time course can be reconstructed through linear combinations of these states. Independent components analysis (ICA) is commonly applied to fMRI data in the spatial dimension to obtain individualized parcellations of the brain into functional ROIs and subnetworks. Spatial ICA works well for fMRI data, which consists of tens of thousands of voxels, but applying ICA in the

temporal dimension is often less robust, as fMRI time series typically only contain a few hundred time points (S. M. Smith et al., 2012). Even so, tICA has been applied both to activation time series (S. M. Smith et al., 2012) as well as windowed connectivity time series (Yaesoubi, Miller, et al., 2015). By accounting for the simultaneous contribution of multiple connectivity states, tICA has shown utility for explaining gender-based differences in TVFC (Yaesoubi, Miller, et al., 2015).

Finally, HMMs provide a probabilistic model-based approach for instantaneous state estimation. HMMs rely on the assumption that a sequence of observed data (i.e., BOLD fMRI signal) is generated by a sequence of unobserved or "hidden" underlying states (i.e., connectivity states). Learning HMMs in the context of TVFC involves estimation of three main components: 1) the distinct activation or connectivity signature of each state, 2) state-to-state transition probabilities, and 3) state membership at each individual time point. In fact, HMMs provide a probabilistic estimate of instantaneous state membership, allowing for the possibility of occupying multiple states at a single time point and thereby affording similar advantages to those of the tICA framework. HMMs have been applied to both windowed estimates of connectivity states, as well as to the BOLD fMRI time series directly. Certain variations on the standard HMM have been proposed, including auto-regressive HMMs (HMM-AR and HMM-MAR) (Vidaurre et al., 2018) and hidden semi-Markov models (HSMMs) (Shappell et al., 2021), each providing certain contextual benefits depending on the goal of the analysis at hand. In healthy control studies, HMMs have provided evidence for a hierarchical organization of time-varying connectivity states into two distinct meta-states (Vidaurre et al., 2017).

HMMs have also shown utility for uncovering altered connectivity dynamics across a variety of clinical diagnoses including PTSD (Ou et al., 2015) and ADHD (Shappell et al., 2021).

Instantaneous state estimation methods have several advantages and disadvantages. As mentioned above, each of the three approaches introduced in this section can be applied in both the activation and connectivity domains, indicating they can serve as stand-alone approaches or as optional post-processing techniques when used in conjunction with instantaneous or windowed estimates of FC described in Sections 2.5.1 and 2.5.2. One major disadvantage of state estimation approaches, in both instantaneous and windowed settings alike, is their dependence on the choice of the number of states to estimate. Often, this is resolved by testing a range of k values and optimizing some evaluation metric, such as the cluster validity index in the case of k-means clustering or the BIC criterion in the case of HMMs.

2.5 Doubts about TVFC

Despite a large body of literature supporting TVFC and its correlates with cognition, behavior and disease, doubts about the underlying processes which give rise to apparent dynamics in FC have been reported. Initial work demonstrated evidence that some level of TVFC could still be identified in an anesthetized state (Hutchison, Womelsdorf, Gati, et al., 2013; Keilholz et al., 2013), suggesting that some portion of the variability in FC cannot be attributed to conscious cognition. A more recent report has challenged the idea that TVFC is cognitively meaningful, instead suggesting that temporal variations in FC can be mainly explained by head motion, changing arousal state and sampling

variability imposed by windowed approaches (Laumann et al., 2017). This work utilized multivariate kurtosis of fMRI time series as a measure of stationarity and found the kurtosis of real resting fMRI data did not significantly differ from that of stationary-by-design simulated data, indicating the null hypothesis of statistical stationarity in resting state fMRI could not be rejected. However, subsequent analyses have presented evidence that contradicts these conclusions, particularly that known dynamic models, such as autoregressive frameworks and HMMs, exhibit statistical stationarity (Liégeois et al., 2017), and that the multivariate kurtosis metric is not always a perfect indicator of stationarity (Miller et al., 2018). These results suggest that statistical stationarity may not be synonymous with a lack of meaningful time-varying structure in FC, or vice versa.

While these doubts are valid, and even if TVFC is not fully encoding spontaneous change in cognitive state and cannot provide mechanistic insights into cognition or psychiatric conditions, it can still be valuable and useful as a potential biomarker (see evidence from Section 2.3.3 above).

2.6 Current Gaps in Knowledge

Considering the doubts presented in the preceding section, significant research into the behavior of TVFC methodologies is required to move the field forward. Since the nature and timescales of the underlying resting dynamics of interest are unknown, methodologies capable of detecting changing temporal patterns in connectivity without imposing arbitrary timescales are necessary. Moreover, as the study of TVFC is still in its infancy, rigorous evaluation of new and existing methodologies is critical to better understand their behavior when applied in resting data,

which lacks ground truth temporal landmarks against which accuracy can be assessed. Related to this, the field of TVFC is in need of standardized benchmarking practices that enable clear comparisons across methodologies. The work presented in the following chapters aims to systematically address each of these areas of need.

2.7 Figures and Tables

Term	Definition
Functional Connectivity (FC)	Statistical dependency of neurophysiological time series derived from individual regions or networks in the brain
Static Functional Connectivity	Functional connectivity analysis computed under the assumption that FC patterns do not change as a function of time
Time-Varying Functional Connectivity (TVFC)	Functional connectivity analysis computed under the assumption that FC patterns change as a function of time, on the order of seconds
Window	Fixed-length and often overlapping slices of the time series, usually in the context of the sliding window TVFC paradigm
Segment	Tailored or variable-length slices of the time series that are discrete (i.e., non-overlapping), often used in the context of the informed segmentation TVFC paradigm
ROI	Region of interest, an anatomical parcel of the brain
fMRI	Functional Magnetic Resonance Imaging
TR	Temporal resolution, i.e., sampling time of fMRI scanner
Connectome/Connectivity Matrix	Square matrix containing FC estimates for all pairs of ROIs

Table 2.1. A glossary of common terms and abbreviations used throughout this dissertation.

Chapter 3 - Validating Dynamicity in Resting State fMRI with Activation-Informed Temporal Segmentation

3.1 Abstract

Confirming the presence (or absence) of TVFC states during rest is an important open question in the field of cognitive neuroscience. The dominant TVFC framework aims to identify dynamics directly from connectivity estimates with a sliding window approach, however this method suffers from several drawbacks including sensitivity to window size and poor test-retest reliability. We hypothesize that time-varying changes in functional *connectivity* are mirrored by significant temporal changes in functional *activation*, and that this coupling can be leveraged to study TVFC without the need for a predefined sliding window. Here we introduce a data-driven TVFC framework, which involves informed segmentation of fMRI time series at candidate FC state transition points estimated from changes in whole-brain functional activation, rather than a fixed-length sliding window. We show this approach reliably identifies true cognitive state change points when applied on block-design working memory task data and outperforms the standard sliding window approach in both accuracy and computational efficiency in this context. When applied to data from four resting state fMRI scanning sessions, our method consistently recovers five reliable FC states, and subject-specific features derived from these states show significant correlation with behavioral phenotypes of interest (cognitive ability, personality). Overall, these results suggest abrupt whole-brain changes in activation can be used as a

marker for changes in connectivity states and provides strong evidence for the existence of time-varying FC in rest.

3.2 Introduction

Over the past two decades the study of functional connectivity has emerged as a preeminent method in cognitive and clinical neuroscience, aiming to characterize the functional network organization of the brain, and to identify objective markers of neuropsychiatric diseases and clinically relevant phenotypes. FC describes the interconnection (often computed as temporal correlation) in activation patterns of spatially distinct regions of the brain, typically measured by BOLD fMRI. Originally, the entire field of FC was built on a critical assumption: that patterns of connectivity are static during any given measurement interval in a resting state, i.e., the absence of any cognitive task (Biswal et al., 1995). Static FC has been used to identify global differences in functional network organization of the brain between cognitive task states and resting state (Greicius et al., 2003), as well as to characterize differences in FC between healthy controls and subjects with neuro-psychiatric diagnoses, such as schizophrenia (Lynall et al., 2010) or autism spectrum disorder (ASD) (Hull et al., 2017).

Recently, however, a number of studies have questioned this assumption, instead advocating the "dynamic" or "time-varying" connectivity view that functional connectivity patterns exhibit substantial moment-to-moment changes over time, specifically within a standard fMRI measurement interval of five to fifteen minutes (Calhoun et al., 2014; Chang & Glover, 2010; Cohen, 2018;

Hutchison, Womelsdorf, Allen, et al., 2013; Lurie et al., 2019; Preti et al., 2017). These changing FC patterns are thought to correspond to cognitively meaningful discrete FC network configurations, or connectivity states, that are reproducible both within and between individual subjects. Dynamic states have been documented across different populations including children (Marusak et al., 2018) and adults (Allen et al., 2014; Cai et al., 2018; T. Chen et al., 2016; Choe et al., 2017; Liu & Duyn, 2013; D. M. Smith et al., 2018), and have been supported with concurrent electroencephalography (EEG) data (Allen et al., 2018; Chang et al., 2013; Tagliazucchi et al., 2012). Furthermore, it has been shown that other characteristics such as the amount of time spent in specific states and the number of transitions between states vary with meaningful individual differences such as age (Cabral et al., 2017; Hutchison & Morton, 2015; Marusak et al., 2016), sex (Mao et al., 2017; Yaesoubi, Miller, et al., 2015), or disease status (Cordes et al., 2018; Damaraju et al., 2014; Jones et al., 2012; Rashid et al., 2014).

By definition, the presence of TVFC in the resting state is marked by changes in the connectivity structure of the fMRI time series. The prevailing sliding window framework aims to identify these second-order changes using functional connectivity "snapshots" obtained from time windows of fixed length slid across the entire fMRI time series. The resultant windowed connectomes are then flattened into feature vectors, concatenated across subjects, and clustered into k distinct connectivity states. Importantly, there are two distinct elements of the sliding window paradigm (windowing and connectome estimation) that present several methodological choices that can be mixed-and-matched to create numerous potential sliding window workflows. For example, the windowing step involves the choice of the size and shape of the window (Mokhtari et al., 2019; Shakil et al., 2016, 2018, 2015), the

optimal choice of which still constitutes an active area of research. There are also several choices of connectivity estimation, including Pearson correlation (Allen et al., 2014), Spearman correlation (Savva et al., 2019), instantaneous shared trajectory (Faghiri et al., 2020), and instantaneous phase synchrony (Pedersen et al., 2018). Each of these methods presents its own benefits, but Pearson correlation is generally the most commonly used connectivity estimator in sliding window paradigms. The sliding window approach represents an important advance in the study of time-varying brain connectivity, but it nonetheless suffers from several important limitations.

First, the sliding window method relies heavily on the somewhat arbitrary choice of window size, and results can differ substantially across various window widths (Hindriks et al., 2016; Shakil et al., 2016). A second problem is that simulations suggest that sliding window methods can introduce artifactual connectivity variation even under conditions when such variation is known to be absent (Laumann et al., 2017; Lindquist et al., 2014b). Third, perhaps due to one or more of the preceding issues, the sliding window method has been found to have poor test-retest reliability (Choe et al., 2017). Fourth, the overlapping nature of the sliding windows precludes definitive segmentation of the fMRI time series into states, making interpretation of the state dynamics difficult. Finally, the sliding window approach requires constructing a sizable number of overlapping windowed connectivity matrices: with 400 timepoints and a 30 TR window, 370 distinct connectivity matrices are required (at a step = 1 TR = 1s). This poses serious scalability issues for relatively long or more temporally granular fMRI datasets.

Some alternatives to sliding window approaches have been proposed in recent years; however, these too have certain drawbacks and limitations. The dynamic conditional correlation (DCC) model is

a multivariate volatility model that estimates the changing covariance structure at each timepoint in the fMRI time series (Choe et al., 2017; Lindquist et al., 2014b). While the DCC model allows for a parametric approach to estimating framewise FC with robust statistical inference, it increases the number of connectivity matrices to consider in the final clustering step compared to the sliding window method, further hindering its scalability. Furthermore, the formulation of the DCC model has been shown to give biased results in high dimensional data (Hafner & Reznikova, 2012), which poses an issue for application in fMRI data with a large number of ROIs and time points. Two other recently proposed moment-to-moment methods, multiplication of temporal derivatives (Shine et al., 2015) and edge co-fluctuations (Esfahlani et al., 2020), have similar formulations and are both aimed at uncovering the degree of functional coupling for all ROI pairs at each timepoint. Similar to DCC, these methods result in a higher dimensional output than that of the sliding window, and the instantaneous estimates of connectivity at each timepoint are highly susceptible to noise. Hidden Markov models (HMMs), which seek to decompose a time series into a sequence of discrete "hidden" states, are another increasingly popular approach for estimating connectivity dynamics (Baker et al., 2014; Quinn et al., 2018; Vidaurre et al., 2017; G. Zhang et al., 2020). However, HMMs rely on several strong assumptions including a predefined number of *k* hidden states that transition between one another in a Markovian fashion (state transitions depend solely on the state at the previous time point). Moreover, HMMs trained at the group level assume a single governing state-to-state transition structure across all subjects, which may be too strict and miss important individual variability.

Our focus here is on a hybrid approach that bridges windowed and instantaneous methods by leveraging moment-to-moment changes in activation to inform tailored time series segmentation at candidate FC state change points, which reduces both the dimensionality and noisiness that affects many other moment-to-moment TVFC methods. It is well known from the task-based fMRI literature that task-driven changes in activation patterns co-occur with changes in connectivity patterns (Davison et al., 2015; Gonzalez-Castillo et al., 2015; Shine & Poldrack, 2018; Spielberg et al., 2015; Sripada et al., 2014; Telesford et al., 2016). This coupling of activation and connectivity changes suggests the possibility that changes in the *activation structure* of the fMRI time series, which are easily derived, can serve as a reasonably reliable marker for changes in the *connectivity structure*, which are more difficult to obtain in an unbiased way. Though connectivity changes may not always be accompanied by activation changes, as long as there is significant correspondence, we can leverage the latter (straightforwardly identified) to find the former (less so) without the need for sliding windows.

In this work we leverage the coupling between activation and connectivity to present the activation-informed segmentation approach, a data-driven TVFC framework centered around informed segmentation of fMRI time series at candidate FC state change points. Moment-to-moment changes in functional activations have previously been utilized in the literature to investigate dynamic functional connectivity (Shine et al., 2015), but have yet to be used to localize connectivity state changepoints for dynamic time series segmentation. Our approach detects significant instantaneous changes in functional activation patterns and generates data-driven segments of stable connectivity throughout the fMRI time series. For clarity, we will use the term “segments” when referring to our

method and "windows" when referring to the sliding window approach. Separating the time series into discrete time segments rather than a set of highly overlapped sliding windows significantly improves the computational efficiency of TVFC analysis and enhances interpretability of results by enabling precise identification of state transition junctures—something the sliding window method cannot provide. We suggest that these FC-tailored segments provide a useful alternative to standard sliding windows in TVFC analyses and show that our approach significantly outperforms the sliding window paradigm in recovering known FC state transitions in a block-design task. Furthermore, we propose a framework for the comparison of connectomes derived from segments of variable length, as well as a graph embedding step for summarizing connectomes into low-dimensional representations that we show are better suited for downstream clustering and machine learning tasks than current approaches.

3.3 Methods

3.3.1 Data Description

3.3.1.1 HCP Data

In this work, we utilize the Human Connectome Project (HCP) S1200 Young Adult dataset made publicly available through the Washington University and the University of Minnesota HCP consortium (http://humanconnectome.org). It is one of the richest collections of neuroimaging data to date, consisting of structural and functional MRI, behavioral assessments, and genotypes for 1200 healthy subjects ages 22-35. A full description of the acquisition protocol can be found in (Van Essen et al., 2013). In short, all HCP fMRI data were acquired on a modified Siemens Skyra 3T scanner using

multiband gradient-echo EPI (TR = 720 ms, TE = 33 ms, flip angle = 52°, multiband acceleration factor = 8, 2 mm isotropic voxels, FOV = 208 × 180 mm, 72 slices, alternating RL/LR phase encode direction). Participants completed four total resting state fMRI scanning sessions (two sessions collected on each of two different days). Each resultant resting state fMRI time series consisted of 1200 volumes sampled every 0.72 seconds, for a total acquisition time of 14 minutes and 24 seconds. During the resting state sessions participants were instructed to keep their eyes open and fixated on a cross hair on the screen, while remaining as still as possible. For clarity, we will refer to resting state data from the first collection day as sessions 1A (RL) and 1B (LR), and similarly sessions 2A and 2B for those collected on the second day.

Though our main objective is to assess FC dynamics during rest, we also leverage the repeating task/rest block structure of the working memory (WM) task data available in HCP as a natural ground truth to test the performance of our method in identifying the known transitions between the task and rest conditions. The HCP WM task consists of four repeating task/rest blocks, where each block is structured as follows: 27.5 seconds Task 1 (0-back), 27.5 seconds Task 2 (2-back), 15 seconds rest. Using the same acquisition details outlined above, each WM task fMRI time series consisted of 405 volumes sampled every 0.72 seconds, for a total acquisition time of 4 minutes and 52 seconds. Two sessions of WM task fMRI were acquired back-to-back, alternating between RL and LR phase encoding directions. We will refer to these as WM session 1 (RL) and WM session 2 (LR).

3.3.1.2 Data Preprocessing

Processed volumetric data from the HCP minimal preprocessing pipeline including ICA-FIX denoising were used. Full details of these steps can be found in (Glasser et al., 2013; Salimi-Khorshidi et al., 2014). Briefly, BOLD fMRI data were gradient-nonlinearity distortion corrected, rigidly realigned to adjust for motion, fieldmap corrected, aligned to the structural images, and then registered to MNI space with the nonlinear warping calculated from the structural images. Then FIX was applied on the data to identify and remove motion and other artifacts in the timeseries. These files were used as a baseline for further processing and analysis (e.g., MNINonLinear/Results/rfMRI_REST1_RL/rfMRI_REST1_RL_hp2000_ clean.nii.gz from released HCP data).

Images were smoothed with a 6mm FWHM Gaussian kernel, and then resampled to 3mm isotropic resolution. This step as well as the use of the volumetric data, rather than the surface data, were done to allow comparability with other large datasets in ongoing and planned analyses that are not amenable to surface-based processing. The smoothed images then went through a number of resting state processing steps, including motion artifact removal steps comparable to the type B (i.e., recommended) stream of (Siegel et al., 2017). Further details on motion artifact removal can be found in (Sripada et al., 2019). Lastly, we calculated spatially averaged time series for each of the 268 ROIs from the parcellation given in (Finn et al., 2015).

For our analysis, we first considered the set of 966 subjects listed in (Sripada et al., 2019) that met the following criteria: structural T1 and T2 data, four complete resting state fMRI sessions, and <

10% of resting state frames censored due to excessive motion (framewise displacement of 0.5 mm). From this set 922 subjects also had two complete WM task fMRI sessions, defining our final subset of subjects.

3.3.2 The Activation-Informed Segmentation Framework

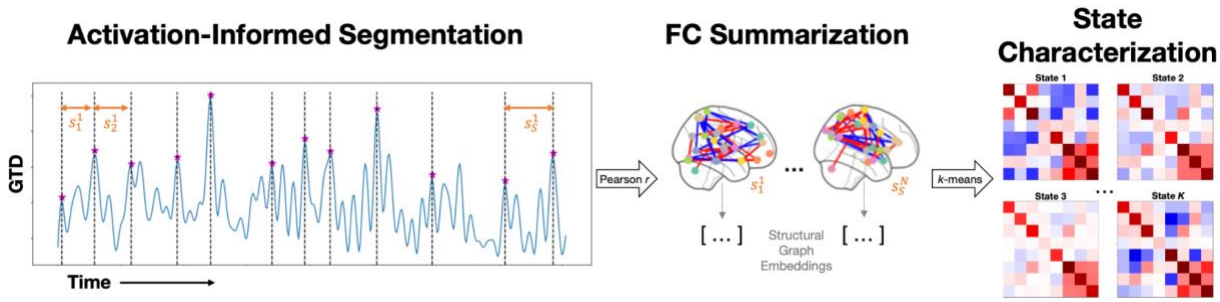

Figure 3.1. Experimental pipeline.
Briefly, peaks in the GTD series define the boundaries of our tailored, non-overlapping stable-FC segments s_1 to s_S (note S can vary between subjects) for all subjects $1 - N$. Next, functional connectivity is summarized using structural graph embeddings for each segment in the set of all segments $\left\{\{s_1^1, s_2^1, \ldots\}, \ldots, \{s_1^N, s_2^N, \ldots\}\right\}$. Finally, k-means is applied to segregate all segments into a set of k connectivity states.

Here we propose a novel framework for identifying time-varying changes in functional connectivity in fMRI time series, termed the activation-informed segmentation method. This method leverages the coupling between changes in connectivity structure and changes in whole-brain activation patterns to produce an intuitive, interpretable, and computationally efficient alternative to the sliding window approach. Our framework consists of three main steps: tailored segmentation of all fMRI time series, summarization of the functional connectivity within each discovered segment, and finally segregation and characterization of a final set of connectivity states (Figure 3.1). These steps are detailed in Sections 3.3.2.1 - 3.3.2.3 below.

3.3.2.1 Activation-informed time series segmentation

The dynamic FC paradigm suggests the presence of significant instantaneous changes in connectivity structure at transition points between two distinct functional states. Using this logic, we sought to identify potential connectivity state transition points within fMRI data and utilize them to perform informed segmentation of the time series as a means for assessing FC dynamics. Based on the phenomenon established in task-based literature (Davison et al., 2015; Gonzalez-Castillo et al., 2015; Shine & Poldrack, 2018; Spielberg et al., 2015; Sripada et al., 2014; Telesford et al., 2016), we hypothesize that changes in the *activation structure* of the fMRI time series, which are easily derived, can serve as a reasonably reliable marker for changes in the *connectivity structure*, which are more difficult to obtain in an unbiased way. To estimate the changes in functional connectivity from one time point *t* to the next, we observe changes in functional activation from one time point to the next by calculating the temporal derivative (*dt*) of each of *n* ROI activation time series (*ts*) of length *T* using first-order differencing similar to that in the multiplication of temporal derivatives (MTD) method (Shine et al., 2015):

$$dt_i(t) = ts_i(t) - ts_i(t-1) \tag{3.1}$$

At this point, our method importantly diverges from the MTD method: while the MTD uses these ROI-wise temporal derivatives to define the connectivity between each pair of ROIs and ultimately generate an $n \times n$ connectome estimate at each time point, our method instead summarizes the regional temporal derivatives to provide a univariate estimate of moment-to-moment changes in

activation on the whole brain scale. At this point in our pipeline, the resulting *n* temporal derivative series of length *T-1* are summarized by taking the L_2-norm, i.e., the root sum of squares, at each time step *t*, resulting in a single vector of length *T-1,* which we have termed the Global Temporal Derivative (GTD) series:

$$GTD\ \ (t)\ =\ ||\ dt_{1:n}\,(t)\ ||_2\ =\sqrt{\sum_{i=1}^{n}\ \ dt_i(t)^2} \tag{3.2}$$

The GTD provides a univariate summarization of instantaneous changes in global brain activation throughout an fMRI time series, therefore peaks in the GTD series correspond to instances of significant moment-to-moment alterations in functional activity. In this way, the GTD is akin to the derivative of the global signal. Growing research suggests the global signal is not noise and carries meaningful information about mental states (Wong et al., 2013). Here, we build on this work to suggest that global signal shifts mark changes in dynamic mental states. We seek to automatedly identify these change points as candidate FC state transitions for the subsequent time series segmentation step. We begin by applying exponentially weighted moving average smoothing (window size = 15 TR, $\alpha = \frac{2}{(window\ size\ +\ 1)}$) to the GTD series to reduce noisy peaks. We then perform moving average peak detection (window size = 20 TR for Rest, 10 TR for WM task) on the smoothed GTD series, identifying points in the time series that are >=2.5 standard deviations above the moving average. To avoid identification of multiple points that surpass this threshold but actually correspond to a single true peak, we collapsed points in close proximity to one another to the local maximum (within 10 TR, corresponding to 7 seconds or the approximate time-to-peak of the hemodynamic response function

(Friston, 2003)). Furthermore, as these change points define our tailored segments for downstream calculation of functional connectivity, we set a minimum inter-peak distance of 25 TR to ensure sufficiently large segments for calculating Pearson correlation (Schönbrodt & Perugini, 2013; Thirion et al., 2007; Turner et al., 2018) (note: we reduce this to 15 TR for the case of WM task data to accommodate the shorter resting state segments we intend to capture). This final set of change points define the boundaries of the tailored time segments, within which we compute FC and between which we investigate potential dynamic FC shifts.

3.3.2.2 Functional Connectivity Estimation

For each tailored segment *s*, we compute the functional connectivity matrix $C^{(s)}$, where the *i,j*th entry is the Pearson correlation of the activation time series of ROIs *i* and *j* within the time segment, $ts_i(s)$ and $ts_j(s)$:

$$C_{i,j}^{(s)} = \frac{cov(ts_i(s), ts_j(s))}{\sigma_{ts_i(s)}\sigma_{ts_j(s)}} \tag{3.3}$$

We then apply the Fisher transformation followed by z-scoring on each FC matrix $C^{(s)}$, to allow for better comparisons between connectivity matrices of segments of differing lengths. Connectivity matrices derived from shorter segments have, on average, higher correlation values than those from longer segments, resulting in a skewed sample distribution. Applying the Fisher transformation enforces an approximately normal distribution of the connectivity values within each segment (Fisher, 1915), and the z-score then translates these connectivity values in terms of their standard deviations from the

mean. While these connectome transformations are common practice in the field of FC, they are especially important when attempting to compare connectomes from segments of variable lengths, which is illustrated in Figure 3.2.

Thresholding is another common pre-processing step in functional connectivity analysis, as it preserves only the high-fidelity connections within connectomes and effectively filters out noise. Though the Fisher transformation with z-scoring helps to align the sample distributions of connectivity values between longer and shorter segments, we still observed the effects of segment length when thresholding on z-scores alone—connectomes from shorter segments were denser (i.e., had more edges preserved) after thresholding than connectomes from longer segments. This segment-length discrepancy in connectome density with z-score thresholding had significant downstream effects in our pipeline, as we found the resultant FC state clusters were highly correlated with segment length. To avoid these segment length effects, we fix the density of all connectomes by thresholding to the top-K connections (or edges) in each connectome. Recent work has suggested that such rank-based schemes are optimal for reliability and reproducibility in FC analyses (Bridgeford et al., 2020). Here, we set top-K = 10,000, which preserves the strongest (i.e., highest magnitude) 27.95% edges, thereby providing sufficient noise reduction.

3.3.2.3 State Clustering

The final step of our TVFC framework involves using k-means clustering to separate all thresholded connectomes into a discrete set of k connectivity states. This state clustering occurs on the

aggregated set of *m* connectomes, where *m* is the total number of time segments across all subjects in a single fMRI scanning session (Table 3.1). In traditional TVFC streams, this approach involves performing *k*-means clustering on the flattened upper triangular of all *m* connectomes, however we found poor performance with this method, likely due to the high dimensionality of the flattened connectomes (>35,000) (Supplementary Table 3.1). We address this issue of high dimensionality by generating low-dimensional latent representations of each thresholded connectivity matrix that sufficiently summarize the connectivity patterns within the time segment. Specifically, we utilize state-of-the-art graph embedding methods, which are commonly used in the field of data mining to generate low-dimensional representations of graphs (i.e., networks) (Rossi et al., 2020). Connectomes are graphs by definition, consisting of a set of nodes (ROIs) connected by edges (z-scored correlations), so graph mining methods naturally extend to the connectome space. To generate our graph embeddings, we first apply GraphWave (Donnat et al., 2018) on the top-*K*-thresholded connectomes to produce a set of *d*-dimensional *node embeddings* for each of the *n* ROIs per connectome. GraphWave learns structural node embeddings, which individually capture the structural role of each node (ROI) within its local network neighborhood and in aggregate provide insights into the topological organization of the connectome graph. We then utilize principal components analysis (PCA) to summarize the set of *n d*-dimensional *node embeddings*, concatenated into one long node embedding vector of length *n*d*, into a single *graph embedding* vector by extracting the top 100 principal components (PCs). Aggregating these connectome graph embeddings across all time segments from all subjects results in a feature matrix of size $m \times 100$.

We performed *k*-means clustering on the resultant group-level feature matrix, varying the number of clusters *k* in the range [2-10]. To determine the optimal number of clusters we utilized the elbow criterion of the cluster validity index, computed as the ratio of within-cluster distance to between-cluster distance (Allen et al., 2014). We mapped corresponding clusters across the session replicates to a single overall state based on shortest Euclidean distances between the cluster centroid connectomes. Reproducibility of FC state clusters was tested across scanning sessions (two sessions for WM task, four sessions for resting state). Test-retest reliability was calculated across scanning sessions between centroid connectomes of corresponding states using the image intra-class correlation (I2C2) (Shou et al., 2013). I2C2 is the generalization of the intra-class correlation (ICC) coefficient to high-dimensional multivariate data, such as images (or in our case, connectomes). As a brief description, let $X_i(c)$ be the true, unknown connectome for state i and $W_{ij}(c)$ be the estimated connectome for state i during session j at connectome edge c. The classical measurement error model for the connectome images across replication studies can then be written as

$$W_{ij}(c) = X_i(c) + U_{ij}(c) \tag{3.4}$$

where connectomes are represented as $C \times 1$ vectors; $\boldsymbol{W}_{ij} = \{W_{ij}(c) : c = 1, ..., C\}$ are the observed connectomes; $\boldsymbol{X}_i = \{X_i(c) : c = 1, ..., C\}$ are the true connectomes, and $\boldsymbol{U}_{ij} = \{U_{ij}(c) : c = 1, ..., C\}$ are the measurement error of the connectomes. In this framework, $i = 1, ..., I$, where I = total states = 5, and $j = 1, ..., J_i$, where J_i = total sessions = 4. Connected to the classical measurement error model above and analogous to the standard ICC formulation, the I2C2 is defined as

$$I2C2 = \frac{trace(K_X)}{trace(K_W)} = \frac{trace(K_W) - trace(K_U)}{trace(K_W)} = 1 - \frac{trace(K_U)}{trace(K_W)} \quad (3.5)$$

Where $K_U = \text{cov}(\boldsymbol{U}_{ij}, \boldsymbol{U}_{ij})$, $K_X = \text{cov}(\boldsymbol{X}_i, \boldsymbol{X}_i)$, and $K_W = \text{cov}(\boldsymbol{W}_{ij}, \boldsymbol{W}_{ij})$, and both K_U and K_X cannot be estimated directly since U_{ij} and X_i are unobserved. Therefore, the I2C2 is computed using the following method of moments estimators:

$$\widehat{trace(K_U)} = \frac{1}{\sum_{i=1}^{I} (J_i - 1)} \sum_{i=1}^{I} \sum_{j=1}^{J_i} \sum_{c=1}^{C} \{W_{ij}(c) - \underline{W_{i\cdot}}(c)\}^2 \quad (3.6)$$

$$\widehat{trace(K_W)} = \frac{1}{\sum_{i=1}^{I} (J_i - 1)} \sum_{i=1}^{I} \sum_{j=1}^{J_i} \sum_{c=1}^{C} \{W_{ij}(c) - \underline{W_{\cdot\cdot}}(c)\}^2 \quad (3.7)$$

Where $\underline{W_{i\cdot}}(c) = \frac{\sum_{j=1}^{J_i} W_{ij(c)}}{J_i}$ is the average connectome for state i over all sessions j, and $\underline{W_{\cdot\cdot}}(c) = \frac{\sum_{i,j,c} W_{ij(c)}}{IJ}$ is the average connectome across all states and sessions. Utilizing these estimators, I2C2 metrics were computed in R using the package provided by the authors in Neuroconductor (https://rdrr.io/github/neuroconductor/I2C2/man/I2C2.html). We further characterize the resultant connectivity states with standard TVFC features including average dwell time and state-to-state transition probabilities and go on to correlate these TVFC features with neurophenotypes of interest.

3.3.3 Evaluation against ground truth

As described in Section 3.3.1.1, the WM task consists of four repeating task/rest blocks, where each block is structured as follows: 27.5s Task 1 (0-back), 27.5s Task 2 (2-back), 15s rest. This repeating task/rest block structure of the WM Task data serves as a natural ground truth for validation of our framework: if activation changes can truly be used as markers for connectivity changes, then one should

be able to show that the discovered activation-informed change points align well with true onsets of WM task conditions. In fMRI data, signals are expected to be observed shortly after the stimulus, rather than directly aligned to the stimulus onset, due to lag in the hemodynamic response. Furthermore, the nature of block-design tasks results in sustained task-related activation changes rather than instantaneous spikes and subjects may require an additional 1-2s after the condition onset to fully enter the task state and experience the full effects of the task-induced activation response. Based on this, we defined a state change response window of 12 TR (8.6s) to account for the hemodynamic response time of 10 TR (7.2s) as well as an additional buffer of 2 TR (1.4s) for subjects to fully enter the task condition state. All peaks identified in the GTD series were labeled as either true positives or false positives based on whether they fell within the state change response window following a known task condition transition or not. Based on these labels, we calculate the overall precision and recall of our activation-informed change point detection, as well as the recall for transitions into each of the three task conditions (Task 1, Task 2, and Rest).

3.3.4 Comparison to Sliding Window

While the sliding window framework has been widely used to estimate dynamic FC states in resting fMRI where ground truth state changes cannot be known, it has not, to the best of our knowledge, been validated against a block-design task structure where the ground truth state changes are in fact known. To enable a direct comparison with the performance of our activation-informed segmentation method we applied the sliding window framework to the WM task data using the Group ICA of fMRI toolbox (GIFT) (https://trendscenter.org/software/gift/; Center for Translational

Research in Neuroimaging and Data Science, Atlanta, Georgia) implementation, following the parameterization detailed in (Allen et al., 2014) as closely as possible. Specifically, we first performed group-level spatial independent component analysis (gICA) (Calhoun et al., 2001) to extract 50 independent components (ICs). IC time series then underwent a standard post-processing procedure to remove low-frequency trends associated with scanner drift, motion related variance and any other non-specific "spikes" or possible noise artifacts. Next, we utilized the dFNC function in the GIFT toolbox to perform the sliding window analysis. As in (Allen et al., 2014), we use a tapered window created by convolving a rectangle (window size = 44 seconds/61 TR) with a Gaussian (σ = 3 TR) and sliding in steps of 1 TR, resulting in 344 total windows per WM fMRI session, and a total of 317,168 windows across all 922 subjects for each WM Session 1 and Session 2. Finally, the upper triangular of the windowed connectomes were used as feature vectors of length $(50 \times (49))/2 = 1225$, and *k*-means clustering was applied to separate all windows into a set of *k* states. We utilized the 'estimate_clusters' option in the GIFT toolbox to identify the optimal value of *k* from the range of 2-10. Further details regarding the implementation of the GIFT toolbox steps can be found in the software manual (https://trendscenter.org/trends/software/gift/docs/v4.0b_gica_manual.pdf). To evaluate the accuracy of the resultant sliding window state clustering and compare against that of our proposed method, we implemented the common design choice of setting the ground truth label (i.e., "task" or "rest") for each window as the label assigned to the time point at the center of the window, in this case timepoint 31.

3.4 Results

3.4.1. The GTD Method Accurately Identified Known Transitions During a Working Memory Task

Results of GTD-based peak discovery in WM task data are shown in Figure 3.3. The distribution of the discovered GTD peaks across all subjects showed a concentration of peaks immediately after a new condition onset (Figure 3.3B). In fMRI data, signals are expected to be observed shortly after the stimulus, rather than directly aligned to the stimulus onset, due to lag in the hemodynamic response. Using the true positive and false positive labels detailed earlier in Section 2.4, we found an average precision of 0.72 and average recall of 0.66 of all discovered change points against ground truth state transitions (Table 3.2). We found that Task 1 and Rest state onsets were more readily identifiable by our method than Task 2 onsets (Recall 0.67, 0.75, 0.57 respectively), indicating that transitions from task state to rest state and vice-versa elicit more significant changes in moment-to-moment activations than transitions from an easier 0-back WM task (Task 1) to a more difficult 2-back WM task (Task 2).

We found the optimal number of clusters $k = 3$ for both WM Session 1 and WM Session 2. Figure 3.3A illustrates the alignment of our segments, colored by their respective clusters, to the ground truth WM task conditions. Overall, we found good segregation between task and rest conditions, with improved accuracy in later block repetitions. As observed with the change point detection, the separation between Task 1 and Task 2 conditions is more difficult, owing both to the similarity in connectivity between the two working memory task conditions and to the lack of change point

detection at Task 2 onset points resulting in segments that span the time frame of both Task 1 and Task 2. Homogeneity and normalized mutual information (NMI) metrics of our discovered clusters compared to the known ground truth are reported in Table 3.2. As our temporal segments may not directly align to the ground truth task blocks, we derived ground truth labels for each discovered segment based on the corresponding task condition throughout the majority of the segment.

3.4.2. In the Working Memory Task, Activation-informed Segmentation Performance Was Superior to Sliding Window

We report the results of the GIFT toolbox sliding window pipeline for k = 5 states, which was estimated as the optimal k using the automated cluster estimation available in the GIFT toolbox. (Table 3.2). Though the sliding window approach does capture some repeating task versus rest signal (Figure 3.4), we found the GIFT sliding window approach had significantly decreased performance in segregating between known task and rest condition windows compared to our activation-informed segmentation approach (homogeneity = 0.037 vs. 0.280, respectively). Based on these results, we can conclude that our method more effectively and efficiently summarized the FC in each time segment, resulting in a 99.8% reduction in size of the final feature set passed to k-means compared to that of the sliding window approach (8740×100 vs. $317{,}168 \times 1225$ in WM Session 1). Furthermore, our method proved to be much more computationally efficient than the sliding window approach, completing in < 2 hours for all subjects in a single WM session while the GIFT toolbox required > 24 hours to complete the requisite ICA and dFNC steps for the same data. Considering together the accuracy, data reduction and the runtime, we found our activation-informed segmentation method to

outperform the traditional sliding window paradigm in recovering dynamics in the context of a block-design ground truth.

3.4.3. The Activation-informed Segmentation Method Identified Five Connectivity States During Rest

We applied our activation-informed segmentation pipeline separately on four sessions of resting state fMRI data. Using the elbow criterion of the cluster validity index, we consistently found the optimal number of clusters $k = 5$ across the four sessions (Figure 3.5). Though our state clusters were derived using the graph embedding vectors as described above, we characterized the connectivity of each discovered cluster using the more interpretable top-K thresholded connectomes derived upstream in our pipeline for all segments in each cluster. We mapped corresponding clusters across the four session replicates to a single overall "dynamic state" based on shortest Euclidean distances between the cluster centroid connectomes and found that each centroid was mapped only to one overall state by this criterion, indicating each state did indeed exhibit a unique connectivity signature.

3.4.4. Connectivity States During Rest Exhibit Excellent Test-Retest Reliability

To assess the stability of these clusters we use the I2C2 metric, which was developed to assess the reliability of MRI images for a set of subjects across several image acquisition sessions. The I2C2 metric is a high-dimensional multivariate generalization of the intra-class correlation coefficient for use on images and other multi-dimensional data, such as connectomes (Shou et al., 2013). A brief description of I2C2 and its application in our case can be found in Section 3.3.2.3 above. We found very

high replicability of our states across the four sessions (I2C2 = 0.96), suggesting that the dynamic states recovered by our method are indeed persistent across subjects and time, and may also be cognitively meaningful.

3.4.5. Activation Peaks Observed During Rest Closely Resemble Peaks Found When Transitioning In and Out of Cognitively Demanding Task States

We found that the magnitude of the GTD peaks that correspond to our discovered FC change points and define our dynamic states in rest are of the same order and mirror the distribution of the peaks found in the WM task setting (Kullback-Leibler divergence = 0.030) (Figure 3.6). This indicates that the changes in functional brain activity between dynamic states in rest are as strong as those observed when transitioning in and out of a cognitively demanding task state.

3.4.6. Connectivity States Involve Brain-Wide Connectivity Patterns and Prominently Involve Prefrontal/Sensory-Motor Coupling

We further characterized the overall connectivity signature of each resultant dynamic state by averaging the corresponding cluster centroids across the four sessions. This signature connectome for each of the five overall dynamic states is presented in Figure 3.7. Overall, we observed states that reflect shifting connectivity across network modules, rather than within network modules, consistent with prior work (Betzel et al., 2016; Zalesky et al., 2014). In particular, we observed changing patterns of brain integration and segregation, prominently involving the frontoparietal network and the default mode network (Zalesky et al., 2014). States 1, 3, and 5 all involve sensory/motor anti-correlation with the

frontoparietal network and default mode network. State 1 encompassed all sensory and motor networks, while state 3 had greater visual network specificity and state 5 had greater motor specificity. State 2 was characterized by anticorrelation between frontoparietal and medial frontal network, without sensory/motor involvement. State 4 exhibited none of the above motifs — just the within network connectivity that was common to all of the states. Importantly, the five states we observed are highly similar to the states identified in this same HCP dataset using the classic sliding window paradigm as reported in (Nomi et al., 2017).

3.4.7. Resting Connectivity States Exhibit Complex Patterns of Transitioning

In addition to summarizing each dynamic state by its unique connectivity patterns, we also extracted common TVFC features including state-to-state transition probabilities, average dwell times per state, and number of occurrences of each state across the four resting sessions. We extracted these TVFC features on a per-subject basis and then averaged them to capture the general patterns for all five dynamic states at the group level. The average state-to-state transition matrix, average dwell times, and average number of occurrences per state across all subjects are depicted in Figure 3.8. Overall, we found the highest probabilities of transitioning into state 4 from any of the other states. Interestingly, state 4 also exhibits the shortest dwell time of all five states, averaging a duration of 29.8 ± 2.5s, as well as the highest average number of occurrences. This coupled with the lower overall connectivity observed in state 4 suggests that this may represent a "buffer" state between the other dynamic states.

3.4.8. Resting Connectivity States are Predictive of Behavioral Phenotypes Including Cognition, Personality, and Psychopathology

We performed a regression analysis to assess the combined relationship between subject-specific TVFC feature vectors, averaged across the four resting state sessions, and several neuro-relevant phenotypes. Specifically, we consider ten cognitive metrics: a general factor of intelligence (G; generated from a bifactor model as described in (Sripada et al., 2020)), processing speed (generated from factor modeling of three NIH Toolbox tasks as described in (Sripada et al., 2019)), the five facets of personality given by the Revised NEO Personality Inventory (openness to experience, conscientiousness, extraversion, agreeableness, and neuroticism), and the three dimensions of psychopathology given by the Adult Self Report Scale (Internalizing, Attention Problems, Externalizing). We also included the covariates of age and gender. All features (besides the binary gender marker) were z-scored prior to the regression analysis, so the resultant model β values could be interpreted similarly to correlation values. At a Bonferroni-corrected $\alpha = 0.005$ significance threshold, we found significant relationships between our TVFC features and four phenotypes (G, externalizing behavior, agreeableness, and conscientiousness). Significant regression results are reported in Table 3.3.

3.4.9. Resting Connectivity States are Unrelated to Head Motion

Head motion is a serious confound in studies of functional connectivity (Power et al., 2012, 2015; Satterthwaite et al., 2012; Van Dijk et al., 2012). Moreover, it has recently been argued that head motion may in fact generate the time varying connectivity observed with sliding window methods (Laumann et al., 2017). We thus sought to determine whether the connectivity states we detected at rest

with the GTD method were related to head motion. We found no significant correlation between the mean framewise displacement time series and the GTD series in all four resting state sessions (r = -0.0027; 95% CI = [-0.006, 0.0007]). We report all time-lagged cross-correlations for ± 10TR in each of the four resting state sessions in Supplementary Table 3.2. This lack of correlation between framewise displacement and the GTD series suggests that there is no significant contribution of head motion to our discovered change points, and thereby our final dynamic states in rest. Taken together, these results strongly support the general existence of dynamicity in the resting state and the reliability of the states discovered by our activation-informed framework.

3.5 Discussion

In this work, we introduce a new data-driven approach for assessing dynamic functional connectivity through informed time series segmentation. Our method, termed the activation-informed segmentation method, aims to derive FC states without the limitations of a predefined time scale for the dynamics or highly overlapped sliding windows. This framework is built upon the theory that changes in functional connectivity are mirrored by changes in functional activation. We validated our activation-informed segmentation method in a working memory task setting where ground truth transitions between cognitive states are known. In this validation experiment we found that our method accurately marked known task boundaries, correctly recovered three connectivity states, and displayed a precision and recall profile that compared favorably to a leading sliding window approach. When applying the method to resting state data, we detected five connectivity states that displayed excellent test-retest reliability across four sessions of resting fMRI, exhibited complex transition dynamics, were correlated

with multiple behavioral phenotypes, and were essentially unrelated to head motion. Our work expands the methodological toolkit for quantifying and characterizing time-varying connectivity and provides some of the strongest evidence to date for the existence of distinct dynamic states during rest.

We assessed the activation-informed segmentation method and sliding window approach head-to-head on a block-design working memory task to test whether these methods detect connectivity state changes where ground truth is known. Laumann et al. performed a test of the opposite issue: They examined a task with extended blocks where connectivity is assumed to be stable and found sliding window methods inappropriately found changing connectivity states where such changes are assumed to be absent (Laumann et al., 2017). In our test, the activation-informed segmentation method performed well. We observed an average precision of 0.72, meaning that 72% of activation changes detected by our algorithm corresponded to true changes in functional connectivity. Furthermore, the recall of true state transition points by our method averaged 0.66 and reached as high as 0.77 depending on the strength of the functional connectivity changes, indicating that a majority of known connectivity transitions are indeed marked by changes in global functional activation. In contrast, the GIFT sliding window method precludes the calculation of such precision and recall statistics due to the highly overlapping nature of the resultant windows. When considering the accuracy of the final state clustering, our method indeed performed ~75% better than the sliding window method in separating blocks of true task from true rest. As far as we know, this is the first such test of the sliding window method in task data where ground truth is known. The fact that the sliding window has only fair

accuracy in finding changes in connectivity state suggests there is room for improvement and reinforces our claim that further methods innovation in the study of time varying FC would be beneficial.

The activation-informed segmentation method found five states at rest and these states showed excellent test-retest reliability. These states appear to be broadly consistent with those reported in the previous literature in terms of number of states as well as connectivity patterns (Nomi et al., 2017). Furthermore, the mean dwell times are similar in duration. We also found these states are linked to a number of behavioral phenotypes – with the magnitudes of relationships similar to those reported in prior studies (Nomi et al., 2017). Taken together, these results suggest that there is some continuity in our results with the results from sliding window approaches. Nonetheless, some key differences remain. First, the states identified here have much higher test-retest reliability. Second, the method to identify them is intuitive, computationally efficient, and appears not to be driven by artifactual causes (e.g., head motion).

A key assumption of our method is that activation changes can serve as a marker of changes in connectivity states. Several lines of evidence support this assumption. First, there is a substantial set of studies (discussed in the Introduction) that document connectivity patterns that arise during distinct task conditions. Importantly, these task conditions are antecedently known to produce distinct distributed activation profiles so that transitions into the relevant task conditions would produce activation shifts. Second, in the present study, we observed GTD peaks during the N-back working memory task when subjects shift task conditions, and we observed distinct connectivity states in the segments flanked by these GTD peaks. Third, if our main assumption were false, that is, if activation

shifts *fail to* mark changes in connectivity states, then we should not have found large activation shifts during rest that are associated with distinct, highly test-retest reliable connectivity states. The fact that we did observe these results from rest provides further support that there is in fact a link between activation shifts and connectivity state changes. Finally, as we noted in the previous paragraph, the states identified have similarities along multiple dimensions with states identified through traditional sliding window methods. If our activation-informed segmentation approach can find connectivity states that are broadly similar to those found by sliding window approaches, this can only be explained if activation changes do indeed serve as a marker of connectivity changes.

In a somewhat unexpected finding, we observed GTD peaks during rest (corresponding to state change points) that were similar in magnitude to those seen during a working memory task. This finding is notable because the N-back working memory task is highly cognitively demanding and produces vigorous activations across a distributed "task-positive network" (Cabeza & Nyberg, 2000; Cole & Schneider, 2007; Mazoyer et al., 2001; Niendam et al., 2012). Rest, in contrast, is assumed to be a state of substantially reduced cognitive demands (Andrews-Hanna et al., 2010; Buckner et al., 2008; McKiernan et al., 2003). It is thus remarkable that we observed GTD peaks during the resting state on par with those that occur in response to transitions in and out of a cognitively demanding task. The fact that resting GTD peaks are so large provides additional support for our framework, which is based on the idea that easy-to-detect GTD peaks can be leveraged to identify hard-to-detect changes in connectivity states—large GTD peaks are particularly easy to detect. But critically, large GTD peaks during rest should be of independent interest to the field. That is, irrespective of their link to changes in

connectivity states (which has been our focus in this study), the fact that there are regular and robust GTD peaks during rest is itself a phenomenon that needs follow up investigation and explanation.

There has been some skepticism in the field about the reality of time varying connectivity. A sizable portion of this debate centers on the sliding window methodology for demonstrating varying connectivity states (Laumann et al., 2017; Lindquist et al., 2014a). It is claimed that this method generates artifacts, finds changes where none exist, etc. An important advance of the present study is that it demonstrates time-varying FC during rest without reliance on sliding window methods. Moreover, the associated connectivity states exhibit excellent test-retest reliability. Therefore, we believe that the present study offers some of the strongest evidence to date for the reality of time-varying connectivity at rest. More specifically, we suggest that the state transition points identified by our framework actually represent a lower bound of the "true" dynamic state changes in rest. This is because there is likely only an imperfect relationship between activation shifts and connectivity state changes: the former may be sufficient but not necessary for the latter. Thus, there may be at least some connectivity state changes that are not preceded by prominent (and thus easy-to-detect) GTD peaks, and our method will fail to detect the presence of such connectivity states. One such example is the transition between Task 1 and Task 2 conditions in the WM task experiment, in which we observed lower recall for the GTD peak detection at these points, indicating these particular connectivity state changes are more subtle and nuanced than transitions from rest to task states and do not result in strong whole brain activation changes. Future work should seek to extend the change point detection scheme developed here to enable identification of these "connectivity-only" transitions. Such a method could

be formulated as an extension of existing instantaneous connectivity estimation methodologies (i.e., MTD, ECF, DCC), aimed at identifying significant moment-to-moment changes in multivariate connectivity rather than univariate activation. It is also possible these requirements can be fulfilled through the use of deep learning approaches, specifically recurrent neural network architectures, which are designed to learn complex, non-linear patterns in multivariate time series data (H. Li & Fan, 2018).

This study has several limitations. First, we rely on a key assumption that activation shifts, more specifically those activation shifts that are strong enough to be observed at the whole-brain scale, can serve as a marker for changes in connectivity states. We acknowledge that the relationship is likely imperfect, and our method may underestimate the true number of states. The strength of our method, nonetheless, is simplicity and transparency, enabling the method to yield notably strong evidence for dynamic states at rest. Second, our peak detection scheme is reliant on several empirically tuned parameters as well as an exponentially weighted moving average operation that may be subject to similar criticism as the sliding window Pearson correlation approach. However, it is important to note that the identification of local maxima in a univariate signal (i.e., GTD) is not as sensitive to window size as computation of multivariate cross-correlations - the strongest peaks will survive across a variety of moving average window lengths. Additionally, we note that there are methods available for peak detection that do not rely on moving averages that can be substituted into our pipeline, and future work can explore these approaches. Third, unlike sliding window methods that impose a uniform length on windowed connectivity matrices, the activation-informed segmentation method is sensitive to the duration of states. We mitigated this in multiple ways, including Fisher transformation and z-scoring of

Pearson correlation-based connectivity matrices, as well as employing a top-*K* thresholding to control connectome density across both short and long segment lengths. Fourth, the meaning and importance of the dynamic states uncovered by the GTD method is unclear. We showed activation shifts are large (comparable to transitions in and out of a working memory task). We also presented initial data that connectivity states are linked to phenotypes of interest. But additional work is needed to establish what psychological processes are reflected in these time-varying states, and whether quantifying these transient states will yield significant theoretical and practical insights in psychology and neuroscience.

In sum, we introduce here a novel method for identifying dynamic states in fMRI that generates data-driven segments of stable FC, validate the method in task data where ground truth is known, and demonstrate that the method finds strong evidence--likely among the strongest to date--for the presence of dynamic states at rest.

3.6 Figures and Tables

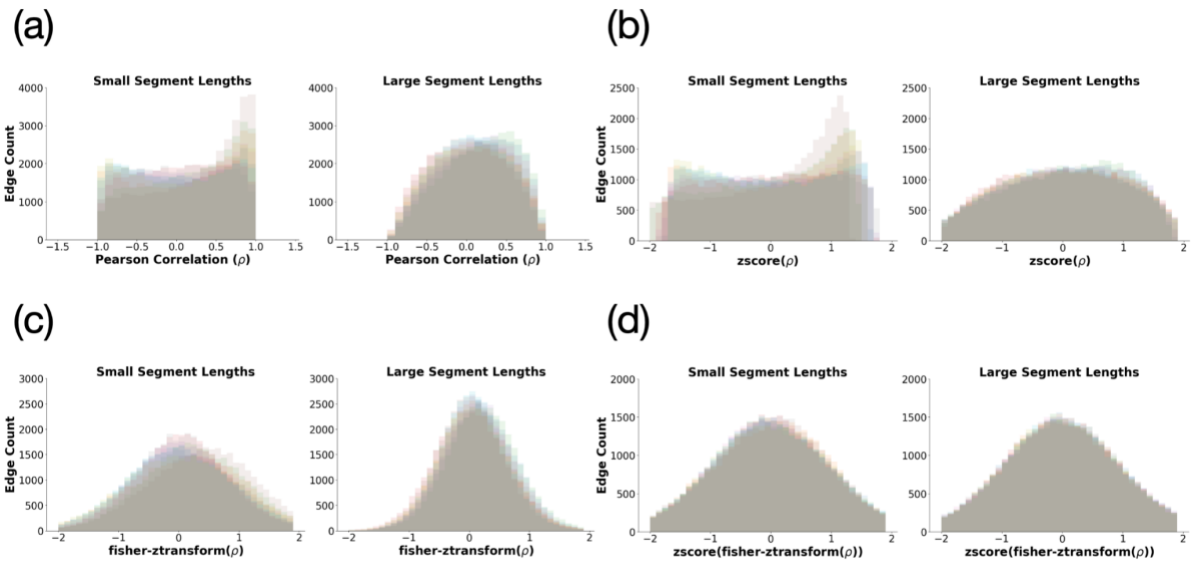

Figure 3.2. Preprocessing Effects.
Effects of (A) no transformation, (B) z-score transformation, (C) Fisher transformation and (D) z-scored(Fisher) transformation on the distribution of Pearson correlation-based connectivity values in short (< 25 TR) and long (> 35 TR) segments.

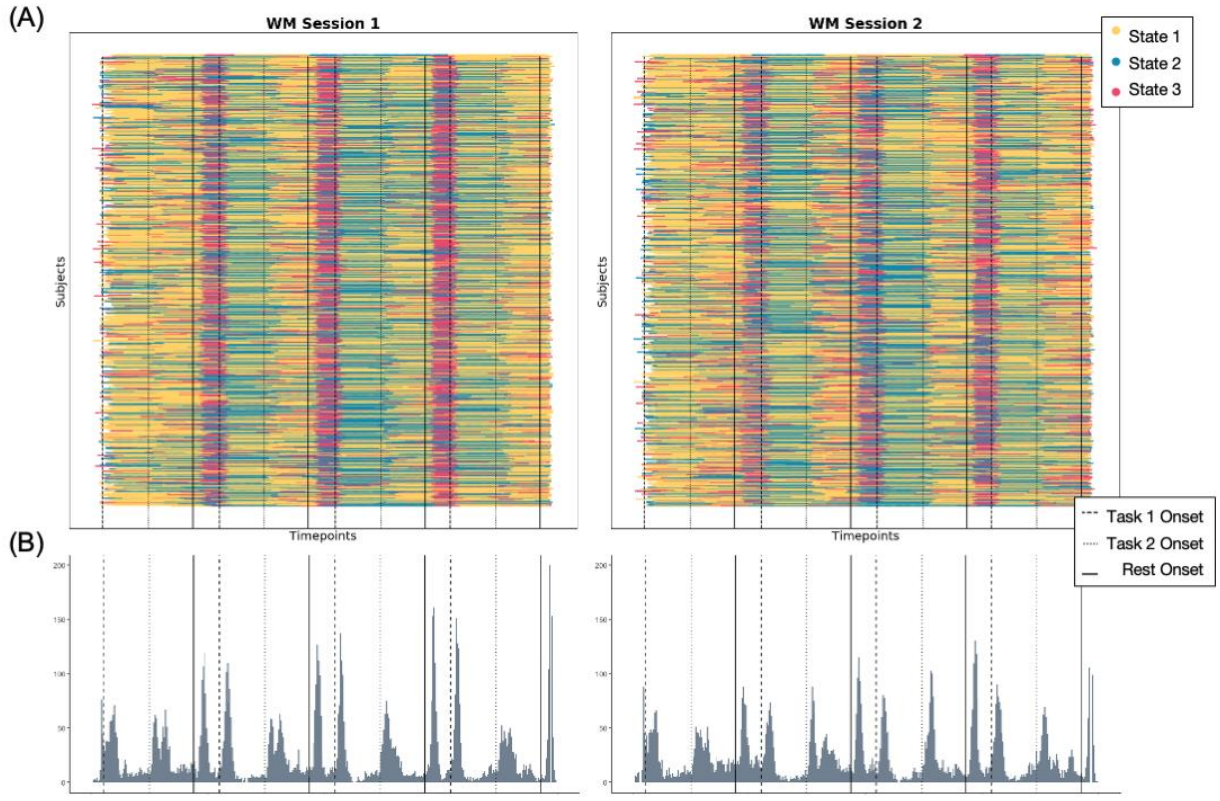

Figure 3.3. Results of the activation-informed segmentation for all subjects in structured WM task data.
(A) Temporal alignment of our discovered segments colored by their corresponding state labels given by *k*-means clustering shows good alignment to known ground truth conditions (onsets marked by vertical lines: dashed for Task 1 onset, dotted for Task 2 onset, solid for Rest onset). (B) Histogram of discovered GTD peak locations show strong alignment to known condition onsets.

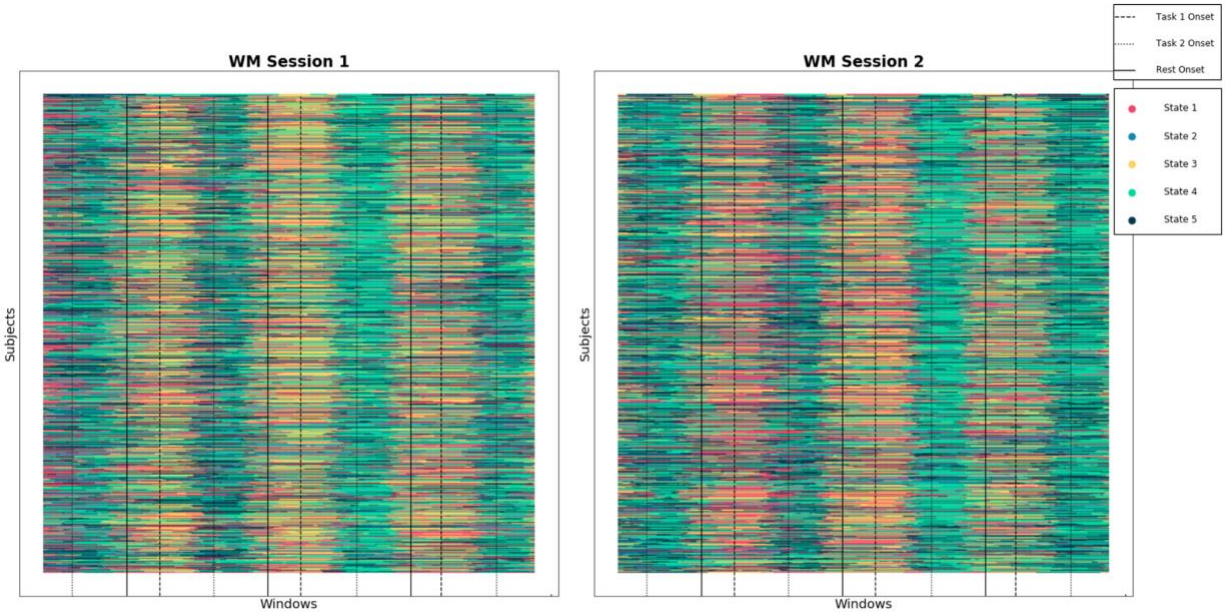

Figure 3.4: Results of GIFT toolbox-based sliding window framework for all subjects in structured WM task data.

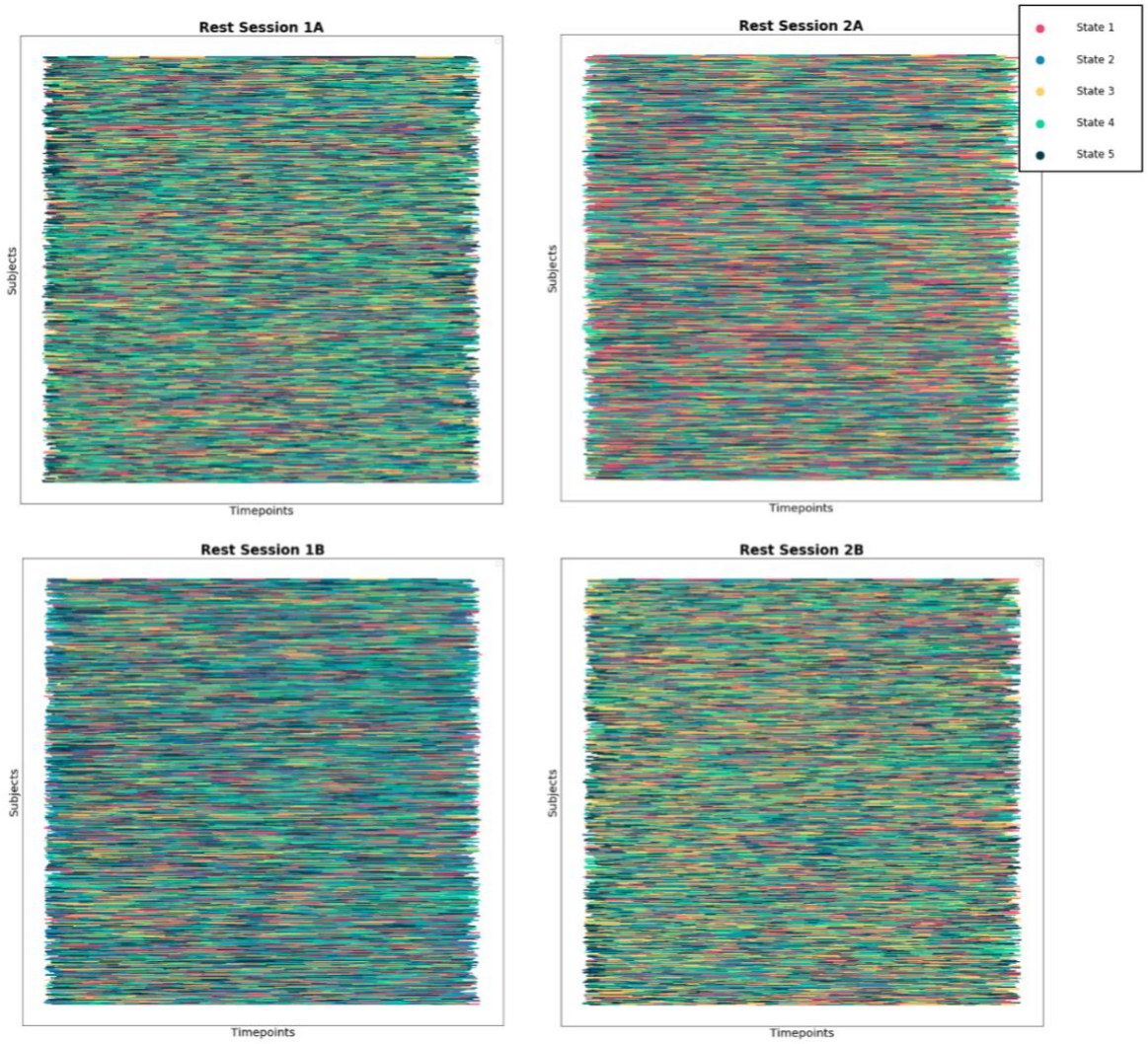

Figure 3.5: Temporal alignment of activation-informed segments and their corresponding state labels given by k-means in all four resting state fMRI sessions.

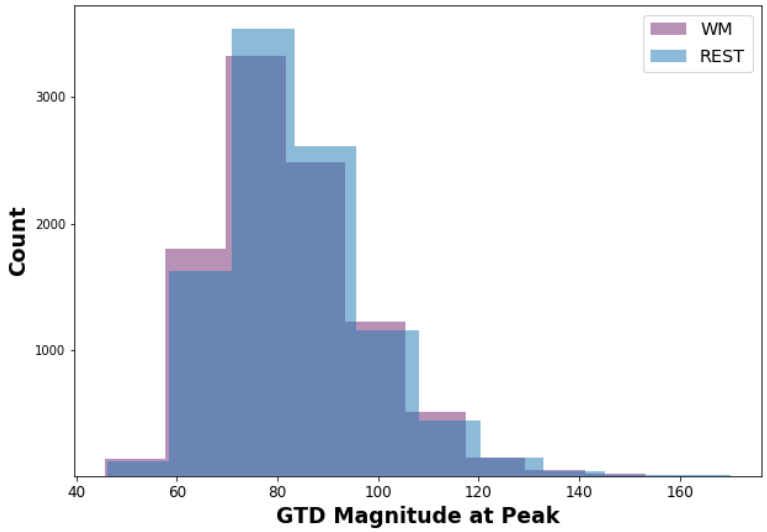

Figure 3.6. Histograms of GTD magnitudes at discovered peaks for 9700 change points in WM Session 1 and a size-matched random sample of change points in Rest Session 1A show similar distributions (Kullback-Leibler divergence = 0.030).

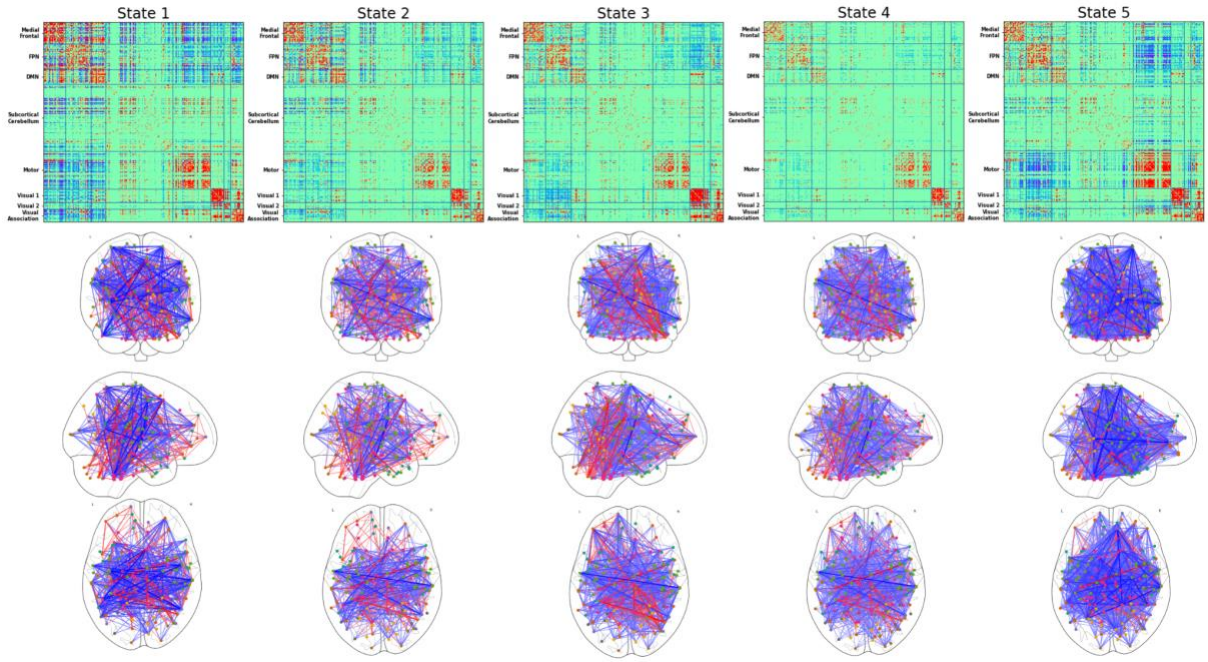

Figure 3.7. Connectivity signatures for each of the five discovered resting FC states.
Connectivity signatures are defined by the centroid (i.e., average) of all connectomes belonging to each state cluster. Glass brain views show the top 0.5% of connections (360 edges) for each state.

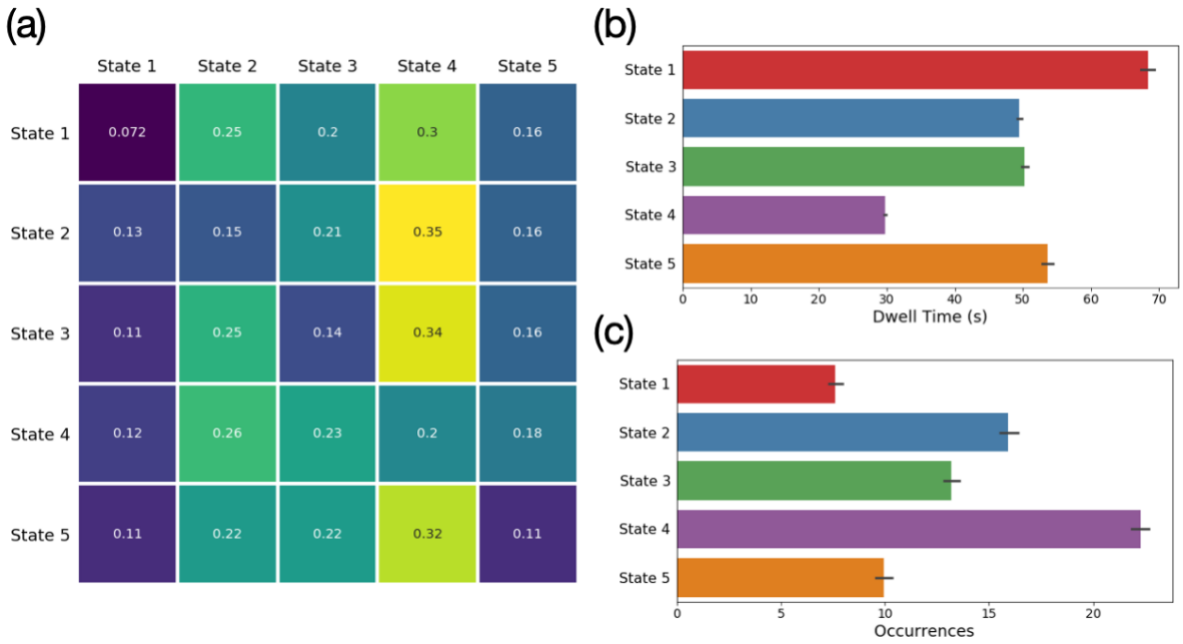

Figure 3.8. Group average TVFC features.
Average transition probabilities of moving from State A (along rows) to State B (along columns) (A), dwell times (B), and number of occurrences (C) across all subjects and resting state fMRI sessions.

Symbol	Meaning	Value
FC	Functional connectivity	-
TVFC	Time-varying functional connectivity	-
WM	Working memory	-
ROI	Region of interest	-
GTD	Global temporal derivative	-
N	Number of subjects	N = 922
n	Number of ROIs	$n = 268$
dt	Temporal derivative	-
ts_i	Time series of ROI i	-
T	Length of time series	$T_{WM} = 405, T_{REST} = 1200$
t	Time point t	-
s, S	Time segment s and total number of segments S, respectively	-
$C^{(s)}$	Functional connectivity matrix for time segment s	-
$ts_i\ (s)$	Time series of ROI i in time segment s	-
K	Number of edges retained in top-K thresholding	$K = 10{,}000$
k	Number of clusters in k-means clustering	$k = (2 - 10)$
m	Total number of time segments/connectomes across all subjects in a single fMRI scanning session	$m_{WM1} = 8740, m_{WM2} = 9052$ $m_{REST1A} = 16{,}104, m_{REST1B} = 16{,}015$ $m_{REST2A} = 15{,}420, m_{REST2B} = 16{,}062$
d	Dimensionality of graph embedding	$d = 100$

Table 3.1. Symbols and abbreviations

Pipeline Step	Metric	Activation-Informed Segmentation			Sliding Window		
		WM Session 1	WM Session 2	Avg	WM Session 1	WM Session 2	Avg
Change Point Discovery	Precision	0.74	0.70	0.72	-	-	-
	Recall Task 1 Task 2 Rest	0.67 0.72 0.54 0.77	0.64 0.62 0.59 0.73	0.66 0.67 0.57 0.75	-	-	-
Clustering	Optimal *k*	3	3	3	5	5	5
	Homogeneity	0.327	0.233	0.280	0.037	0.037	0.037
	NMI	0.231	0.159	0.195	0.018	0.018	0.018

Table 3.2. Performance of our activation-informed segmentation method and the standard sliding window method in recovering ground truth dynamic state changes in WM task data.
The change point discovery step is unique to our framework and unable to be reported for the sliding window method.

	Feature	**β coefficient**	**p-value**
Dependent variable = G; Model p-value = 0.000306			
	Gender	0.30	0.000
	State 1 to State 3 Transition Probability	-0.144	0.041
Dependent variable = Externalizing Behavior; Model p-value = 1.56e-05			
	Gender	2.87	0.000
	State 3 to State 1 Transition Probability	-2.57	0.008
	State 3 to State 2 Transition Probability	-3.38	0.008

	Probability of Remaining in State 3	-2.08	0.025
	State 3 to State 4 Transition Probability	-3.45	0.011
	State 3 to State 5 Transition Probability	-3.24	0.004
	State 5 to State 1 Transition Probability	-1.23	0.050
	State 5 to State 3 Transition Probability	-2.01	0.014
	Probability of Remaining in State 5	-1.40	0.010
	Occurrence of State 5	1.20	0.039
	Age	-0.22	0.006
Dependent Variable = Agreeableness; Model p-value = 1.94e-06			
	Gender	-1.91	0.000
	State 1 to State 5 Transition Probability	0.82	0.030
Dependent Variable = Conscientiousness; Model p-value = 0.00127			
	Gender	-1.21	0.003
	Probability of Remaining in State 1	0.66	0.031
	Dwell Time State 5	-0.73	0.005

Table 3.3. Ordinary least squares regression results for significantly predicted phenotypes (Bonferroni-corrected $\alpha = 0.005$).

3.7 Publication and Acknowledgements

This chapter has been revised from a manuscript that is in late-stage review at the journal Human Brain Mapping, and that has been published as a pre-print (Duda et al., 2020). I would like to thank Parmida Davarmanesh, Aman Taxali, Saige Rutherford and Mike Angstadt for their support and valuable feedback throughout this work. I would also like to acknowledge the contributions of my co-authors of the submitted manuscript, Danai Koutra and Chandra Sripada.

This work was supported by funding from the University of Michigan Precision Health Investigator Award. MD was supported by the National Science Foundation Graduate Research Fellowship Program grant DGE-1256260.

3.8 Supplementary Information

Method	**Optimal *k***		**Homogeneity**		**NMI**	
	WM Session 1	*WM Session 2*	*WM Session 1*	*WM Session 2*	*WM Session 1*	*WM Session 2*
Connectome Vectorization	3	3	0.036	0.037	0.025	0.025
PCA Decomposition	3	3	0.033	0.035	0.024	0.024

Supplementary Table 3.1. Clustering performance of traditional FC summarization methods in our activation-informed segments.
Connectome vectorization involves flattening the upper triangular of each connectome into a single vector of length 35,778. To test whether the difference in performance between our structural graph embedding approach and the classic connectome vectorization approach was due to the difference in dimensionality of the feature vectors, we applied PCA decomposition on the set of vectorized connectomes, retained the top 100 PCs to match the final dimensionality of our approach, and applied k-means clustering on this low-dimensional feature set.

Session	Lag	Mean Correlation	95% CI Lower Bound	95% CI Upper Bound
REST1B	-10	-0.0063	-0.0100	-0.0025
REST1B	-9	-0.0089	-0.0127	-0.0052
REST1B	-8	-0.0126	-0.0164	-0.0088
REST1B	-7	-0.0174	-0.0213	-0.0135
REST1B	-6	-0.0221	-0.0262	-0.0181
REST1B	-5	-0.0259	-0.0301	-0.0217
REST1B	-4	-0.0272	-0.0315	-0.0229
REST1B	-3	-0.0260	-0.0304	-0.0216
REST1B	-2	-0.0228	-0.0273	-0.0184
REST1B	-1	-0.0189	-0.0233	-0.0145
REST1B	0	-0.0152	-0.0195	-0.0109
REST1B	1	-0.0133	-0.0176	-0.0090
REST1B	2	-0.0135	-0.0178	-0.0093
REST1B	3	-0.0149	-0.0192	-0.0107
REST1B	4	-0.0160	-0.0202	-0.0118
REST1B	5	-0.0152	-0.0195	-0.0110
REST1B	6	-0.0122	-0.0164	-0.0080
REST1B	7	-0.0071	-0.0112	-0.0029
REST1B	8	-0.0009	-0.0049	0.0031
REST1B	9	0.0050	0.0010	0.0090
REST1B	10	0.0095	0.0054	0.0135
REST1A	-10	0.0039	0.0008	0.0071
REST1A	-9	0.0035	0.0004	0.0067
REST1A	-8	0.0028	-0.0003	0.0060
REST1A	-7	0.0021	-0.0010	0.0052
REST1A	-6	0.0016	-0.0015	0.0047

REST1A	-5	0.0014	-0.0017	0.0045
REST1A	-4	0.0018	-0.0013	0.0050
REST1A	-3	0.0022	-0.0009	0.0053
REST1A	-2	0.0021	-0.0010	0.0052
REST1A	-1	0.0018	-0.0013	0.0049
REST1A	0	0.0016	-0.0015	0.0048
REST1A	1	0.0014	-0.0018	0.0045
REST1A	2	0.0010	-0.0021	0.0041
REST1A	3	0.0008	-0.0023	0.0038
REST1A	4	0.0008	-0.0022	0.0038
REST1A	5	0.0013	-0.0017	0.0043
REST1A	6	0.0020	-0.0010	0.0049
REST1A	7	0.0027	-0.0002	0.0057
REST1A	8	0.0035	0.0006	0.0064
REST1A	9	0.0040	0.0011	0.0069
REST1A	10	0.0042	0.0013	0.0071
REST2B	-10	0.0029	-0.0001	0.0060
REST2B	-9	0.0028	-0.0002	0.0059
REST2B	-8	0.0028	-0.0003	0.0059
REST2B	-7	0.0027	-0.0004	0.0058
REST2B	-6	0.0024	-0.0006	0.0055
REST2B	-5	0.0020	-0.0010	0.0051
REST2B	-4	0.0017	-0.0013	0.0047
REST2B	-3	0.0013	-0.0018	0.0043
REST2B	-2	0.0005	-0.0026	0.0036
REST2B	-1	0.0000	-0.0031	0.0031
REST2B	0	-0.0001	-0.0031	0.0030
REST2B	1	0.0001	-0.0030	0.0031

REST2B	2	0.0001	-0.0030	0.0032
REST2B	3	0.0000	-0.0030	0.0030
REST2B	4	-0.0001	-0.0031	0.0029
REST2B	5	-0.0001	-0.0030	0.0029
REST2B	6	0.0000	-0.0030	0.0029
REST2B	7	0.0002	-0.0028	0.0031
REST2B	8	0.0005	-0.0025	0.0035
REST2B	9	0.0007	-0.0022	0.0037
REST2B	10	0.0007	-0.0022	0.0037
REST2A	-10	0.0009	-0.0021	0.0038
REST2A	-9	0.0009	-0.0021	0.0039
REST2A	-8	0.0013	-0.0017	0.0042
REST2A	-7	0.0015	-0.0014	0.0044
REST2A	-6	0.0018	-0.0011	0.0047
REST2A	-5	0.0019	-0.0010	0.0048
REST2A	-4	0.0020	-0.0009	0.0049
REST2A	-3	0.0021	-0.0009	0.0050
REST2A	-2	0.0020	-0.0010	0.0050
REST2A	-1	0.0022	-0.0008	0.0053
REST2A	0	0.0029	-0.0002	0.0059
REST2A	1	0.0035	0.0004	0.0065
REST2A	2	0.0038	0.0007	0.0068
REST2A	3	0.0040	0.0010	0.0070
REST2A	4	0.0041	0.0011	0.0071
REST2A	5	0.0043	0.0014	0.0073
REST2A	6	0.0046	0.0016	0.0075
REST2A	7	0.0048	0.0019	0.0078
REST2A	8	0.0050	0.0021	0.0080

REST2A	9	0.0050	0.0020	0.0080
REST2A	10	0.0048	0.0018	0.0078

Supplementary Table 3.2. Relation to head motion.
Mean correlation and 95% confidence interval (CI) between GTD and framewise displacement time series at lags ranging from (-10, 10) TR for four sessions of resting state fMRI.

Chapter 4 - Data-Driven Segmentation of Instantaneous Connectivity Estimates Reveals a Highly Stable Set of Time-Varying States in Resting fMRI

4.1 Abstract

As the field of TVFC continues to expand, the methodological toolkit for identifying time-varying changes in resting state connectivity expands with it. One of the most promising classes of TVFC methods are those which generate instantaneous estimates of FC at each timepoint in the BOLD fMRI time series. This class of instantaneous FC estimators include the edge co-fluctuations (ECF), multiplication of temporal derivatives (MTD) and dynamic conditional correlations (DCC) methodologies. Though each of these methods have been independently tested against the baseline sliding window approach, they have not been tested against one another. In this chapter, I conduct a comprehensive comparative analysis between the ECF, MTD and DCC instantaneous FC estimators using block-design working memory task data as a natural ground truth for assessment. I test a variety of post-processing choices to estimate changing connectivity states from the instantaneous FC estimates, including a newly introduced connectivity-informed segmentation framework to derive data driven, non-overlapping segments of stable FC. Overall, the combination of ECF and connectivity-informed segmentation best recovers the original task structure of the working memory fMRI data. When applied in resting state fMRI, this ECF + connectivity-informed segmentation framework

detected five states that were highly stable across four distinct scanning sessions and closely resembled states derived from our previously described activation-informed segmentation approach. The convergence of results across these distinct, yet analogous, methods underscores the significance of the resultant time-varying states and provides further evidence in support of TVFC during rest.

4.2 Introduction

Resting state functional connectivity (rsFC) is defined by the statistical dependence structure (usually computed as Pearson correlation) in the activity of distinct regions of interest (ROIs) throughout the brain, as measured via neuroimaging modalities, most commonly via blood oxygen level dependent (BOLD) functional magnetic resonance imaging (fMRI). Classically, studies of rsFC have focused on static connectivity, which relies on the assumption that the statistical dependence structure in the resting state does not fluctuate as a function of time. While the static view of rsFC has uncovered several compelling associations with individual variations across a variety of phenotypes including cognition, clinical diagnoses and age, recent interest has shifted towards a dynamic or time-varying view of rsFC (Hutchison, Womelsdorf, Allen, et al., 2013; Lurie et al., 2020; Preti et al., 2017).

The prevailing method in the study of time-varying functional connectivity (TVFC) is the sliding window paradigm, wherein connectivity snapshots are extracted from temporal windows of a given size and shape that are iteratively shifted along the entire length of the fMRI time series. While these sliding window approaches have served an important role in providing some of the earliest evidence for the existence of TVFC (Allen et al., 2014; Chang & Glover, 2010; Sakoğlu et al., 2010),

they are accompanied by several important limitations. Paramount among these limitations is the inability of sliding windows to localize changes in FC on a truly moment-to-moment basis—the sliding window operation serves as a low-pass filter, resulting in a blurred and overly-smooth approximation of the changing functional connectivity over time. This temporal blurring poses issues for the interpretability of sliding window connectivity when paired with the common *k*-means clustering approach for FC state estimation. For example: How does one interpret the case where FC estimates from two adjacent windows that necessarily contain ~95% of the same data are clustered into two separate states? Additionally, it has been suggested that the sliding window approach may artificially induce the appearance of changing connectivity, even in time series that are stationary by design (Laumann et al., 2017).

Due to the limitations associated with sliding window TVFC frameworks, there has been increased interest in the development of "windowless" methodologies, especially those capable of estimating instantaneous connectivity. More specifically, instantaneous FC methods estimate an $n \times n$ functional connectivity matrix for each time point in the fMRI time series, where n is the number of ROIs.

The Multiplication of Temporal Derivatives (MTD) method (Shine et al., 2015) was introduced as a way to estimate functional connectivity at a higher temporal resolution than what was available via windowed methods. Intuitively, the magnitude of the MTD metric captures the degree of functional coupling between each pair of ROIs at each time point, whereas the sign captures the direction of the relationship—a positive MTD value indicates functional change in the same direction

(either both increasing or both decreasing in fMRI amplitude), whereas a negative MTD value indicates anti-coupling. The MTD was shown to outperform the standard sliding window method in identifying connectivity changes in both simulated and real-world data (Shine et al., 2015).

Very recently, another approach that is formulaically related to the MTD method has been proposed for estimating instantaneous FC. This approach, here referred to as the edge co-fluctuation (ECF) metric (Esfahlani et al., 2020) (but sometimes referred to as "node functional connectivity" [nFC]), is described as a "temporal unwrapping" of the Pearson correlation coefficient. The formulation of the ECF metric is equivalent to the Pearson correlation across the entire time series without the averaging step, and so it follows that the temporal average of the ECF series is equivalent to the static FC estimated with pairwise Pearson correlation. In this way, each time-resolved connectivity matrix generated by the ECF can be interpreted as an instantaneous component of static Pearson correlation across the full time series. The authors show that the ECF metric shows inter-subject synchrony during a passive movie watching task, indicating the changing FC patterns captured by the ECF metric in this context may be associated with perception and processing of sensory information, and supporting the hypothesis that the ECF can potentially be used to track an individual's changing cognitive state over time, even in the absence of task.

While the MTD and ECF are both non-parametric methods, parametric models are also available for estimating time-varying statistical dependencies between time series, namely those classically used for financial analysis. Of these the most well studied is the dynamic conditional correlation (DCC) model (Engle, 2000), which is a form of a multivariate generalized autoregressive

conditional heteroscedastic (GARCH) model. A general univariate GARCH(p,q) model estimates the conditional variance of a univariate time series at time t as a linear combination of q prior estimates of the conditional variance and p prior values of the time series itself. From the first application of DCC models to estimate TVFC in BOLD fMRI data, the authors report superior performance in identifying the true time-varying correlation structure across several simulated and real-world datasets as compared to the standard sliding window approach (Lindquist et al., 2014b).

While each of these instantaneous FC estimation frameworks seems promising on its own, there has not been any study which compares the performance of the MTD, ECF or DCC methods against one another. Furthermore, though each of these methods has been validated in one way or another, none of these instantaneous FC estimators has been rigorously evaluated against block-design task data, specifically in the context of recovering *structured* changes in functional connectivity that accompany the onsets of alternating cognitive tasks. Here, we provide a comprehensive head-to-head comparison between these three methodologies of instantaneous FC estimation in conjunction with multiple popular approaches for state estimation from FC time series. As part of this comparative analysis, we propose a novel connectivity-informed segmentation framework, an extension of our previous work on the analogous activation-informed segmentation approach (Duda et al., 2020). We evaluate all methodologies against fMRI data collected during a block-design working memory (WM) task, quantify the accuracy of each distinct framework in recovering the original task structure, and go on to apply the best performing framework in rest to decompose the resting state fMRI data into a set of discrete TVFC states.

4.3 Methods

4.3.1 Data Description

4.3.1.1 HCP Data

In this work, we utilize the Human Connectome Project (HCP) S1200 Young Adult dataset made publicly available through the Washington University and the University of Minnesota HCP consortium (http://humanconnectome.org). It is one of the richest collections of neuroimaging data to date, consisting of structural and functional MRI, behavioral assessments, and genotypes for 1200 healthy subjects ages 22-35. A full description of the acquisition protocol can be found in (Van Essen et al., 2013). In short, all HCP fMRI data were acquired on a modified Siemens Skyra 3T scanner using multiband gradient-echo EPI (TR = 720 ms, TE = 33 ms, flip angle = 52°, multiband acceleration factor = 8, 2 mm isotropic voxels, FOV = 208 × 180 mm, 72 slices, alternating RL/LR phase encode direction). In this work, we leverage the repeating task/rest block structure of the working memory (WM) task data available in HCP as a natural ground truth to test the performance of each considered method in identifying the known transitions between the task and rest conditions. The best performing method was then applied in resting state fMRI to extract TVFC states.

The HCP WM task consists of four repeating task/rest blocks, where each block is structured as follows: 27.5 seconds Task 1 (0-back), 27.5 seconds Task 2 (2-back), 15 seconds rest. Using the acquisition details outlined above, each WM task fMRI time series consisted of 405 volumes sampled every 0.72 seconds, for a total acquisition time of 4 minutes and 52 seconds. Two sessions of WM task

fMRI were acquired back-to-back, alternating between RL and LR phase encoding directions. We will refer to these as WM session 1 (RL) and WM session 2 (LR).

Participants completed four total resting state fMRI scanning sessions (two sessions collected on each of two different days). Each resultant resting state fMRI time series consisted of 1200 volumes sampled every 0.72 seconds, for a total acquisition time of 14 minutes and 24 seconds. During the resting state sessions participants were instructed to keep their eyes open and fixated on a cross hair on the screen, while remaining as still as possible. For clarity, we will refer to resting state data from the first collection day as sessions 1A (RL) and 1B (LR), and similarly sessions 2A and 2B for those collected on the second day.

4.3.1.2 Data Preprocessing

Processed volumetric data from the HCP minimal preprocessing pipeline including ICA-FIX denoising were used. Full details of these steps can be found in (Glasser et al., 2013; Salimi-Khorshidi et al., 2014). Briefly, BOLD fMRI data were gradient-nonlinearity distortion corrected, rigidly realigned to adjust for motion, fieldmap corrected, aligned to the structural images, and then registered to MNI space with the nonlinear warping calculated from the structural images. Then FIX was applied on the data to identify and remove motion and other artifacts in the timeseries. These files were used as a baseline for further processing and analysis (e.g. MNINonLinear/Results/rfMRI_REST1_RL/rfMRI_REST1_RL_hp2000_

clean.nii.gz from released HCP data).

Images were smoothed with a 6mm FWHM Gaussian kernel, and then resampled to 3mm isotropic resolution. This step as well as the use of the volumetric data, rather than the surface data, were done to allow comparability with other large datasets in ongoing and planned analyses that are not amenable to surface-based processing. The smoothed images then went through a number of resting state processing steps, including motion artifact removal steps comparable to the type B (i.e., recommended) stream of (Siegel et al., 2017). Further details on motion artifact removal can be found in (Sripada et al., 2019). Lastly, spatially averaged time series were calculated for each of the 268 ROIs from the parcellation given in (Finn et al., 2015).

For our analysis, we first considered the set of 966 subjects listed in (Sripada et al., 2019) that met the following criteria: structural T1 and T2 data, four complete resting state fMRI sessions, and <10% of resting state frames censored due to excessive motion (framewise displacement of 0.5mm). From this set 922 subjects also had two complete WM task fMRI sessions, defining our final subset of subjects.

4.3.2 Instantaneous FC Estimators

The goal of this work was to provide a comprehensive comparative analysis of the three most popular instantaneous functional connectivity estimators that have been proposed in the TVFC literature to date: edge co-fluctuations (ECF), multiplication of temporal derivatives (MTD) and dynamic conditional correlations (DCC). We provide a detailed description of the formulation of each method in the following subsections.

4.3.2.1 Edge Co-fluctuations (ECF)

The ECF metric is described as a "temporal unwrapping" of the Pearson correlation (Esfahlani et al., 2020), which is widely considered the most popular measure of FC. For a pair of ROIs *i,j*, the ECF metric is computed by first z-scoring (i.e. subtracting its mean, μ, and normalizing by its standard deviation, σ) each of the ROI time series (*ts*) and then computing the element-wise product of the two z-scored time series. The t^{th} value in this element-wise product series thereby represents the ECF connectivity estimate between ROIs i and j at time t.

$$ECF_{i,j}(t) = z_i(t) \times z_j(t) \tag{4.1}$$

where $z_i = \frac{ts_i(t)-\mu_i}{\sigma_i}$ and $z_j = \frac{ts_j(t)-\mu_j}{\sigma_j}$.

Repeating this procedure for all pairs of ROIs results in a ECF tensor of dimensions $T \times n \times n$, representing a pairwise estimate of whole brain functional connectivity at each time point in the fMRI time series. To formalize the ECF metric as a "temporal unwrapping" of the Pearson correlation, we can formulate the Pearson correlation as follows:

$$r_{i,j} = \frac{1}{T-1}\sum_t [\, z_i(t) \times z_j(t) \,] = \frac{1}{T-1}\sum_t [\, ECF_{i,j}(t) \,] \tag{4.2}$$

Based on this formulation, ECF can be interpreted as a calculation of the Pearson correlation that omits the averaging step, essentially preserving the frame-wise components of FC that define the overall static measure of FC between two regions.

4.3.2.2 Multiplication of Temporal Derivatives (MTD)

The MTD metric is another method developed for estimation of functional connectivity at any given time point within an fMRI time series (Shine et al., 2015). Briefly, the MTD is computed by first calculating the temporal derivative (*dt*) of each of *n* ROI time series (*ts*) using first-order differencing.

$$dt_i(t) = ts_i(t) - ts_i(t-1) \tag{4.3}$$

Each temporal derivative series *dt* is then normalized by dividing the entire time course by its standard deviation (σ). Next, at each time point *t* the connectivity between each pair of ROIs *i,j* is defined as the product of their corresponding temporal derivative series (dt_i, dt_j) at time point *t*:

$$MTD_{ij}(t) = \frac{dt_i(t) \times dt_j(t)}{\sigma_i \times \sigma_j} \tag{4.4}$$

Computing the MTD metric for all pairs of ROIs at a given time point yields an instantaneous estimate of FC across the whole brain at that time *t*. Owing to the first-order differencing step, the resulting MTD time series has dimension $T - 1 \times n \times n$, in contrast to the ECF and DCC methods, which both result in FC time series of dimension $T \times n \times n$. From the formulations given in Equations 4.1 and 4.4, it follows that the MTD metric can be interpreted similarly to the ECF metric as computed in the temporal derivative space.

4.3.2.3 Dynamic Conditional Correlation (DCC)

In addition to the non-parametric ECF and MTD methods described above, parametric methods for instantaneous estimation of connectivity matrices at each fMRI frame have also been described, namely the dynamic conditional correlation (DCC) model (Choe et al., 2017; Lindquist et al., 2014a). DCC is a variation on a multivariate generalized autoregressive conditional heteroscedastic (GARCH) model, which have been popularly used in the field of finance to understand the statistical dependency between stocks (Engle, 2000). The DCC model estimates the time-varying correlation structure of multivariate time series using a two-step process: first, a univariate GARCH model is fit to each of the independent time series individually to estimate the conditional variance, and second, the time-varying correlation matrix is estimated from the standardized residuals from step one using an exponentially weighted moving average (EWMA) approach.

The formulation of the DCC model begins with the formulation of the univariate GARCH(1,1) model. We can represent a given a univariate process as

$$y_t = \sigma_t \epsilon_t \tag{4.5}$$

where ϵ_t is a N(0,1) random variable and σ_t is the conditional variance we wish to model. The GARCH(1,1) model would estimate the conditional variance term as follows:

$$\sigma_t^2 = \omega + \alpha y_{t-1}^2 + \beta \sigma_{t-1}^2 \tag{4.6}$$

where $\omega > 0, \alpha, \beta \geq 0$, and $\alpha + \beta < 1$. In this formulation, the α term weights the impact of prior values of the time series itself, while the β term weights the impact of estimates of the conditional variance at previous time points in estimating the conditional variance at the present time point *t*. It is worth noting that more general GARCH(*p*,*q*) models can also be defined, which consider *p* previous values of the time series and *q* previous estimates of the condition variance in the estimate of σ_t.

Using the formulation of the univariate GARCH(1,1) as a basis, we illustrate the following bivariate example of the DCC(1,1) model. Let $\boldsymbol{y_t} = \epsilon_t$ represent a BOLD fMRI time series of two ROIs and Σ_t be the conditional covariance matrix we wish to model. The DCC(1,1) model is defined as follows:

$$\sigma_{i,t}^2 = \omega_i + \alpha_i y_{i,t-1}^2 + \beta_i \sigma_{i,t-1}^2 \text{ for } i = 1,2 \tag{4.7}$$

$$D_t = diag\{\sigma_{1,t}, \sigma_{2,t}\} \tag{4.8}$$

$$\epsilon_t = D_t^{-1} e_t \tag{4.9}$$

$$Q_t = (1 - \theta_1 - \theta_2)\underline{Q} + \theta_1 \epsilon_{t-1} \epsilon_{t-1}' + \theta_2 Q_{t-1} \tag{4.10}$$

$$R_t = diag\{Q_t\}^{-1/2} Q_t \, diag\{Q_t\}^{-1/2} \tag{4.11}$$

$$\Sigma_t = D_t R_t D_t \tag{4.12}$$

The first step of the DCC algorithm consists of fitting a GARCH(1,1) model to each of the two ROI time series in $\boldsymbol{y}_t$ individually (Eq. 3.7) and then used to compute the standardized residuals, ϵ_t(Eqs. 3.8, 3.9). The second step involves the application of an EWMA scheme to the standardized residuals

from the first step to compute the time-varying correlation (R_t) and covariance (Σ_t) matrices (Eqs. 3.10, 3.11, 3.12), . The model parameters ($\omega_1, \alpha_1, \beta_1, \omega_2, \alpha_2, \beta_2, \theta_1, \theta_2$) are estimated in a two-stage approach using a quasi-maximum likelihood method.

In the present study, the DCC model was implemented in R utilizing the packages `rugarch` (https://cran.r-project.org/web/packages/rugarch/index.html) and `rmgarch` (https://cran.r-project.org/web/packages/rmgarch/rmgarch.pdf). Theoretically, the DCC model should be able to scale to estimate the time-varying correlation structure between an arbitrarily large number of time series (Engle, 2000). However, in practice, we found the model estimation became intractable when the number of time series used exceeded 50. In fact, many previous applications of DCC in the TVFC literature only considered 5 ROI time series (Lindquist et al., 2014b; Syed et al., 2017). In another use of the DCC TVFC framework that considered 50 ROI time series, a "massively bivariate" approach is suggested, where a separate bivariate DCC model is fit for each unique ROI pair in the time series, in an effort to better enable parallelization as the number of ROIs increases (Choe et al., 2017). While this may be feasible with tens of ROIs, it quickly becomes intractable for the 268-ROI parcellation utilized here. To put this in perspective, estimating the time-varying correlation structure of a single time series would require the fitting of 35,778 bivariate DCC models, and to apply this framework to both WM fMRI time series across all 922 subjects would total nearly 66 million distinct bivariate DCC models. Furthermore, even if each model fitting only took one second, fitting the full set of required DCC models would require over 763 days of computational time, so even with heavy parallelization, such a study would be infeasible. With these considerations in mind, we first reduced

the dimensionality of the data by transforming the ROI time series into subnetwork time series. Specifically, for each of the 8 subnetworks defined in (Finn et al., 2015) we computed the mean and variance time series across all ROIs included in each subnetwork, reducing the spatial dimensionality of the data from 268 to 16. This reduced subnetwork-level time series helped strike the balance between preserving the spatial and functional specificity of the data while also enabling the analysis to run in a reasonable amount of time.

4.3.3 Post-processing Strategies

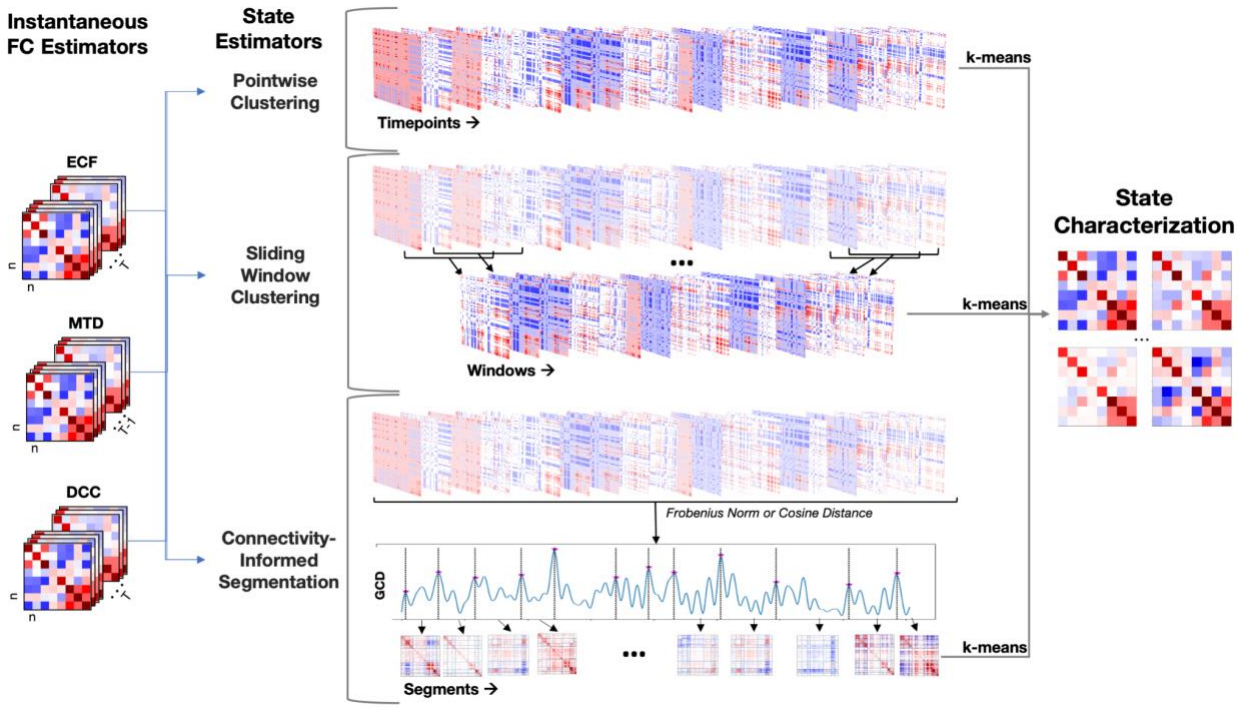

Figure 4.1. Experimental pipeline.
For each of the three instantaneous FC estimators, we apply three post-processing workflows for state estimation: pointwise clustering, sliding window clustering, and connectivity-informed segmentation. Each workflow culminates in the application of *k*-means clustering for characterization of *k* final states.

While instantaneous FC estimators are valuable for providing a temporally granular view of the changing connectivity landscape, additional post-processing steps are necessary to translate the

time-resolved FC estimates into connectivity states. Here, we compared three post-processing schemes for state estimation (Figure 4.1). First, we applied pointwise *k*-means clustering, similar to the CAP approach, to group individual time points into a set of discrete FC states based on their instantaneous FC signatures. While this approach preserves the temporal granularity of the instantaneous FC estimations, it is the most susceptible to pointwise noise that can occur with instantaneous FC estimations and comes at a cost of higher dimensionality compared to the other windowing or segmentation approaches tested.

Second, we applied a sliding window + *k*-means approach, computing the average FC estimate within each window in an effort to induce smoothness on the otherwise potentially noisy instantaneous FC methods. We tested the effect of window size on the accuracy of the state predictions by implementing sliding windows of three different lengths: 15 TR, 25 TR, and 35 TR. These choices of window size are comparable to those utilized in other sliding window TVFC paradigms and are also compatible with the length of the ground truth cognitive processes we attempt to uncover in the WM task structure (38 TR for task conditions and 21 TR for rest conditions). The averaging nature of the sliding window procedure helps reduce instantaneous noise, but the highly overlapped windows create issues for interpretation of resultant states.

Finally, we applied two variants of an informed segmentation framework, here termed the connectivity-informed segmentation, inspired by the activation informed-segmentation approach described in Section 3.3.2 and (Duda et al., 2020). The goal of the informed segmentation paradigm is to identify moments of significant instantaneous change in functional connectivity (or activation) and

to use these change points as boundaries for the creation of tailored, non-overlapping temporal segments. Informed segmentation serves as a hybrid approach, utilizing the time-resolved estimates of FC to generate data-driven boundaries between connectivity states while reaping similar averaging and smoothing benefits from the tailored segmentation as obtained from windowing approaches. Furthermore, as the resultant segments are discrete (i.e., non-overlapping), offering the added benefits of improved interpretability and reduced dimensionality over the sliding window approach.

The first connectivity-informed segmentation variant, similar to the activation-informed segmentation, involves the calculation of a temporal connectivity derivative (dC) via first-order differencing:

$$dC_{i,j}(t) = C_{i,j}(t) - C_{i,j}(t-1) \tag{4.13}$$

where $C_{i,j}(t)$denotes the FC estimate between ROIs i and j at time t for the instantaneous FC estimator C. The resultant dC tensor has dimension $T-1 \times n \times n$ where T is the total length of the instantaneous FC time series and n is the total number of ROIs. Analogous to the relationship between the temporal activation derivative dt and the GTD in the activation-informed segmentation framework (Section 3.3.2), the multivariate connectivity derivative dC is simplified to a univariate, whole-brain summary of connectivity change, here termed the Frobenius global connectivity derivative (GCD_F), by applying the Frobenius matrix norm to the dC matrix at each time point t.

$$GCD_F(t) = ||dC_{1:n,1:n}(t)||_F = \sqrt{\sum_{i=1}^{n}\sum_{j=1}^{n}|dC_{i,j}(t)|^2} \tag{4.14}$$

The variant of the connectivity-informed segmentation framework that utilizes the GCD_F series will be referred to as the Frobenius variant.

The second connectivity-informed segmentation variant combines the first-order differencing and the univariate summarization into a single step utilizing cosine similarity. Recently, cosine similarity has been proposed as a metric for measuring the change in connectivity configuration from one time point to the next (Fu et al., 2021). The cosine similarity θ between two square $n \times n$ matrices, X and Y, can be formulated as:

$$\theta(X, Y) = \frac{J(X \circ Y)J^T}{||X||_F ||Y||_F} \tag{4.15}$$

where J is a $1 \times n$ vector of ones, $\circ$ is the Hadamard product and $||\ ||_F$ is the Frobenius norm. Computing the cosine distance (i.e. $1 - \theta$) at each step in the instantaneous FC time series C results in the cosine variant of the global connectivity derivative (GCD_{cos}), another univariate summarization of instantaneous whole-brain change in connectivity.

$$GCD_{cos}(t) = 1 - \theta(\ C(t), C(t-1)\ ) \tag{4.16}$$

The variant of the connectivity-informed segmentation framework that utilized the GCD_{cos} series will be referred to as the cosine variant.

Analogous to the GTD, peaks in each GCD series denote moments of significant instantaneous change in global, i.e., whole brain, functional connectivity. We apply peak detection to identify these FC change points. As described in Section 3.3.2.1, we begin by applying exponentially

weighted moving average smoothing (window size = 15 TR, $\alpha = \frac{2}{(window\ size + 1)}$) to the GCD series to reduce noisy peaks. We then perform moving average peak detection (window size = 10 TR) on the smoothed GCD series. Using a subset of 10% (n=92) subjects, we optimized the moving average peak detection parameters to maximize the average precision and recall of discovered peaks against ground truth transition points and perform peak detection using the resultant optimum parameters on the remaining 90% of subjects (n=830). As a post-processing procedure, peaks in close proximity to one another (within 10 TR, corresponding to 7 seconds or the approximate time-to-peak of the hemodynamic response function (Friston, 2003)) were collapsed to the local maximum, and a minimum inter-peak distance of 15 TR was applied to ensure sufficiently large segments for calculating Pearson correlation (Schönbrodt & Perugini, 2013; Thirion et al., 2007; Turner et al., 2018).

This final set of peaks served as the boundaries for tailored time series segmentation. Within a given segment, FC was summarized by the mean instantaneous FC estimates of all time points within that segment. Finally, *k*-means clustering was applied to the aggregated set of segment connectomes across all segments and subjects.

4.3.4 Experimental Design

We applied ECF, MTD, and DCC approaches as described above to fMRI time series data from WM Sessions 1 and 2 for all 922 subjects in our HCP dataset. Within each session dataset, instantaneous FC time series are concatenated across the entire set of 922 subjects. The resultant

dimensionality for each method was as follows: $373{,}410 \times 35{,}778$ for ECF, $372{,}488 \times 35{,}778$ for MTD and $373{,}410 \times 120$ for DCC. In addition to the point-wise connectivity estimates, sliding window and informed segmentation post-processing procedures were also applied to each of the three instantaneous FC estimation results at the subject level, and then similarly concatenated at the group level. Before employing the *k*-means clustering step, we performed PCA dimensionality reduction to reduce the spatial dimension for both ECF and MTD datasets at all levels of post-processing (since the DCC data was already reduced to the subnetwork level, PCA dimensionality reduction was not necessary). Previous work suggests 50-150 PCs are sufficient for capturing robust inter-individual differences in functional connectivity (Sripada et al., 2019). Aligned with this recommendation, we generated low-dimensional representations of FC by retaining the top 100 principal components in each dataset. We then applied *k*-means clustering on each of the PCA-reduced pointwise, windowed, and segmented measures of FC to generate state estimates at each respective level of temporal granularity. We repeated the *k*-means clustering procedure for values of *k* in the range [2-10] and selected the optimal value of *k* for each dataset using the elbow criterion of the cluster validity index, computed as the ratio of within-cluster distance to between-cluster distance (Allen et al., 2014).

We evaluated the accuracy of the state estimation against the ground truth task condition for each combination of instantaneous FC estimator and post-processing technique using three common cluster evaluation metrics: homogeneity, completeness and NMI. Homogeneity is a measure of how homogeneous each cluster is given the ground truth labelling—a perfectly homogenous cluster would only contain samples from a single ground truth class. The completeness metric is essentially the

inverse of the homogeneity metric—perfect completeness would indicate all samples from a given ground truth class were members of a single cluster. Finally, NMI is a metric that measures the mutual dependence between two labelings of the same data, (U, V), given by:

$$NMI(U,V) = \sum_{i=1}^{|U|}\sum_{j=1}^{|V|}\frac{M|U_i \cap V_j|}{\sum U \sum V} log\frac{M|U_i \cap V_j|}{|U_i||V_j|} \quad (4.15)$$

where $|U_i|, |V_j|$ are the number of samples in clusters U_i, V_j, respectively, and M is the total number of samples in the data. Each of these metrics ranges from 0-1, where 1 indicates perfect correspondence between the clustering and the ground truth labels. For the pointwise clustering the ground truth labelling is quite straightforward—each time point is labelled by the task condition at that instant. For sliding window clustering the ground truth for each window is defined by the task condition at the midpoint of the window. Finally, for informed segmentation clustering the ground truth of each segment is defined by the task condition active during a majority of time points in the segment.

4.3.5 Baseline Measures

In addition to the comparison across instantaneous FC estimators, we also present a comparison of other TVFC approaches as baselines for comparison. Namely, we test against the popular sliding window framework and the hybrid activation-informed segmentation paradigm.

4.3.4.1 Sliding Window Pearson Correlation

The sliding window Pearson correlation framework was implemented using the GIFT toolbox and applied as described in Section 3.3.4.

4.3.4.2 Activation Informed Segmentation

The activation-informed segmentation framework was applied as described in Section 3.3.2.

4.3.6 Application in Resting State fMRI

After identifying the best-performing instantaneous FC pipeline in the WM task experiments, we apply this top pipeline to each of the four resting state fMRI scans (REST1A, REST1B, REST2A, REST2B) across the full set of 922 subjects. The optimal number of clusters is tuned by varying the value of k in the range [2,10] during k-means clustering and identifying the elbow point of the cluster validity index across this range. The FC signature for each of the k resultant states is defined by the cluster centroid connectivity matrix. Subsequently, clusters are matched across experimental replicates (i.e. scanning sessions) based on shortest Euclidean distances between the cluster centroid connectomes, and the reliability of the state centroids across these replicates is computed using the I2C2 metric (Section 3.3.2.3). We further characterize the resultant connectivity states with standard TVFC features including average dwell time (i.e., the amount of time spent uninterrupted in a given state), total occurrences of a given state, and specific state-to-state transition probabilities.

4.3.7 Connection to Phenotypes

We performed a regression analysis to assess the combined relationship between subject-specific TVFC feature vectors, averaged across the four resting state sessions, and several neuro-relevant phenotypes. Specifically, we consider ten cognitive metrics: a general factor of intelligence (G), generated from a bifactor model as described in (Sripada et al., 2020), processing speed, generated

from factor modeling of three NIH Toolbox tasks as described in (Sripada et al., 2019), the five facets of personality given by the Revised NEO Personality Inventory (openness to experience, conscientiousness, extraversion, agreeableness, and neuroticism), and the three dimensions of psychopathology given by the Adult Self Report Scale (Internalizing, Attention Problems, Externalizing). We also included the covariates of age and gender. All features (besides the binary gender marker) were z-scored prior to the regression analysis, so the resultant model β values could be interpreted similarly to correlation values. We used a Bonferroni-corrected $\alpha = 0.005$ significance threshold to identify significant relationships between our TVFC features and the ten cognitive phenotypes.

4.4 Results

4.4.1 Informed Segmentation Offers Improved Noise Reduction Over Sliding Window Smoothing

In all frameworks utilizing ECF and MTD, we applied dimensionality reduction by extracting the top 100 PCs prior to the *k*-means clustering step. The percentage of the total variance of the data that is explained by these top 100 PCs in each instance is listed in Table 4.1. The percentage of variance explained (PVE) in the pointwise frameworks provide the baselines for comparison of the various windowing and segmentation approaches tested for both ECF and MTD pipelines. When the number of PCs extracted is constant across various treatments of the data, the change in the PVE can be observed to understand the effect of that treatment on the original data—an increase in PVE would

indicate a reduction in noise, whereas a decrease in PVE would suggest the unintentional introduction of noise compared to the original data.

In the case of ECF, the PVE increases compared to the pointwise baseline for all windowing and segmentation schemes, suggesting these treatments result in a reduction in noise. We found that the largest sliding window size of 35 TR provided the largest boost in PVE of the three sliding window schemes compared to the pointwise framework; however, the maximum PVE observed across all ECF pipelines was attained by applying the cosine variant of the connectivity-informed segmentation framework. This treatment resulted in an increase of PVE from 28.42% to 33.73% and 28.30% to 32.78% compared to the pointwise baseline for WM Session1 and Session 2, respectively. In contrast to ECF, we observed a slight decrease in PVE when applying sliding window operations to MTD in relation to the pointwise framework, suggesting this type of fixed-window averaging does not provide effective noise reduction for instantaneous MTD estimates. While the cosine variant of the connectivity-informed segmentation framework also yielded the maximum PVE in the top 100 PCs across all MTD frameworks, this increase compared to the baseline pointwise framework was negligible, only amounting to 0.10-0.22%.

4.4.2 ECF-Derived Estimates Best Summarize Changing FC Patterns

In total, we tested the performance of 18 distinct connectivity-based TVFC pipelines (six state estimation schemes across three instantaneous FC estimators) at recovering the ground truth task structure of a block-design working memory task-based fMRI. The accuracies of these pipelines (as measured by homogeneity, completeness and NMI) as applied to both WM Sessions 1 and 2 are listed

in Table 4.2. To evaluate the ability of each of the three instantaneous FC estimators to identify true changes in connectivity structure on their own, we first consider the performance of the pointwise clustering. State-time plots showing the temporal alignment of the states identified via pointwise clustering of ECF, MTD and DCC estimates is presented in Figure 4.2.

We found k=3 was optimal across all pointwise clustering experiments. States were matched across experiments to enable direct comparisons. From the pointwise clustering results, we found that ECF estimates outperformed the MTD and DCC estimates in recovering the ground truth states (Table 4.2). By observing the ECF state-time plot in Figure 4.2, we find that State 3 has a strong correspondence to the Rest condition segments, State 2 shows moderate correspondence to the onsets of Task 1 and Task 2 conditions but is also found throughout the Task 1 and Task 2 segments, and State 1 corresponds broadly to the general WM task positive condition. In the MTD pointwise clustering, we find a similar correspondence of State 1 to the general WM task-positive condition, with State 2 showing less specificity for any certain experimental condition. In contrast to the ECF-based results, State 3 shows strong correspondence to the onset of the Task 1 condition, as well as moderate correspondence with the onset of the Rest condition. This result is particularly noteworthy, as the transitions from a task-positive condition to a rest condition and vice-versa evoke the strongest changes in cognitive demands within the WM paradigm. The DCC pointwise clustering results are comparatively noisy. We observe both States 1 and 2 distributed throughout the WM task-positive condition, with some minor specificity of State 2 to the Task 2 onsets. State 3 aligns to the Rest condition and extends through the onset of the Task 1 condition.

4.4.3 ECF + Connectivity-Informed Segmentation Framework Best Recovers Ground Truth Task Structure

In addition to the pointwise clustering, we applied three variations of the sliding window framework (window size 15 TR, 25 TR and 35 TR; Figure 4.3) as well as two variations of the connectivity-informed segmentation framework (Frobenius-variant and cosine-variant; Figure 4.4) for state estimation from each of the three baseline instantaneous FC time series. The accuracies of the sliding window and connectivity-informed segmentation frameworks are listed in Table 4.2.

In accordance with the PVE results in Table 4.1, we observe an increase in clustering accuracy when sliding window or connectivity-informed segmentation frameworks are applied compared to the baseline pointwise clustering accuracy across all instantaneous FC time series (Table 4.2). In the sliding window framework, state correspondences remained largely consistent with those observed in the pointwise clustering experiments, with various degrees of blurring depending on the size of the sliding window smoothing applied (Figure 4.3). Again, ECF exhibited the best specificity of discovered states to ground truth task conditions, which is reflected in the clustering evaluation metrics (Table 4.2). Additionally, we observed that the connectivity-informed segmentation framework yielded improved (in the case of ECF and MTD) or similar (in the case of DCC) performance compared to the sliding window pipeline. The state-time plots for the connectivity-informed segmentation frameworks illustrate the improved performance of the cosine-variant over the Frobenius-variant across all frameworks, with the best performance exhibited when paired with the ECF instantaneous FC base time series (Figure 4.4).

Due to the explicit change-point identification step in the connectivity-informed segmentation pipelines, the accuracy of identifying boundaries between ground truth states can be calculated with precision and recall statistics. In this context, precision can be interpreted as the percentage of discovered change-points that correspond to ground truth state transitions, and recall can be understood as the percentage of ground truth change-points that are identified by the discovered peaks. Transition-dependent recalls can also be calculated to assess the specificity of the informed-segmentation algorithm in identifying each type of onset (i.e., Task 1 → Task 2; Task 2 → Rest; Rest → Task 1). Precision and recall statistics for all connectivity-informed segmentation experiments are presented in Table 4.3. The ECA + connectivity-informed segmentation (cosine-variant) significantly outperforms all other connectivity-informed segmentation pipelines in change-point accuracy, exhibiting an average precision of 0.59 ±0.13 and average recall of 0.66 ±0.14. We found this framework to be fairly well suited to identify all three transition types, with slightly improved performance in the identification of Task 2 → Rest transitions (recall: 0.70±0.23). Taken together, these results point to the ECF + connectivity-informed segmentation (cosine-variant) as the best overall pipeline for instantaneous FC + state estimation (Table 4.2).

4.4.4 Comparison to Baseline Approaches

We considered two baseline frameworks that operate in the activation domain for comparison—the standard sliding window Pearson correlation approach as implemented in the GIFT toolbox, as well as the GTD-based activation-informed segmentation framework. Results for these baselines are reported in Table 4.4. We found that sliding window smoothing of the connectivity-

based frameworks tested here generally outperform the standard sliding window Pearson correlation frameworks, with the exception of the MTD + sliding window clustering framework. Notably, the best-performing instantaneous FC framework (ECF + cosine-based connectivity-informed segmentation) did not outperform the analogous activation-informed segmentation, both in homogeneity of clustering and overall accuracy of change-point detection; however, we did observe certain improvements afforded by the connectivity-informed segmentation over the activation-centric baseline segmentation. Namely, we note an increase in recall of Task 2 boundaries compared to the activation-informed segmentation approach, which correspond to the smallest change in cognitive demands in the context of the WM task, as well as a similar overall trend of specificity (i.e., higher recall) for Rest condition onsets compared to the task-positive onsets.

4.4.5 ECF + Connectivity-Informed Segmentation Framework Detects Five High-Fidelity Resting States

We applied the ECF + connectivity-informed segmentation (cosine-variant) to data from four distinct runs of resting state fMRI. Using the elbow criterion of cluster validity index, we identified k=5 as the optimal number of clusters in all four resting replicates (Supplementary Figure 4.1). Discovered states were matched across the four experimental replicates and characterized by the average cluster centroids across the four resting sessions (Figure 4.5). We found these states to be highly reliable across experimental replicates (I2C2=0.90).

Overall, we observed states that reflect shifting connectivity across network modules, rather than within network modules, consistent with prior work (Betzel et al., 2016; Zalesky et al., 2014). In particular, we observed changing patterns of brain integration and segregation, prominently involving the frontoparietal, medial frontal, and default mode networks (FPN, MF and DMN, respectively) (Zalesky et al., 2014). States 1, 3, and 5 all involve sensory/motor anti-correlation with the FPN, MFN and DMN. Interestingly, in the context of this motif the MFN and DMN exhibit some degree of coupling that appears to be anti-coupled with the FPN—the anticorrelations with the motor/visual subnetworks in States 1 and 3 shows specificity for both MFN/DMN, whereas the anticorrelations with the motor/visual subnetworks in State 5 show specificity for the FPN. Conversely, States 2 and 4 are characterized strictly by positive correlations. Specifically, State 2 is characterized by a high degree of segregation (i.e., cross-network connectivity) and a moderate degree of integration (i.e., within-network connectivity). Sate 4 is mainly characterized by patterns of integration and exhibits an overall lowered degree of connectivity, namely within the subcortical cerebellum network. Importantly, the five states we observed are highly similar to the states identified in this same HCP dataset using the classic sliding window paradigm as reported in (Nomi et al., 2017) and those resulting from the activation-informed segmentation framework presented in Chapter 3. Overall, we observed no temporal alignment of states within or between subjects (Figure 4.6)

4.4.6 Discovered Resting States are Predictive of Personality Traits

Lastly, we extracted TVFC features including state-to-state transition probabilities, dwell times and state occurrences for each subject and performed a regression analysis to identify significant

relations between our discovered states in rest and 10 neuro-relevant phenotypes (Group average metrics shown in Figure 4.7). At a Bonferroni-corrected α=0.005 threshold, we identified significant relationships for three cognitive metrics: G, agreeableness, and openness to experience (Table 4.5). Specifically, we observed moderate relationships between the State 2 to State 4 transition probability and G (β = 0.043; p-value = 0.041), and the State 5 to State 4 transition probability and agreeableness (β = 0.052; p-value = 0.012). Conversely, we found relatively strong relationships between the occurrence of State 1 (β = -0.332; p-value = 0.020) and all transition probabilities from State 3 to all other states (β-values = 0.284 - 0.421; p-values = 0.011 - 0.036) and NEO personality inventory measure of openness to experience. In addition to the comparatively strong β-values in these relationships, it is notable that gender does not appear as a significant predictor in the openness to experience regression model, whereas it consistently appears as the strongest predictor in the other 9 models. This result indicates that the combined effects from the TVFC features listed above outweigh the effects of gender in predicting this facet of personality.

4.5 Discussion

In this work, we performed a comprehensive comparative analysis of instantaneous functional connectivity estimation approaches for assessing TVFC. Specifically, we tested three distinct instantaneous FC estimators (ECF, MTD and DCC) in combination with three methods of state estimation: pointwise clustering, sliding window clustering, and our newly proposed connectivity-informed segmentation framework. We validated each combination of FC and state estimators in a working memory task setting where ground truth transitions between cognitive states are known.

Across this set of validation experiments, we observed that 1) the ECF estimates of instantaneous FC best approximated the changing connectivity structure governed by the WM task structure, 2) the cosine-variant of the data-driven connectivity-informed segmentation approach offered the best noise reduction on the baseline pointwise FC estimates, and 3) the ECF + connectivity-informed segmentation framework (cosine variant) best recovered the underlying task structure of the WM fMRI time series. When applied to resting state data, this ECF + connectivity-informed segmentation framework detected five connectivity states that displayed excellent test-retest reliability across four sessions of resting fMRI, exhibited complex transition dynamics, and were highly consistent with the states uncovered by the activation-informed segmentation approach described in Chapter 3. Our work provides a head-to-head evaluation of the foremost methods in the class of instantaneous FC estimators in the context of a structured ground truth, proposes a novel approach for data-driven segmentation of connectivity time series and presents converging evidence for a highly stable set of time-varying resting states.

This work is the first to conduct a direct comparison between these popular instantaneous FC methods and, to the best of our knowledge, is also the first attempt to quantify accuracy of these frameworks against the natural ground truth of structured, block-design task fMRI. The lack of inherent ground truth in the resting state is one of the largest challenges in the development of TVFC methods. Often, validation studies are performed on simulated data, but such simulations can be susceptible to pitfalls such as oversimplification or over-exaggeration of connectivity changes compared to true spontaneous FC in rest. Thus, evaluating the performance of TVFC methods in

structured block-design task fMRI is advantageous, as it provides naturalistic examples of changing FC and is accompanied by well-defined temporal labels that can serve as a ground truth progression of cognitive states against which accuracy statistics can be measured.

We observed moderate success in recovering the ground truth task structure when MTD-based estimates of FC were used. In the baseline MTD experiments using pointwise clustering we observed two key findings: 1) the MTD appeared to identify instantaneous onsets of changing connectivity states rather than unique patterns of sustained FC, and 2) the MTD method similarly clustered onsets of the Task 1 condition and Rest condition, transitions that are both associated with the strongest changes in cognitive load. Considering these results in conjunction with formulation of the MTD, which computes instantaneous correlations in activation *changes* rather than in activations directly (as in the ECF), it is logical that the MTD would be more selective for *changes* in connectivity rather than sustained governance of a single FC state. Furthermore, the lack of specificity between the Task 1 and Rest condition onsets indicates that there may be some induced lack of directionality stemming from the computation of correlations in the temporal derivative space, as these transitions are effectively opposites (Task-positive → Rest vs. Rest → Task-positive), but the net connectivity effects of the associated activation changes appear to be similar.

The effects of the first-order differencing involved in the MTD may also be relevant in light of the formulation of the informed segmentation approach. We observed relatively poor performance of both the cosine- and Frobenius-variants of our proposed connectivity-informed segmentation pipeline on the MTD-estimated FC time series compared to the other instantaneous FC estimators. Since both

the MTD and the GCD, the series on which the connectivity-informed segmentation relies, compute temporal derivatives, the combination of these methods layers these first-order differencing operations. Such treatment of the data can be effectively similar to computing a second derivative and demonstrates decreased utility in identifying true changes in FC, as evidenced by the results of the MTD + connectivity-informed segmentation approaches. One potential future direction that merits further exploration would be applying peak detection directly to the MTD series itself as a method of informed segmentation, thereby omitting the redundant temporal derivative operations.

We also tested the utility of the parametric DCC model for TVFC analysis. Our work adds to the DCC-based TVFC literature in two important ways. First, ours is the first attempt to apply the DCC framework to fMRI data with a relatively high spatial resolution, here n=268 ROIs. Previous works have only considered fMRI data with spatial dimensions ranging from 5 ROIs (Lindquist et al., 2014b; Syed et al., 2017) to 50 ROIs (Choe et al., 2017). Each of these works comments on the theoretical ability of the DCC framework to scale to an arbitrarily large number of ROIs, however practical applications of DCC at these larger scales and computational considerations required to complete such experiments are notably missing from the current TVFC literature. Even the use of a "massively bivariate" implementation of DCC, as suggested in (Choe et al., 2017) would be computationally infeasible on our in-house compute cluster, despite the reduction in memory requirements and potential for parallelization offered by this strategy compared to the multivariate DCC alternative. Our work provides valuable direct commentary on these computational considerations that is thus far missing from the literature. Second, our results strongly support the

utility of the DCC framework for accurately estimating the changing connectivity structure from fMRI time series. To circumvent the computational issues encountered at the full spatial granularity of our data, we generated coarse subnetwork-level time series rather than the granular ROI-level time series that are generally used. Somewhat surprisingly, we observed fair performance of this application of the DCC method in recovering the ground truth task structure of the WM fMRI. Even with this substantially simplified time series as input, the DCC generates FC estimates that capture the differing connectivity signatures between the task and rest conditions and merits further study in the context of TVFC. Based on our experimental results, we suggest the DCC model be used in conjunction with coarser spatial parcellations of the fMRI data, those on the order of tens of ROIs rather than hundreds. Specifically, we suggest that the combination of parametric DCC with data-driven spatial ICA methods (Calhoun et al., 2001) would provide informative time-resolved estimates of TVFC, however subsequent validation in similar block-design task experiments is needed to first evaluate the accuracy of such an approach.

Finally, we found that the instantaneous FC estimates derived from the ECF framework best approximated the changing connectivity structure underlying the progression of cognitive conditions in the WM task, evidenced by its superior clustering accuracy compared to the other instantaneous FC estimators across all treatments of the data. As formulated, the FC time series estimated by the ECF is described as a "temporal unwrapping" of the static Pearson correlation. The Pearson correlation is the most common metric for defining FC (Preti et al., 2017), and accordingly one of the most robust. Therefore, it follows that a mathematically exact decomposition of the Pearson correlation into its

temporal components would be similarly robust for capturing changing connectivity signatures. Furthermore, we identified the ECF + connectivity-informed segmentation as the best instantaneous FC framework overall. This result complements the findings in our previous work, where we found that data-driven segmentation approaches that result in discrete, non-overlapping segments of stable connectivity outperform the rigid and highly overlapping sliding windows.

In addition to a head-to-head comparison, this work presents two important innovations in TVFC methodology. First, we propose a framework for the data-driven segmentation of instantaneous FC time series to derive a time-resolved progression of functional brain states. This connectivity-informed segmentation framework is based on the analogous activation-informed segmentation pipeline presented in our previous work, extending this data-driven temporal segmentation paradigm to the connectivity domain. As consensus has not yet been reached in the field as to the "best" or "most informative" method for defining time-varying brain states at rest (Lurie et al., 2020), testing methods that operate across different domains of the fMRI data will be crucial for moving the field forward. Second, in addition to the framework utilizing the Frobenius-norm method of summarizing multivariate temporal derivative series into a univariate series of instantaneous changes in activation (or connectivity) proposed in our previous work, we also suggest an alternative framework that utilizes cosine distances to quantify the change in connectivity between estimates of FC at consecutive time points. Recently, the use of cosine distances has been proposed as a metric for quantifying the degree functional connectivity network reconfiguration between adjacent time points (Fu et al., 2021). We build on this work with the introduction of the cosine variant of the connectivity-informed

segmentation framework, which adds elements of change-point identification and data-driven segmentation to their baseline approach. Furthermore, the considerable boost in performance observed with the cosine-variant compared to the Frobenius-variant suggests that the cosine distance is indeed a superior metric for summarizing changes between connectivity matrices than the Frobenius norm.

Perhaps the most consequential result of this work is the convergence of the time-varying states discovered with the ECF + connectivity-informed segmentation pipeline and those discovered via activation-informed segmentation, reported in our previous work. While the two methods are indeed analogous, it is important to consider that they are not only derived from different domains of the data (activation time series vs. connectivity time series), but also reliant on univariate time series computed via two distinct distance metrics (L_2-norm vs. cosine distance). The consequence of such divergent approaches resulting in such closely related states is two-fold: first, it lends support to the informed-segmentation paradigm as a whole, and second, it suggests that this set of five resting states, that are highly stable across fMRI sessions and methodologies, are meaningful and merit further study. In addition to the convergence across our analogous informed-segmentation pipelines, these states also resemble those discovered via classic sliding window approaches in the same HCP dataset (Nomi et al., 2017), providing further support for this set of resting states specifically, and the larger idea of resting TVFC in general.

This work has a few key limitations that must be considered. First, instantaneous estimation of FC necessarily results in a high-dimensional output, on the order of $T \times (\frac{n(n-1)}{2})$ (T: length of time

series, *n*: number of ROIs) when only the upper triangulars of the connectivity matrices are retained. Further concatenation of these FC series across a large number of subjects for state estimation necessitates dimensionality reduction techniques for feasibility of *k*-means clustering. While we find our PCA-based strategy for dimensionality reduction sufficient in practice, we acknowledge that there may be room for further improvement in this aspect of our methods, as only about ~30% of the variance in the original data is retained in the reduced set of 100 PCs. Second, while we improved our peak detection strategy from our prior work to include a parameter optimization step, this aspect of our connectivity-informed segmentation pipeline is still reliant on the exponentially weighted moving average operation that may be subject to similar criticism as the sliding window Pearson correlation approach. However, it is important to note that the identification of local maxima in a univariate signal (i.e., GCD) is not as sensitive to window size as computation of multivariate cross-correlations—the strongest peaks will survive across a variety of moving average window lengths. Additionally, we note that there are methods available for peak detection that do not rely on moving averages that can be substituted into our pipeline, and future work can explore these approaches. Finally, while converging evidence across methodologies suggests the discrete set of states described in this work are meaningful, the exact importance of the time-varying states uncovered by the ECF + connectivity-informed segmentation method is unclear. We showed that changes in ECF connectivity align well with known changes in cognitive state (as evoked by alternating WM task conditions) and that the set of five resting states are highly reliable across replicate sessions of resting state fMRI. We also presented initial data showing that TVFC features extracted from these connectivity states are

linked to phenotypes of interest. But additional work is needed to establish what psychological processes are reflected in these time-varying states, and whether quantifying these transient states will yield significant theoretical and practical insights in psychology and neuroscience.

Finally, in addition to the future directions specified for both the MTD and DCC methods above, we recognize another avenue of potential future exploration related to the ECF, which we have shown as the best of the three methods. The authors of the ECF metric have also proposed an edge-centric approach for estimating static FC, aptly named edge functional connectivity (eFC) (Faskowitz et al., 2020). The eFC metric computes the statistical dependency (i.e., Pearson correlation) of all pairs of edges in the ECF (also referred to by the authors as the nodal functional connectivity [nFC]) series, resulting in a $m \times m$ edge-centric connectivity matrix, where $m = \frac{n(n-1)}{2}$. The resultant edge-by-edge connectivity matrix can be utilized to uncover overlapping communities of edges that co-fluctuate with one another and probe the differences in the organization of these communities under various cognitive conditions. It may be useful to explore the utility of the eFC "super connectome" to characterize the functional connectivity within each tailored segment (rather than the average ECF matrix) to capture time-varying edge functional connectivity and the changing underlying edge community structure. However, the large dimensionality and associated high computational cost of generating the eFC metric may preclude its use in TVFC studies.

In summary, we have conducted a comprehensive comparative analysis of three instantaneous FC estimators (ECF, MTD and DCC) in conjunction with several state estimation techniques. We introduce a novel connectivity-informed segmentation framework for assessing TVFC via data-driven

segmentation of connectivity time series. Using this newly proposed framework, we identify five distinct time-varying states in rest that are highly stable across fMRI replicates and correspond well with states identified previously via activation-informed segmentation and classic sliding window paradigms.

4.6 Figures and Tables

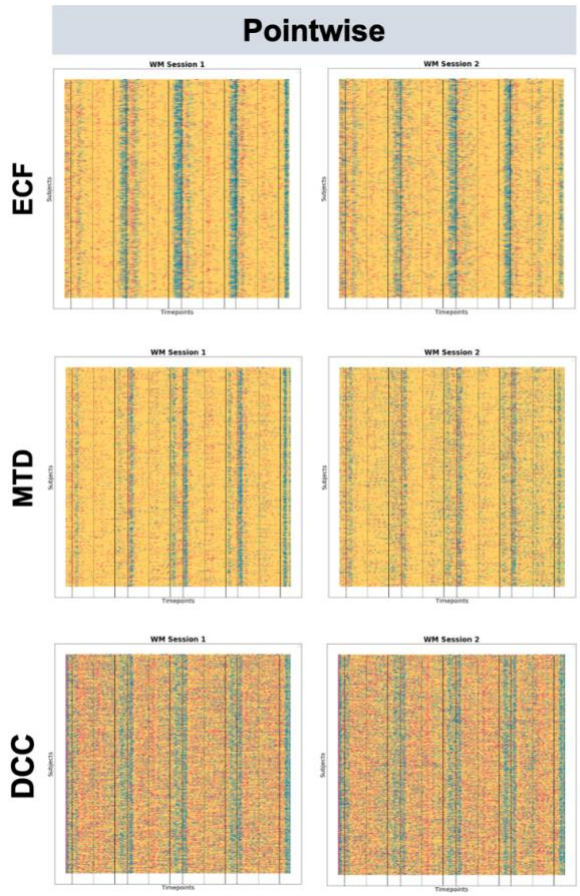

Figure 4.2. Temporal alignment of states discovered in WM via pointwise clustering of FC estimates derived by the ECF, MTD and DCC methods.
Onsets of task conditions are marked by vertical lines: dashed for Task 1 onset, dotted for Task 2 onset, and solid for Rest onset.

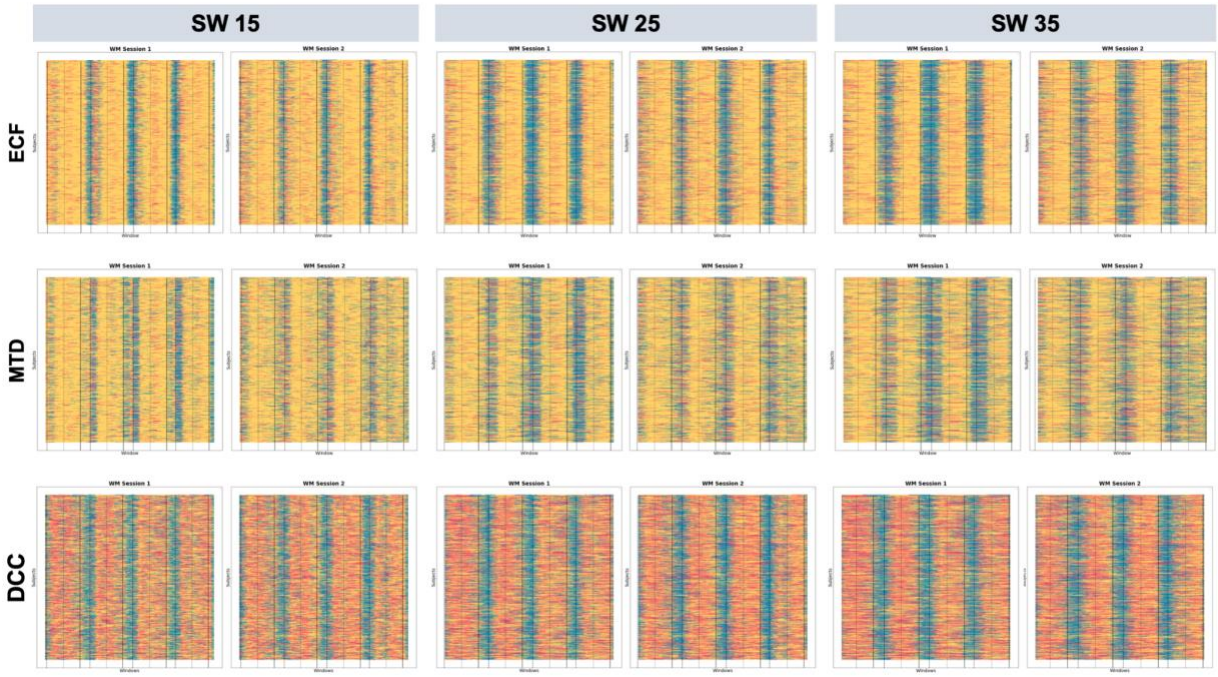

Figure 4.3. Temporal alignment of states discovered via sliding window clustering applied to pointwise FC estimates derived by the ECF, MTD and DCC methods.
Three different window sizes (SW 15: w = 15 TR; SW 25: w = 25 TR; SW 35: w = 35 TR) are reported. Onsets of task conditions are marked by vertical lines: dashed for Task 1 onset, dotted for Task 2 onset, and solid for Rest onset.

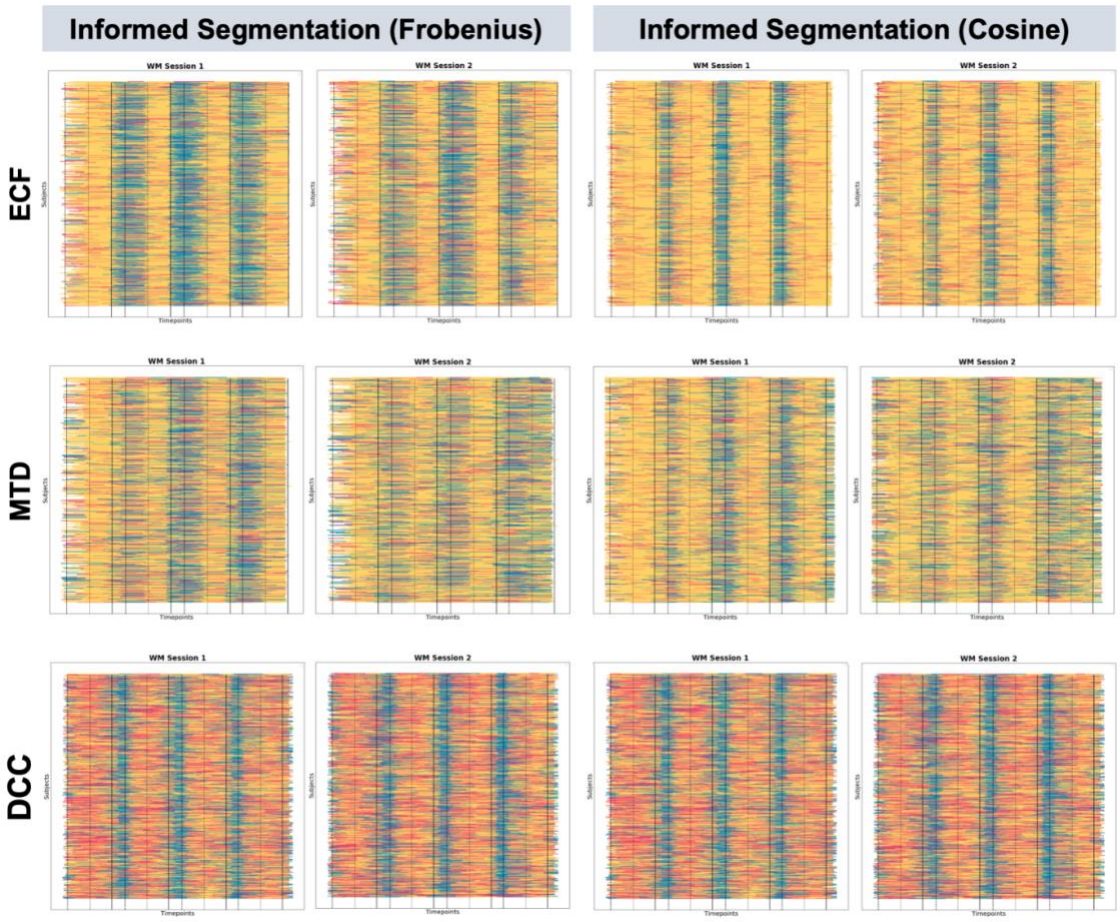

Figure 4.4. Temporal alignment of states discovered via informed segmentation applied to pointwise FC estimates derived by the ECF, MTD and DCC methods.
Two variations of informed segmentation (Frobenius and cosine) are presented. Onsets of task conditions are marked by vertical lines: dashed for Task 1 onset, dotted for Task 2 onset, and solid for Rest onset.

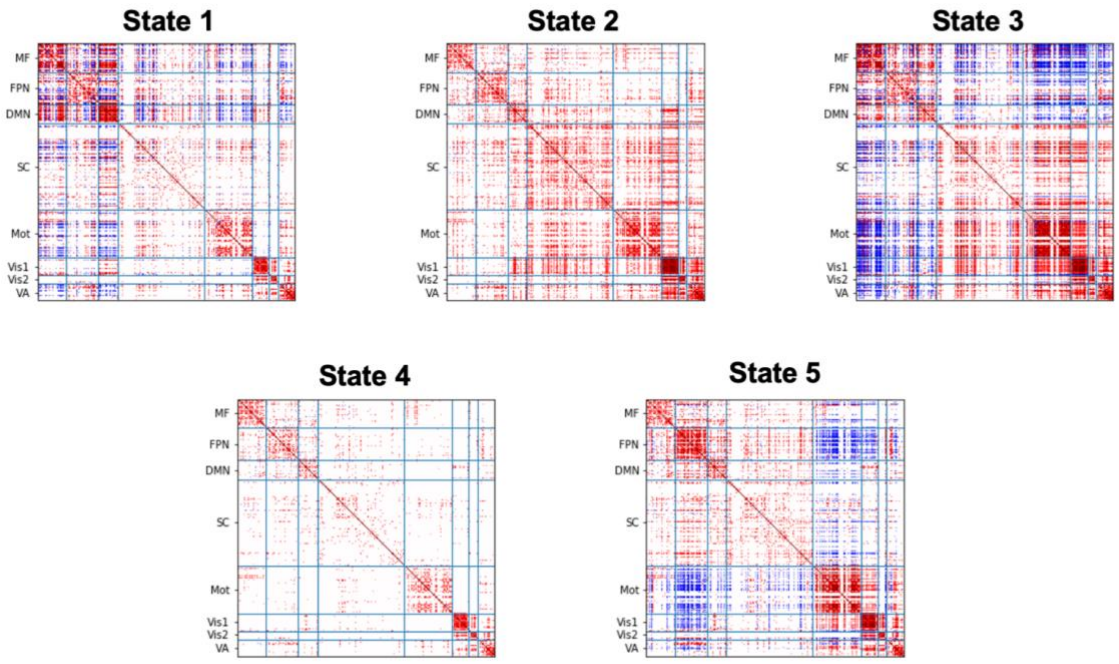

Figure 4.5. Connectivity signatures for each of the five resting states discovered by the ECF + connectivity-informed segmentation framework.

For each of the four resting state experiments, the connectivity signature for each state is defined by the centroid of the corresponding *k*-means cluster, and the mean is computed across the four session replicates to generate overall state connectivity signatures. Connectivity signatures for each of the four resting fMRI scanning sessions are provided in the Supplementary Material. (Subnetwork Abbreviations—MF: Medial Frontal Network; FPN: Frontal Parietal Network; DMN: Default Mode Network; SC: Subcortical Cerebellum Network; Mot: Motor Network; Vis1: Visual 1 Network; Vis2: Visual 2 Network; VA: Visual Association Network).

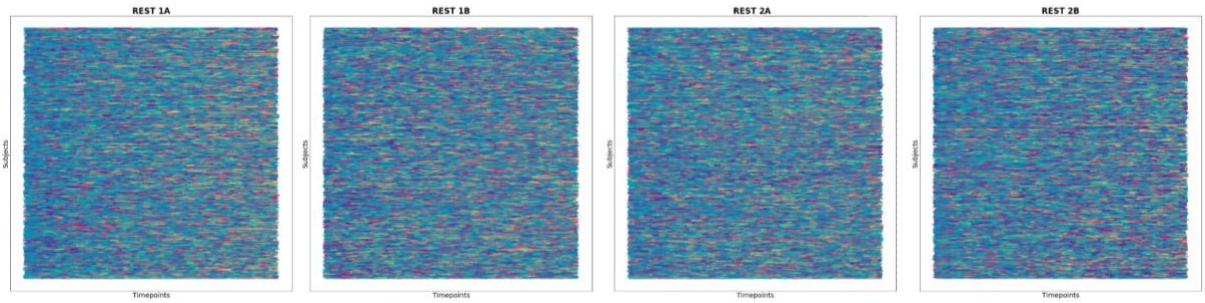

Figure 4.6. Temporal decomposition of resting state fMRI data with respect to states discovered by the ECF + connectivity-informed segmentation framework across four resting state scanning sessions.
As expected, there are no clear temporal patterns within or between subjects at rest.

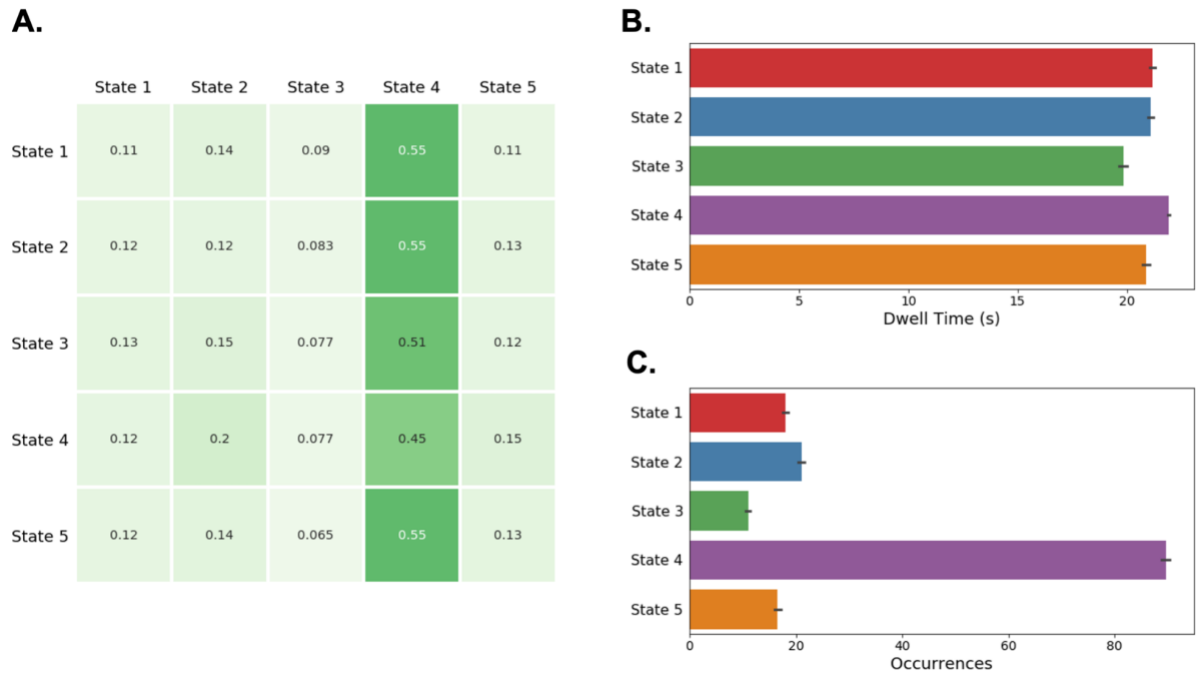

Figure 4.7. TVFC features extracted from resting states discovered by the ECF + connectivity-informed segmentation framework.
Average A) transition probabilities of moving from State X (along rows) to State Y (along columns), B) dwell times, and C) number of occurrences, computed across all 922 subjects and four resting state fMRI sessions.

State Estimator	ECF		MTD	
	WM1	WM2	WM1	WM2
Pointwise Clustering	0.2842	0.2830	0.2339	0.2329
SW 15 Clustering	0.3010	0.3072	0.2334	0.2334
SW 25 Clustering	0.3170	0.3122	0.2302	0.2304
SW 35 Clustering	0.3231	0.3168	0.2305	0.2304
Informed Segmentation (Frobenius)	0.3221	0.3116	0.2299	0.2275
Informed Segmentation (Cosine)	0.3373	0.3278	0.2349	0.2351

Table 4.1 Percent variance explained (PVE) by the top 100 PCs across all treatments of ECF and MTD instantaneous FC estimates.

In both cases, the cosine-variant of the connectivity-informed segmentation approach retains the highest PVE in the top 100 PCs.

State Estimator	Instantaneous FC Estimator					
	ECF		**MTD**		**DCC**	
	WM1	WM2	WM1	WM2	WM1	WM2
Pointwise Clustering						
Homogeneity	0.040	0.023	0.013	0.006	0.009	0.011
Completeness	0.075	0.044	0.027	0.011	0.011	0.013
NMI	0.055	0.032	0.019	0.008	0.010	0.012
SW 15 Clustering						
Homogeneity	0.071	0.048	0.028	0.013	0.032	0.044
Completeness	0.107	0.058	0.042	0.019	0.033	0.045
NMI	0.087	0.072	0.035	0.016	0.032	0.045
SW 25 Clustering						
Homogeneity	0.102	0.071	0.032	0.017	0.055	0.068
Completeness	0.137	0.092	0.046	0.023	0.054	0.068
NMI	0.118	0.081	0.037	0.020	0.054	0.068
SW 35 Clustering						
Homogeneity	0.115	0.076	0.034	0.020	0.057	0.061
Completeness	0.142	0.094	0.042	0.024	0.056	0.060
NMI	0.127	0.085	0.038	0.022	0.056	0.060
Informed Segmentation (Frobenius)						
Homogeneity	0.152	0.089	0.055	0.021	0.052	0.068
Completeness	0.173	0.104	0.064	0.024	0.052	0.067
NMI	0.163	0.096	0.059	0.023	0.052	0.067
Informed Segmentation (Cosine)						
Homogeneity	0.138	0.093	0.042	0.022	0.052	0.068
Completeness	0.197	0.131	0.054	0.028	0.052	0.068
NMI	0.165	0.110	0.047	0.025	0.052	0.068

Table 4.2. Clustering accuracy for all combinations of instantaneous FC estimation and state extraction applied in data from WM Session 1 (WM1) and Session 2 (WM2).

	Metric	Informed Segmentation (Frobenius)		Informed Segmentation (Cosine)	
		WM 1	WM 2	WM 1	WM 2
ECF	Precision	0.46 (0.16)	0.45 (0.14)	0.59 (0.13)	0.58 (0.12)
	Recall	0.39 (0.14)	0.42 (0.14)	0.66 (0.14)	0.65 (0.14)
	Recall Task 1	0.29 (0.10)	0.30 (0.11)	0.65 (0.24)	0.65 (0.24)
	Recall Task 2	0.39 (0.19)	0.46 (0.22)	0.61 (0.23)	0.65 (0.24)
	Recall Rest	0.67 (0.24)	0.66 (0.23)	0.74 (0.22)	0.66 (0.23)
MTD	Precision	0.23 (0.12)	0.25 (0.12)	0.30 (0.12)	0.30 (0.12)
	Recall	0.20 (0.11)	0.21 (0.10)	0.33 (0.13)	0.32 (0.13)
	Recall Task 1	0.26 (0.05)	0.27 (0.07)	0.35 (0.16)	0.35 (0.16)
	Recall Task 2	0.36 (0.17)	0.34 (0.15)	0.38 (0.18)	0.37 (0.17)
	Recall Rest	0.30 (0.12)	0.32 (0.13)	0.40 (0.19)	0.39 (0.18)
DCC	Precision	0.42 (0.12)	0.42 (0.12)	0.43 (0.12)	0.42 (0.12)
	Recall	0.51 (0.15)	0.51 (0.15)	0.51 (0.15)	0.51 (0.15)
	Recall Task 1	0.56 (0.23)	0.56 (0.23)	0.55 (0.23)	0.55 (0.23)
	Recall Task 2	0.53 (0.23)	0.53 (0.23)	0.51 (0.23)	0.51 (0.23)
	Recall Rest	0.50 (0.26)	0.50 (0.26)	0.52 (0.23)	0.52 (0.23)

Table 4.3. Precision and recall of informed segmentation approaches across the ECF, MTD and DCC time series. Results are reported in mean (standard deviation) format.

Metric	Activation-Informed Segmentation		Sliding Window	
	WM 1	WM 2	WM 1	WM 2
Homogeneity	0.327	0.233	0.037	0.037
NMI	0.231	0.159	0.018	0.018
Precision	0.74	0.70	N/A	N/A
Recall	0.67	0.64		
Recall Task 1	0.72	0.62		
Recall Task 2	0.54	0.59		
Recall Rest	0.77	0.73		

Table 4.4. Performance of the baseline activation-domain frameworks in recovering ground truth dynamic state changes in WM task data.
The change point discovery step is unique to our framework and unable to be reported for the sliding window method.

Feature	**β coefficient**	**p-value**
Dependent variable = G; Model p-value = 9.83e-05		
Gender	0.348	0.000
State 2 to State 4 Transition Probability	0.043	0.041
Dependent variable = Agreeableness; Model p-value = 6.17e-05		
Gender	-0.351	0.000
Age	0.069	0.041
State 5 to State 4 Transition Probability	0.052	0.012
Dependent Variable = Openness to Experience; Model p-value = 7.22e-05		
Age	-0.079	0.020
Occurrence of State 1	-0.332	0.020
State 1 to State 5 Transition Probability	0.071	0.015
State 2 to State 4 Transition Probability	0.046	0.028
State 3 to State 1 Transition Probability	0.284	0.036
State 3 to State 2 Transition Probability	0.323	0.028
Probability of Remaining in State 3	0.193	0.014
State 3 to State 4 Transition Probability	0.421	0.031
State 3 to State 5 Transition Probability	0.349	0.011
State 4 to State 1 Transition Probability	-0.063	0.029

Table 4.5. Ordinary least squares regression results for significantly predicted phenotypes (Bonferroni-corrected significance threshold at $\alpha = 0.005$).

4.7 Acknowledgements

This chapter has been revised from a manuscript that is in preparation. I would like to thank Parmida Davarmanesh, Aman Taxali, Saige Rutherford and Mike Angstadt for their support and valuable feedback throughout this work. I would also like to acknowledge the contributions of my co-authors of the manuscript, Danai Koutra and Chandra Sripada.

This work was supported by funding from the University of Michigan Precision Health Investigator Award and the National Science Foundation Graduate Research Fellowship Program grant DGE-1256260.

4.8 Supplementary Material

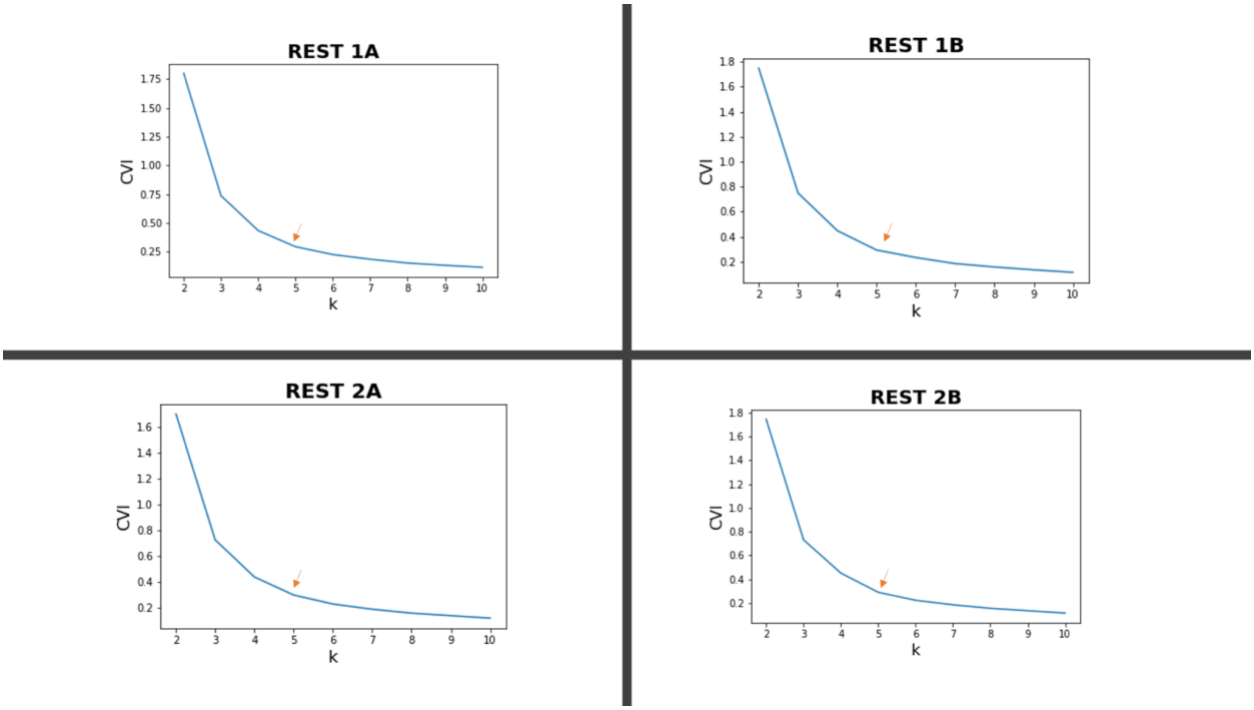

Supplementary Figure 4.1. Cluster validity index (CVI) as a function of *k* in *k*-means clustering of ECF + connectivity-informed segmentation-derived states across four replicate resting fMRI scanning sessions.
In all experiments, the elbow point falls at $k = 5$, suggesting decomposition into 5 states to be optimal.

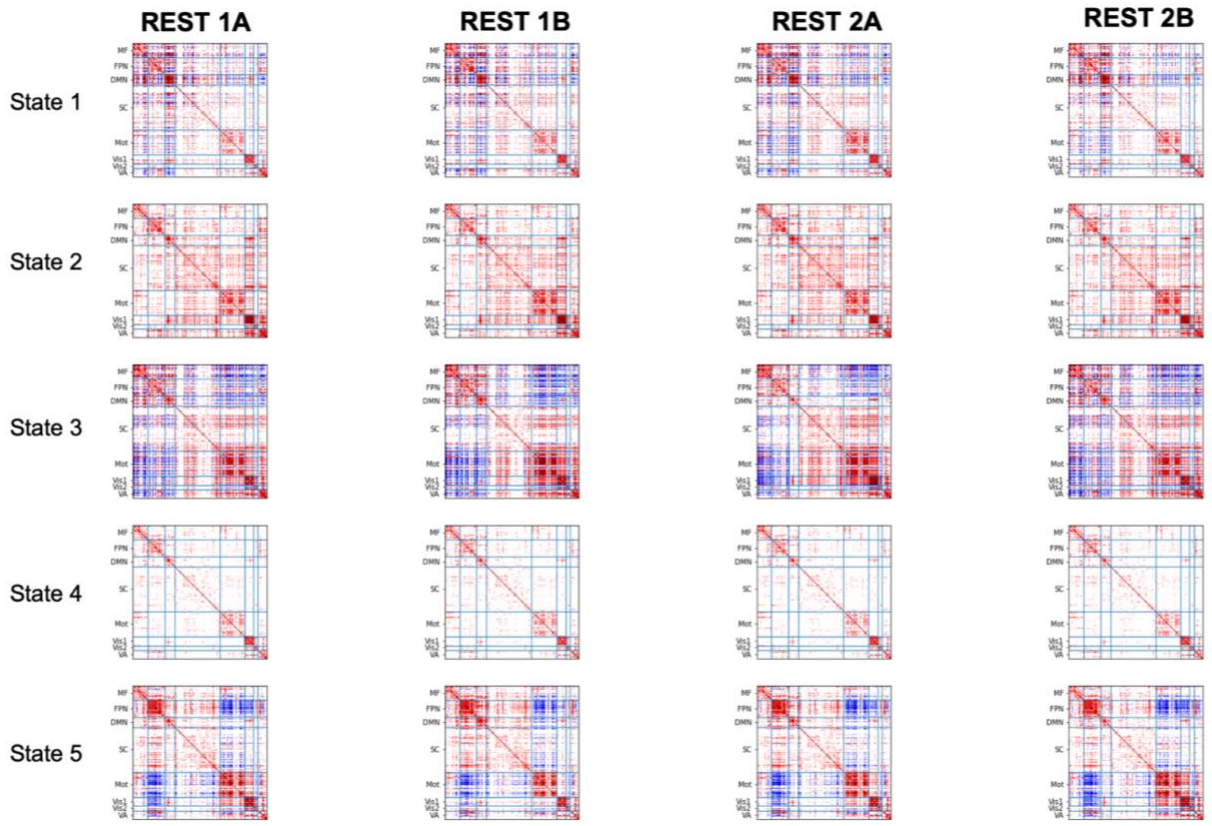

Supplementary Figure 4.2. Replication of resting states discovered by the ECF + connectivity-informed segmentation framework across four sessions of resting state fMRI.
For each of the four resting state experiments, the connectivity signature for each state is defined by the centroid of the corresponding *k*-means cluster. (Subnetwork Abbreviations—MF: Medial Frontal Network; FPN: Frontal Parietal Network; DMN: Default Mode Network; SC: Subcortical Cerebellum Network; Mot: Motor Network; Vis1: Visual 1 Network; Vis2: Visual 2 Network; VA: Visual Association Network).

Chapter 5 - Comparative Analysis Between Data-Driven and Model-Based Instantaneous State Estimation Approaches in Activation and Connectivity Domains

5.1 Abstract

While one goal of TVFC analysis is to simply determine the presence or absence of statistically significant changes in functional connectivity over time, another area of interest within the field of TVFC is to decompose the fMRI time series into a progression through a discrete set of meaningful FC states. Co-activation pattern (CAP) analysis is one such approach, which identifies clusters of time points marked by similar instantaneous patterns activation (or connectivity) via *k*-means clustering. Another popular state estimation framework utilizes hidden Markov modeling (HMM), a generative probabilistic approach that operates under the assumption that a sequence of observed variables (here BOLD fMRI time series) is generated by a sequence of hidden internal states. CAP analysis and HMMs represent two very different means to the same end—a time series labeled by instantaneous membership in a given brain state. Despite their overlapping use-case, these methods have not been directly compared to one another, nor have they been tested in the context of recovering known transitions in cognitive state associated with the implementation of a block-design cognitive task. We provide these direct comparisons and evaluations against task-based ground truth in this work. We found that the use of instantaneous FC time series improved the accuracy of HMM-predicted states;

however, the data-driven CAP approach applied to the activation domain resulted in the best approximation of the changing ground truth cognitive states overall. When applied in resting state, this CAP framework detected four brain states that exhibited unique signatures of both activation and connectivity, and subject's characteristic progressions through these states were found to be predictive of individual variation in cognitive, behavioral and personality traits.

5.2 Introduction

Resting state functional connectivity (rsFC) is a measure of the functional coupling between spatially distinct regions in the brain in the absence of explicit task demands. It has been shown that task-unrelated thought and behavior accounts for nearly 50% of our waking time (Killingsworth & Gilbert, 2010) and may even explain a much larger portion of individual neural variability than that of task-evoked cognition (Musall et al., 2019). For this reason, gaining a more complete understanding of the functional underpinnings of resting cognition is of paramount importance to the field of cognitive neuroscience. Without explicit stimuli to evoke a neural response, rsFC was traditionally thought of as "static" or unchanging throughout the entire fMRI scanning session. However, recent evidence suggests that rsFC may be decomposed into a set of meaningful and reproducible dynamic states (Chang & Glover, 2010; Sakoğlu et al., 2010), catalyzing the growth of the field of time-varying functional connectivity (TVFC).

The classic method of time-varying state estimation centers around the use of a sliding window for estimating changing FC as a function of time, paired with *k*-means clustering to decompose the

series of time-progressing connectivity matrices into a set of *k* discrete brain states (Allen et al., 2014). While this method has proven useful for initial study of FC states, the sliding window paradigm is known to have several limitations, moving the field in the direction of windowless methodologies (Laumann et al., 2017; Lindquist et al., 2014b).

One such windowless approach is the study of co-activation patterns (CAPs), which instead produces an instantaneous (i.e., pointwise) estimate of changing FC states. The standard CAP approach involves the choice of a seed region and the selection of an activation threshold for defining "high-activity" frames. For all timepoints in which activation in the seed region exceeds the selected threshold, activation values across all voxels or ROIs are extracted and aggregated across all subjects. Finally, *k*-means clustering is applied to this aggregated set of activation patterns to identify a set of *k* distinct CAPs, or brain states. Each distinct CAP is defined by the average activation signature of each timepoint in the cluster. Based on this formulation, the standard CAP approach is not fully instantaneous, as only a subset of high activity timepoints are considered. However, the CAP paradigm can be extended by applying the clustering learned from the high-activity frames to all time points, or by omitting the framewise thresholding of the time series and simply applying *k*-means clustering to all time points. The CAP approach has been applied in a variety of contexts (J. E. Chen et al., 2015; Liu et al., 2018), and certain variations on this method have been proposed, such as the iCAP method that includes a deconvolution step in attempts to distinguish between temporally overlapping CAPs (Karahanoğlu & Van De Ville, 2015). Recently, CAP analysis has been utilized to gain insights into the altered functional dynamics associated with ASD (Marshall et al., 2020).

While CAP analysis represents a purely data-driven approach, hidden Markov models (HMMs) provide a model-based alternative for instantaneous state estimation from fMRI time series data. The key assumption of HMMs is that a series of observed data are generated by an underlying progression of latent (i.e., "hidden") states, which take on the form of a first-order Markov chain. Once model parameters (i.e., initial state probabilities and state-to-state transition probabilities) are estimated, the highest-likelihood progression of states under that model can be calculated. In the context of TVFC, BOLD activation time series serve as the observed data and the progression of underlying FC states is what the model seeks to estimate. Certain variations on the standard HMM have been proposed, including auto-regressive HMMs (HMM-AR and HMM-MAR) (Vidaurre et al., 2018) and hidden semi-Markov models (HSMMs) (Shappell et al., 2021), each providing certain contextual benefits depending on the goal of the analysis at hand. In healthy control studies, HMMs have provided evidence for a hierarchical organization of time-varying connectivity states into two distinct meta-states (Vidaurre et al., 2017). HMMs have also shown utility for uncovering altered connectivity dynamics across a variety of clinical diagnoses including PTSD (Ou et al., 2015) and ADHD (Shappell et al., 2021).

Until recently, BOLD activation signals were among the only available time series upon which instantaneous state estimators could operate. As part of the progression towards windowless TVFC methodologies several methods for estimating instantaneous functional connectivity have also been proposed, including edge co-fluctuation (ECF) (Esfahlani et al., 2020), multiplication of temporal derivatives (MTD) (Shine et al., 2015) and dynamic conditional correlations (DCC) (Lindquist et al.,

2014b). Each of these methods derives an $n \times n$ functional connectivity matrix at each time point in the fMRI time series. In theory, state estimation approaches can be applied to such FC series to uncover the underlying progression of functional states responsible for the observed data in the connectivity domain, rather than the activation domain. However, to date such an analysis has not been performed, neither with an adapted CAPs approach, nor with HMMs. In the past, HMMs have been applied to time-varying state estimates of changing FC states derived from a sliding window + *k*-means framework, but to the best of our knowledge HMMs have not been applied to time-varying functional connectivity data directly. Beyond this, the existing instantaneous state estimation literature does not provide any analysis aimed at directly comparing the CAP and HMM approaches. Understanding the concordance of the data-driven CAP and probabilistic HMM state estimates would provide valuable contextualization of these methods in the larger field of TVFC; however, the lack of knowledge regarding the timings of functional state changes in resting data to serve as ground truth makes impartial comparisons of such methods difficult.

In this work, we conduct a comparative analysis between the CAP and HMM approaches for instantaneous state estimation, using data from a block-design working memory task as a naturalistic ground truth. We apply CAP and HMM methods in both the activation and connectivity domains, using ECF, MTD and DCC estimates of FC as the baseline connectivity time series. We then apply the best-performing model to resting fMRI data to generate a set of discrete rsFC states, comment on the replicability of these states across scanning sessions within the same population and compare the resultant functional characterization of each state to results from prior rsFC decomposition studies.

5.3 Methods

5.3.1 Data Description

5.3.1.1 HCP Data

In this work we utilize the Human Connectome Project (HCP) S1200 Young Adult dataset made publicly available through the Washington University and the University of Minnesota HCP consortium (http://humanconnectome.org). It is one of the richest collections of neuroimaging data to date, consisting of structural and functional MRI, behavioral assessments, and genotypes for 1200 healthy subjects ages 22-35. A full description of the acquisition protocol can be found in (Van Essen et al., 2013). In short, all HCP fMRI data were acquired on a modified Siemens Skyra 3T scanner using multiband gradient-echo EPI (TR = 720 ms, TE = 33 ms, flip angle = 52°, multiband acceleration factor = 8, 2 mm isotropic voxels, FOV = 208 × 180 mm, 72 slices, alternating RL/LR phase encode direction). In this work, we leverage the repeating task/rest block structure of the working memory (WM) task data available in HCP as a natural ground truth to test the performance of each considered method in identifying the known transitions between the task and rest conditions. The best performing method was then applied in resting state fMRI to extract TVFC states.

The HCP WM task consists of four repeating task/rest blocks, where each block is structured as follows: 27.5 seconds Task 1 (0-back), 27.5 seconds Task 2 (2-back), 15 seconds rest. Using the acquisition details outlined above, each WM task fMRI time series consisted of 405 volumes sampled every 0.72 seconds, for a total acquisition time of 4 minutes and 52 seconds. Two sessions of WM task

fMRI were acquired back-to-back, alternating between RL and LR phase encoding directions. We will refer to these as WM session 1 (RL) and WM session 2 (LR).

Participants completed four total resting state fMRI scanning sessions (two sessions collected on each of two different days). Each resultant resting state fMRI time series consisted of 1200 volumes sampled every 0.72 seconds, for a total acquisition time of 14 minutes and 24 seconds. During the resting state sessions participants were instructed to keep their eyes open and fixated on a cross hair on the screen, while remaining as still as possible. For clarity, we will refer to resting state data from the first collection day as sessions 1A (RL) and 1B (LR), and similarly sessions 2A and 2B for those collected on the second day.

5.3.1.2 Data Preprocessing

Processed volumetric data from the HCP minimal preprocessing pipeline including ICA-FIX denoising were used. Full details of these steps can be found in (Glasser et al., 2013; Salimi-Khorshidi et al., 2014). Briefly, BOLD fMRI data were gradient-nonlinearity distortion corrected, rigidly realigned to adjust for motion, fieldmap corrected, aligned to the structural images, and then registered to MNI space with the nonlinear warping calculated from the structural images. Then FIX was applied on the data to identify and remove motion and other artifacts in the timeseries. These files were used as a baseline for further processing and analysis (e.g., MNINonLinear/Results/rfMRI_REST1_RL/rfMRI_REST1_RL_hp2000_

clean.nii.gz from released HCP data).

Images were smoothed with a 6mm FWHM Gaussian kernel, and then resampled to 3mm isotropic resolution. This step as well as the use of the volumetric data, rather than the surface data, were done to allow comparability with other large datasets in ongoing and planned analyses that are not amenable to surface-based processing. The smoothed images then went through a number of resting state processing steps, including motion artifact removal steps comparable to the type B (i.e., recommended) stream of (Siegel et al., 2017). Further details on motion artifact removal can be found in (Sripada et al., 2019). Lastly, spatially averaged time series were calculated for each of the 268 ROIs from the parcellation given in (Finn et al., 2015).

For our analysis, we first considered the set of 966 subjects listed in (Sripada et al., 2019) that met the following criteria: structural T1 and T2 data, four complete resting state fMRI sessions, and <10% of resting state frames censored due to excessive motion (framewise displacement of 0.5mm). From this set 922 subjects also had two complete WM task fMRI sessions, defining our final subset of subjects.

5.3.2 Instantaneous State Estimators

5.3.2.1 Co-activation Patterns (CAPs)

CAP analysis is a form of instantaneous state estimation that defines states with whole-brain activation patterns at each individual time point via *k*-means clustering. CAP analysis was first proposed with an initial temporal thresholding step involving the choice of both a seed region and activation threshold, and in this formulation only time points with suprathreshold BOLD signal in the chosen seed region were considered in the clustering step (Liu & Duyn, 2013). Subsequent analyses

have suggested omitting this initial thresholding step (Liu et al., 2013) as a means of decomposing the entire fMRI time series, rather than just a subset of high-activity frames, into a set of discrete states. Here, we employ the latter approach to generate state estimates at each time point and to allow for direct comparison of the CAP framework to all other tested approaches across the entire fMRI time series.

While the CAP approach was initially proposed for clustering of similar *activation* patterns, an analogous approach can be defined for clustering similar *connectivity* patterns. To achieve this, we apply *k*-means clustering to time series of instantaneous (i.e., pointwise) estimates of functional connectivity matrices.

5.3.2.2 Hidden Markov Models (HMMs)

Let $Y_{i1}, \ldots, Y_{iT}$ denote the fMRI time series data, where each vector $Y_{it} \in \mathbb{R}^{1\times n}$ represents the BOLD signal amplitude for each of *n* ROIs at time point *t* for subject *i*. Each Y_{it} is assumed to follow a multivariate Guassian distribution $Y_{it} \sim N(\mu_{s=k}, \Sigma_{s=k})$, where the mean μ and covariance Σ depend on the current state *k* at time point *t*. Let S_{iT} denote the latent (i.e., hidden) state at time point *t* for subject *i*. We denote the total set of fMRI time series data across all subjects and time points, $Y_{i1}, \ldots, Y_{iT}$, by $\tilde{Y}$ and the full series of accompanying state estimates by $\tilde{S}$.

As with most traditional HMMs, our HMM framework makes the following assumptions: 1) Transitions between hidden states are assumed to take on the form of a first order Markov chain, meaning the state at time *t* depends only on the state at time *t-1*, and 2) the observed BOLD fMRI

signal vectors at each time point *t* are conditionally independent given the latent state process. In our framework, we fit one HMM model using the observed fMRI data across all subjects, $\tilde{Y}$. The number of states, *k*, that are fit by the HMM must be defined *a-priori*. In the WM experiments, with knowledge of the underlying ground truth structure of the cognitive task progressions, we fit each HMM to model *k*=3 states.

We fit all HMM models using the `hmmlearn` Python package (https://hmmlearn.readthedocs.io/en/stable/#). To generate the series $\tilde{Y}$, we concatenate the ROI time series across all subjects, resulting in a matrix of dimension $(T \cdot N) \times n$, where T is the total number of time points (T=405), N is the total number of subjects (N=922) and n is the total number of ROIs (n=268). All models were fitted using an iterative version of the Expectation-Maximization algorithm, in this context referred to as the Baum-Welch algorithm (Baum et al., 1970). Once all model parameters were estimated, the highest likelihood sequence of latent states was generated using the Viterbi algorithm (Forney, 1973).

5.3.3 Instantaneous FC Time Series

We tested the utility of the CAP and HMM approaches when applied in both the activation and connectivity domains of fMRI time series. Testing these methods in the activation domain is quite straightforward, as the methods are applied directly to the ROI activation time series. To test the performance of each state estimator in the connectivity domain, we compare across three instantaneous FC estimators: edge co-fluctuations (ECF), multiplication of temporal derivatives

(MTD) and dynamic conditional correlations (DCC). Full descriptions of the ECF, MTD and DCC metrics can be found in Sections 4.3.2.1, 4.3.2.2, and 4.3.2.3, respectively.

Briefly, each instantaneous FC estimator generates a connectivity matrix at each time point in the fMRI time series. The ECF can be interpreted as a calculation of the Pearson correlation that omits the averaging step, essentially preserving the frame-wise components of FC that define the static measure of FC between two regions computed over the entire fMRI time series. The MTD metric is formulaically similar to the ECF but operates on the temporal derivative, capturing the degree of functional coupling between pairs of regions at each fMRI time step. Lastly, the DCC is a variation of the multivariate GARCH model, which estimates the conditional correlation matrix at a given time point in the fMRI time series in terms of prior estimates of the conditional correlation as well as prior values of the time series itself. As described in Section 4.3.2.3, spatial dimensionality reduction was required to achieve computational feasibility of fitting the DCC models to each time series. Specifically, for each of the 8 subnetworks defined in (Finn et al., 2015) we computed the mean and variance time series across all ROIs included in each subnetwork, reducing the spatial dimensionality of the data from 268 to 16. This reduced subnetwork-level time series helped strike the balance between preserving the spatial and functional specificity of the data while also enabling the DCC model fitting to run in a reasonable amount of time.

5.3.4. Experimental Design

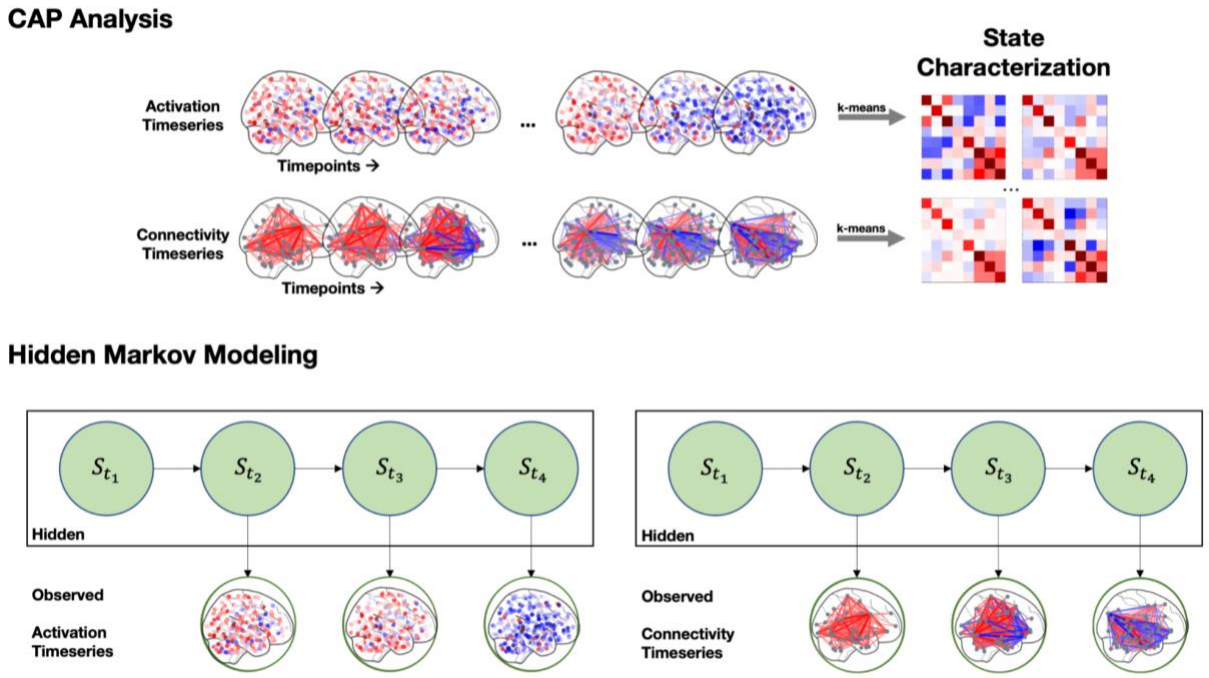

Figure 5.1. Experimental pipeline.
CAP analysis and HMMs were applied to the activation time series, as well as to each of the ECF, MTD, and DCC connectivity time series.

We applied ECF, MTD, and DCC approaches as described above to fMRI time series data from WM Sessions 1 and 2 for all 922 subjects in our HCP dataset. Within each session dataset, instantaneous FC time series are concatenated across the entire set of 922 subjects. The resultant dimensionality for each method was as follows: $373{,}410 \times 35{,}778$ for ECF, $372{,}488 \times 35{,}778$ for MTD and $373{,}410 \times 120$ for DCC. Before employing the instantaneous state estimation procedures, we performed PCA dimensionality reduction to reduce the spatial dimension for both ECF and MTD datasets at all levels of post-processing (since the DCC data was already reduced to the subnetwork level, PCA dimensionality reduction was not necessary). Previous work suggests 50-150

PCs are sufficient for capturing robust inter-individual differences in functional connectivity (Sripada et al., 2019). Aligned with this recommendation, we generated low-dimensional representations of FC by retaining the top 100 principal components in each dataset. For the CAP approach, we applied pointwise *k*-means clustering on each of the activation and PCA-reduced (or subnetwork-reduced) connectivity time series. We repeated the *k*-means clustering procedure for values of *k* in the range [2-10] and selected the optimal value of *k* for each dataset using the elbow criterion of the cluster validity index, computed as the ratio of within-cluster distance to between-cluster distance (Allen et al., 2014). HMMs were also fit to each of the activation, PCA-reduced ECF, PCA-reduced MTD and subnetwork-reduced DCC time series, and the most likely state progressions were estimated using HMM model parameters for each subject time series. HMM models were trained in WM Session 1 data and applied to both WM Sessions 1 and 2 data, to evaluate the model's ability to approximate ground truth state progressions (Session 1) as well as its generalizability to new data (Session 2). The experimental pipeline is depicted in Figure 5.1.

We evaluated the accuracy of the state estimation against the ground truth task condition for each combination of instantaneous state estimator and baseline time series using three common cluster evaluation metrics: homogeneity, completeness and NMI. Homogeneity is a measure of how homogeneous each cluster is given the ground truth labeling—a perfectly homogenous cluster would only contain samples from a single ground truth class. The completeness metric is essentially the inverse of the homogeneity metric—perfect completeness would indicate all samples from a given

ground truth class were members of a single cluster. Finally, NMI is a metric that measures the mutual dependence between two labelings of the same data, (U, V), given by:

$$NMI(U,V) = \sum_{i=1}^{|U|}\sum_{j=1}^{|V|}\frac{M|U_i \cap V_j|}{\sum U \sum V} log\frac{M|U_i \cap V_j|}{|U_i||V_j|} \quad (4.15)$$

where $|U_i|, |V_j|$ are the number of samples in clusters U_i, V_j, respectively, and M is the total number of samples in the data. Each of these metrics ranges from 0-1, where 1 indicates perfect correspondence between the clustering and the ground truth labels.

5.3.5 Application in Resting State

After identifying the best-performing instantaneous state estimation pipeline in the WM task experiments, we apply this top pipeline to each of the four resting state fMRI scans (REST1A, REST1B, REST2A, REST2B) across the full set of 922 subjects. The functional signature for each of the k resultant states is defined by the cluster centroid activation pattern or connectivity matrix, depending on the method identified. Subsequently, clusters are matched across the four experimental replicates (i.e., scanning sessions) based on shortest Euclidean distances between the cluster centroids, and the reliability of the state centroids across these replicates is computed using the I2C2 metric (Section 3.3.2.3). We further characterize the resultant connectivity states with standard TVFC features including average dwell time (i.e., the amount of time spent uninterrupted in a given state), total occurrences of a given state, and specific state-to-state transition probabilities.

5.3.6 Connection to Phenotypes

We performed a regression analysis to assess the combined relationship between subject-specific TVFC feature vectors, averaged across the four resting state sessions, and several neuro-relevant phenotypes. Specifically, we consider ten cognitive metrics: a general factor of intelligence (G), generated from a bifactor model as described in (Sripada et al., 2020), processing speed, generated from factor modeling of three NIH Toolbox tasks as described in (Sripada et al., 2019), the five facets of personality given by the Revised NEO Personality Inventory (openness to experience, conscientiousness, extraversion, agreeableness, and neuroticism), and the three dimensions of psychopathology given by the Adult Self Report Scale (Internalizing, Attention Problems, Externalizing). We also included the covariates of age and gender. All features (besides the binary gender marker) were z-scored prior to the regression analysis, so the resultant model β values could be interpreted similarly to correlation values. We used a Bonferroni-corrected $\alpha = 0.005$ significance threshold to identify significant relationships between our TVFC features and the ten cognitive phenotypes.

5.4 Results

5.4.1 Instantaneous Co-Activation Patterns are More Informative Than Co-Connectivity Patterns in CAP analysis

We applied CAP analysis on ROI activation time series, as well as ECF-, MTD- and DCC-derived functional connectivity time series. Resulting state-time plots are presented in Figure 5.2 and

accuracy measures computed against the ground truth states at each time point are reported in Table 5.1. We observed that clustering of pointwise co-activation patterns was overall more informative than clustering of pointwise co-connectivity patterns. Specifically, CAP analysis performed on activation patterns resulted in about a three-fold increase in accuracy metrics over the next-best performing CAP pipeline operating on the ECF-derived FC time series (average homogeneity/completeness/NMI = 0.122/0.123/0.123 vs. 0.032/0.060/0.044, respectively). We found that the activation-based CAP analysis resulted in a clustering that not only segregated resting time points (State 3) from task-positive time points (States 1 and 2) exceptionally well, but that also discriminated between landmarks within the task condition, namely onests of Task 1 and 2 (State 2) conditions and points throughout the duration of the task.

5.4.2 Connectivity Time Series Improve HMM State Estimation

We also fit HMM models to each of the activation and connectivity time series from WM Session 1 and used the fitted models to derive the highest-likelihood state progressions in both WM Session 1 and 2 data. This enabled evaluation of both the accuracy of the HMM predictions (in Session 1) and their generalizability to new data (in Session 2). Resulting state-time plots are presented in Figure 5.3 and accuracy measures computed against the ground truth states at each time point are reported in Table 5.1. We observed three main takeaways from the HMM results. First, we found that HMM state predictions on ECF estimates of instantaneous FC best recover the ground truth WM task structure. Second, we observed that HMM-derived states better approximated the ground truth state progressions than the corresponding CAP-derived states across all three instantaneous FC time series.

Finally, we found that all four HMM models generalize fairly well to new data, evidenced by the performance in the WM Session 2 data. Overall, our results indicated that the CAP procedure applied to the ROI activation time series yielded the best approximation of the ground truth structure of the WM task data and was therefore used as the analysis framework for the remaining resting state experiments.

5.4.3 CAP Analysis Reliably Detects Four Distinct Brain States

We applied the CAP analysis pipeline to BOLD activation data from four distinct runs of resting state fMRI. Due to the increased number of time points in the resting state (1200 vs. 405 in WM), the dramatically increased dimensionality of the group-level dataset ($1{,}106{,}400 \times 268$) precluded the generation of a full distance matrix required to compute the cluster validity index (CVI). Instead, we implemented the following procedure to identify the optimal number of states. We began with k=5, informed by the optimal number of clusters identified by the CVI in our prior analyses (Chapter 3, Chapter 4), and performed state matching across the four resting state replication experiments based on shortest Euclidean distances between the cluster centroids. The clustering at k=5 did not yield a 1:1 match across session replicates, so we similarly tested the clustering at k=4, which did yield a 1:1 match across states. Moreover, visual inspection of the cluster centroids across session replicates indicated a unique activation signature for each state that was highly reliable across replicates, lending further support for the optimal clustering at k=4 (Supplementary Figure 5.1). This reliability was underscored by the high I2C2 score across session replicates (I2C2 = 0.97). Figure 5.6 illustrates the temporal decomposition of the resting state data with respect to these four states.

Each state was characterized by the average cluster centroid across the four resting state sessions (Figure 5.4). As the CAP approach was applied on BOLD activation time series, cluster centroids correspond to *activation* patterns, rather than *connectivity* patterns. We found States 1 & 2 exhibited opposing activation patterns, where State 1 was characterized by increased activation across most networks and decreased activations in the default mode and medial frontal networks, and State 2 what characterized by lower overall activity across subnetworks and increased activity in the default mode and medial frontal networks. A similar relationship was seen between States 3 & 4: State 3 exhibited low amplitude BOLD signals throughout, with high amplitude signals in the sensory networks, especially the visual 1 network, and State 4 showed the opposite pattern—high activity overall and low activity in the visual 1 network.

To enable direct comparison with the CAPs-derived states and the connectivity states derived in our prior analyses, we also generated connectomes to characterize each of the four resultant brain states. To do this, we identified all instances of five or more consecutive time points assigned to the same state, generated functional connectomes via Pearson correlation within these consecutive segments, and averaged the connectomes within each state. To emphasize the unique connectivity signature of each state, we subtracted the mean group connectome from each mean state connectome, characterizing each state by its deviation from the mean connectivity (Figure 5.5). State 1 was characterized by increased connectivity within and across the frontoparietal, medial frontal and default mode networks, as well as increased connectivity between the default mode/medial frontal networks with sensory/motor networks, in parallel with decreased connectivity between frontoparietal and

sensory/motor networks. State 2 was marked by decreased connectivity within the default mode network, and across the default mode network and the medial frontal, frontoparietal and subcortical cerebellar networks. State 3 was characterized by increased connectivity between the frontoparietal network and visual networks, whereas State 4 was marked by decreased connectivity between the visual networks and the frontoparietal, default mode and subcortical cerebellar networks. Notably, States 1 & 2 showed little characterization within the largest subcortical cerebellum network, whereas State 3 was marked by increased integration within this network, and State 4 was conversely marked by decreased integration (i.e., within-network connectivity) of the subcortical cerebellum. Overall, we observed repeated connectivity motifs that marked states derived by our activation- and connectivity-informed segmentation frameworks in prior work (Chapter 3, Chapter 4), including seemingly coupled connectivity between the medial frontal and default mode networks that appear to oppose connectivity patterns of the frontoparietal network, as well as characteristic patterns of coupling/anti-coupling between the frontoparietal/medial frontal/default mode networks and the sensory/motor networks. Importantly, these four states are also highly similar to the states identified in this same HCP dataset using the classic sliding window paradigm as reported in (Nomi et al., 2017).

5.4.4 Discovered Resting States are Predictive of Cognitive, Behavioral, and Personality Traits

Lastly, we extracted TVFC features including state-to-state transition probabilities, dwell times and state occurrences for each subject (Figure 5.7) and performed a regression analysis to identify significant relations between our discovered states in rest and 10 neuro-relevant phenotypes. At a

Bonferroni-corrected α=0.005 threshold, we identified significant relationships for five cognitive metrics: G, processing speed, attention problems, externalization, and agreeableness (Table 5.2). Specifically, we observed moderate relationships between the State 1 to State 3 transition probability and G (β = 0.061; p-value = 0.024), the State 1 to State 3 and State 1 to State 4 transition probabilities and processing speed (β = 0.071, 0.046; p-value = 0.004, 0.017, respectively), and State 2 to State 3 transition probabilities and attention problems (β = 0.063; p-value = 0.024). Conversely, we found relatively strong relationships between the State 3 to State 1 and State 4 to State 3 transition probabilities and processing speed (β = 0.284, 0.323; p-value = 0.015, 0.042, respectively), the occurrence of State 3 and externalization (β = -0.212; p-value = 0.010), and both the dwell time and occurrence of State 1 with agreeableness (β = 0.303, -0.299; p-value = 0.005, 0.002, respectively).

5.5 Discussion

In this work, we performed a comparative analysis of instantaneous brain state estimation approaches for assessing TVFC. Specifically, we compared the data-driven CAPs framework with the model-based HMM approach in both the activation and connectivity domains, through the use of three instantaneous FC estimators (ECF, MTD and DCC). We validated each combination of state estimator and baseline time series in a working memory task setting where ground truth transitions between cognitive states are known. Across this set of validation experiments, we observed that 1) data-driven clustering of instantaneous activation patterns enabled better approximation of the changing connectivity structure governed by the WM task structure than the alternative instantaneous connectivity patterns, 2) conversely, the accuracy of the HMM state predictions improved when

models were fit using instantaneous FC time series (estimated via ECF), rather than BOLD activation time series, and 3) overall, the activation-based CAP framework best recovered the underlying task structure of the WM time series. When applied to resting state data, this CAP framework detected four connectivity states that displayed excellent test-retest reliability across four sessions of resting fMRI, exhibited complex transition dynamics, and were highly consistent with the states uncovered by the activation- and connectivity-informed segmentation approaches described in Chapter 3 and Chapter 4. Our work provides a head-to-head evaluation of the foremost methods in the class of instantaneous state estimators in the context of a structured ground truth and presents converging evidence for a highly stable set of time-varying resting states across diverse methodologies.

This work is the first to conduct a direct comparison between the popular instantaneous state estimation methods of CAP analysis and HMMs, and, to the best of our knowledge, is also the first attempt to quantify accuracy of these frameworks against the natural ground truth of structured, block-design task fMRI. While HMMs were applied to data from a finger tapping motor task in prior work (Vidaurre et al., 2016), this prior study was performed in a much smaller sample (N=8 subjects), only attempted to localize discrete finger tapping events rather than sustained FC state changes and did not explicitly report any accuracy statistics for recovering expected ground truth state transitions. For these reasons, it is unclear how these results translate to the accurate detection of transient cognitive (rather than motor) states, as we expect in the resting state. Thus, evaluation of the performance of TVFC methods in structured block-design task fMRI as presented herein is advantageous, as it provides naturalistic examples of changing FC and is accompanied by well-defined temporal labels that

can serve as a ground truth progression of cognitive states against which accuracy statistics can be measured.

Importantly, this work is also the first application of HMMs in the connectivity domain. The use of HMMs in the study of TVFC is not new—HMMs have been used to decompose neuroimaging time series into sets of underlying brain states, and even to connect variations in the resultant state progressions to clinical diagnoses (Baker et al., 2014; Shappell et al., 2021; Vidaurre et al., 2017, 2018). However, all of these applications have been applied directly on the activation time series (both fMRI and MEG), rather than in the connectivity domain. We note that in one recent study, HMMs were paired with sliding window estimates of time-varying FC, but in that work the HMMs were applied to the state progressions derived from a sliding window + *k*-means approach rather than directly to the sliding window connectivity estimates themselves (Ou et al., 2015). Considering this context, our work represents an important new branch in the HMM-based TVFC literature.

This work further meets the moment of current TVFC literature by incorporating the very recently proposed ECF method (Esfahlani et al., 2020) in addition to more established instantaneous FC estimation methods (DCC (Lindquist et al., 2014a) and MTD (Shine et al., 2015)). In our previous work, the moment-to-moment estimates of FC generated by the new ECF framework were found to outperform the more established instantaneous FC estimators (Chapter 4), and we found this pattern continued in the current work. This result further underscores the utility of the ECF framework, a mathematically exact "temporal unwrapping" of the Pearson correlation metric. Moreover, we found the ECF to be computationally efficient and easy to implement, with the

additional advantages of being highly interpretable and familiar, due to its connection to the well-known and commonly utilized Pearson correlation. Taken together, the performance, efficiency, and interpretability of the ECF suggests that future work aiming to localize instantaneous changes in functional connectivity should consider incorporation of this method.

Beyond the standard Gaussian HMM utilized in this work, other variations of the HMM framework have been applied in TVFC analyses. Early HMM-based studies of TVFC combined HMM and multivariate auto-regressive (MAR) models to define the HMM-MAR approach (Vidaurre et al., 2016, 2018). More recently, the hidden semi-Markov model (HSMM) has been proposed, which is analogous to the standard HMM with the added step of explicitly modeling dwell times for each state. HSMM analyses have shown utility for deriving brain states that capture attention-based differences in individuals (Shappell et al., 2019, 2021). Future studies may build on the work presented here by evaluating the accuracy of such variants of the HMM framework against block-design WM tasks and comparing to the baselines reported herein.

Despite the increase in performance afforded by the ECF in the context of HMMs, we found that the activation-based CAP approach best approximated the ground truth structure of the WM task overall. Specifically, we noted that this approach resulted in the best separation between Task 1 and Task 2 (representing 0-back and 2-back working memory tasks, respectively), not only of the methods reported here, but of any of the methods evaluated within this dissertation. This result is not entirely surprising—Task 1 and Task 2 probe the same cognitive process, but to varying degrees of difficulty, therefore should evoke the same *pattern* of functional activity, but with varying *strengths*

(i.e., BOLD signal amplitudes). Such a pattern would be better recognized in the activation domain, rather than the connectivity domain, and this is consistent with the results presented across our varying analyses.

There are a few key limitations to this work. Firstly, the dimensionality of the pointwise data precluded generation of a full distance matrix in order to utilize the CVI for selection of k. To work around this, we manually set k = 3 in the WM task experiments, based on knowledge of the ground truth structure of the data. For the application of CAP in rest, we used the optimal value of k selected by prior experiments utilizing the CVI (k=5) and decreased the value of k until a 1:1 matching of states was identified across the four experimental replicates, resulting in the selection of k=4. We found this approach to work well in practice, yielding states with unique connectivity signatures that exhibited high reliability across experiments (I2C2 = 0.97). Future work may consider other approaches for selecting the best value of k when the dimensionality of the data is exceedingly large. Secondly, the results of CAP and HMM analysis in the connectivity domain are affected by the limitations of the MTD and DCC methodologies discussed in Section 4.5. To reiterate those limitations here, the DCC results are limited by the necessary subnetwork-level summarization required to make the DCC estimation process computationally feasible. It may be useful to repeat these DCC analyses with a lower-dimensional brain parcellation, perhaps derived via the data-driven spatial ICA method. In CAP analysis of MTD, we observe that MTD estimates of instantaneous FC showed greater specificity for identifying transitions in FC states rather than distinguishing between sustained occupancy in a given

state. Thus, using MTD as a baseline time series for HMM state detection can lead to similarly lowered accuracy.

In sum, we have provided a comparison of two popular methodologies for instantaneous brain state estimation from fMRI data—CAP analysis and HMMs. We apply these methods in the standard activation domain, as well as in the previously unexplored connectivity domain. We provide evidence that measures of instantaneous FC, specifically the ECF metric, improve HHM-derived state estimations, and observe that activation-centric CAP analysis best recovers changes FC evoked by changing cognitive task demands.

5.6 Figures and Tables

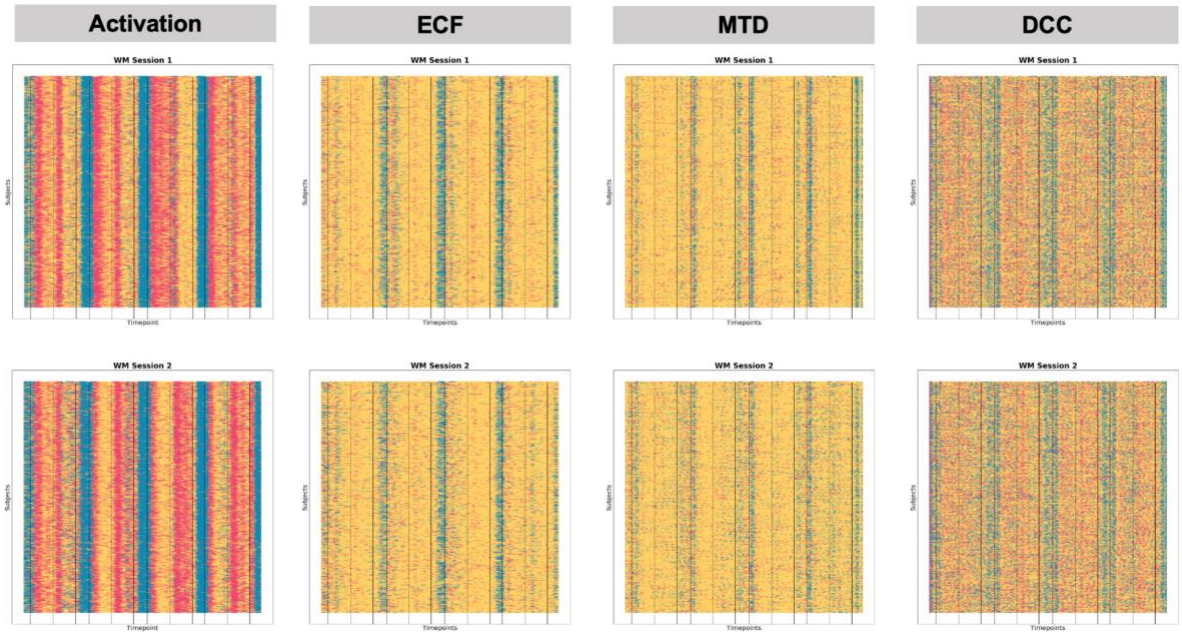

Figure 5.2. Temporal alignment of states discovered via CAP analysis applied to fMRI BOLD activation time series and pointwise FC estimates derived by the ECF, MTD and DCC methods.
Onsets of task conditions are marked by vertical lines: dashed for Task 1 onset, dotted for Task 2 onset, and solid for Rest onset.

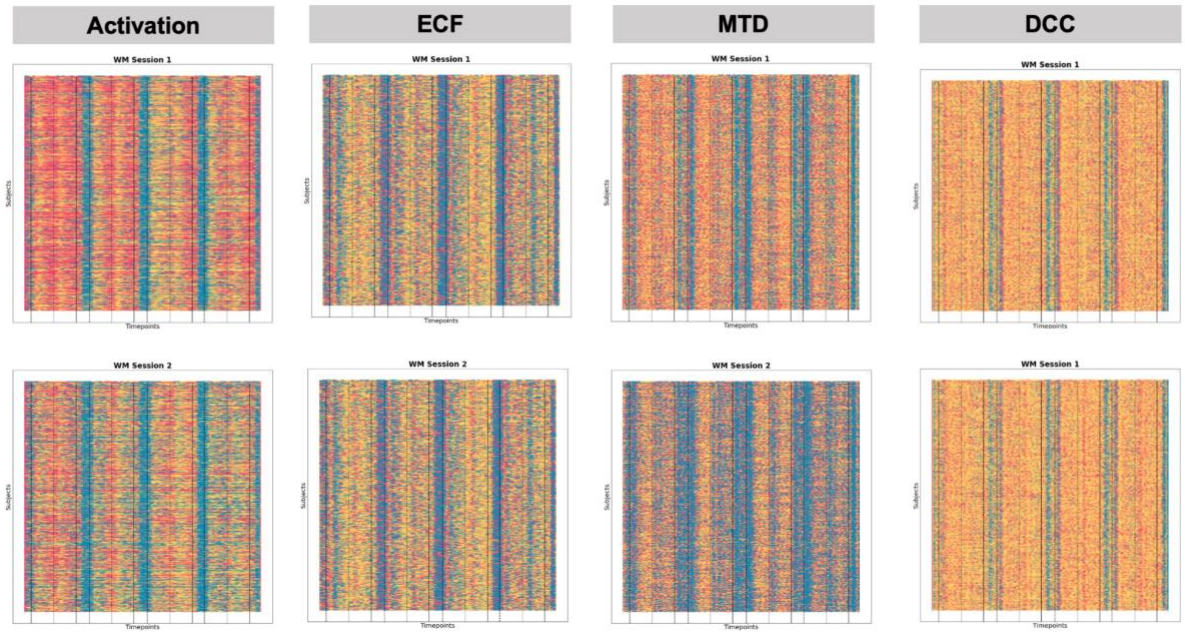

Figure 5.3. Temporal alignment of states discovered via HMMs applied to fMRI BOLD activation time series and pointwise FC estimates derived by the ECF, MTD and DCC methods.
Onsets of task conditions are marked by vertical lines: dashed for Task 1 onset, dotted for Task 2 onset, and solid for Rest onset.

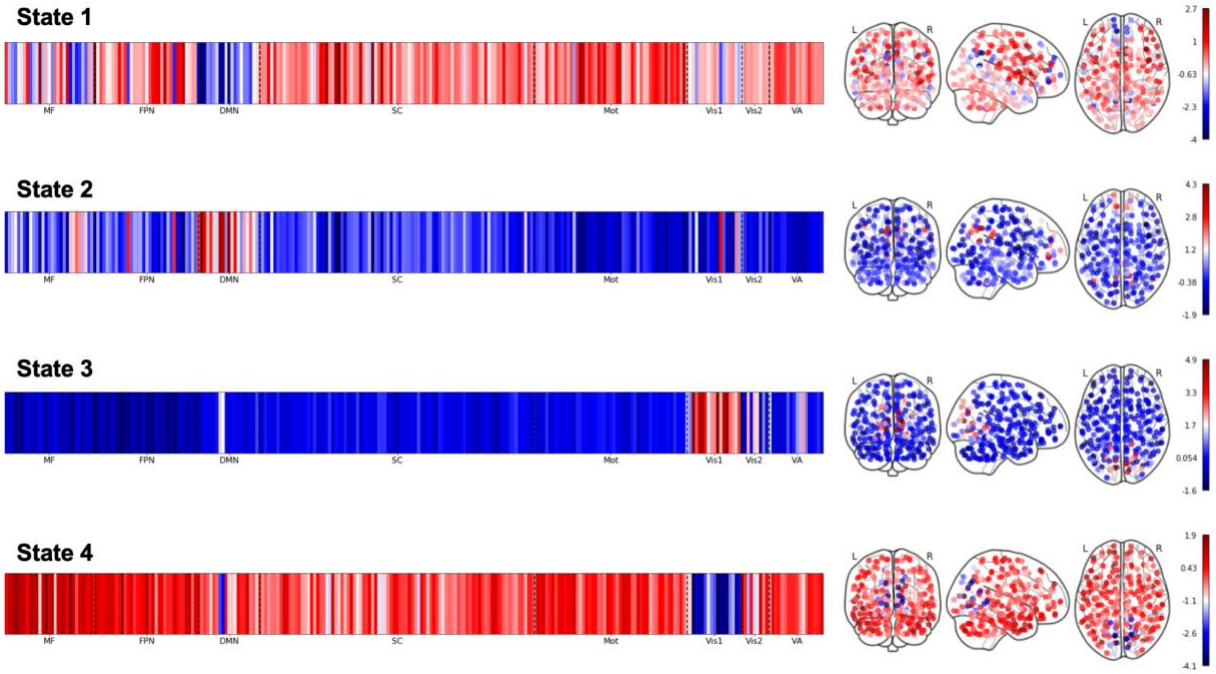

Figure 5.4. Activation signatures for each of the four resting states discovered by the CAP approach. For each of the four resting state experiments, the activation signature for each state is defined by the centroid of the corresponding *k*-means cluster, and the mean is computed across the four session replicates to generate overall state activation signatures. Activation signatures for each of the four resting fMRI scanning sessions are provided in the Supplementary Material. (Subnetwork Abbreviations—MF: Medial Frontal Network; FPN: Frontal Parietal Network; DMN: Default Mode Network; SC: Subcortical Cerebellum Network; Mot: Motor Network; Vis1: Visual 1 Network; Vis2: Visual 2 Network; VA: Visual Association Network).

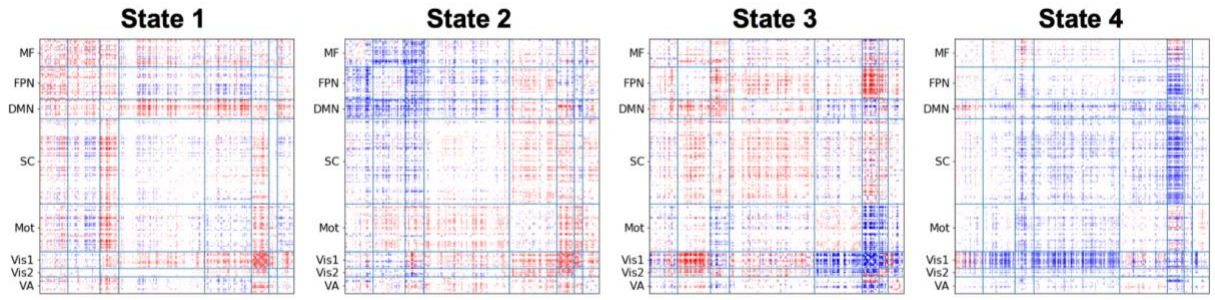

Figure 5.5. Connectivity signatures for each of the four resting states discovered by the CAP approach.
For each of the four resting state experiments, connectomes are computed within consecutive runs of a given state (i.e. *k*-means cluster) and subsequently averaged across all subjects and again across all sessions. Here, the plotted connectivity signatures for each state show the deviation of the mean state connectivity from the mean connectivity across all subjects and sessions, computed by subtracting the average overall connectome from the average state connectome. (Subnetwork Abbreviations—MF: Medial Frontal Network; FPN: Frontal Parietal Network; DMN: Default Mode Network; SC: Subcortical Cerebellum Network; Mot: Motor Network; Vis1: Visual 1 Network; Vis2: Visual 2 Network; VA: Visual Association Network).

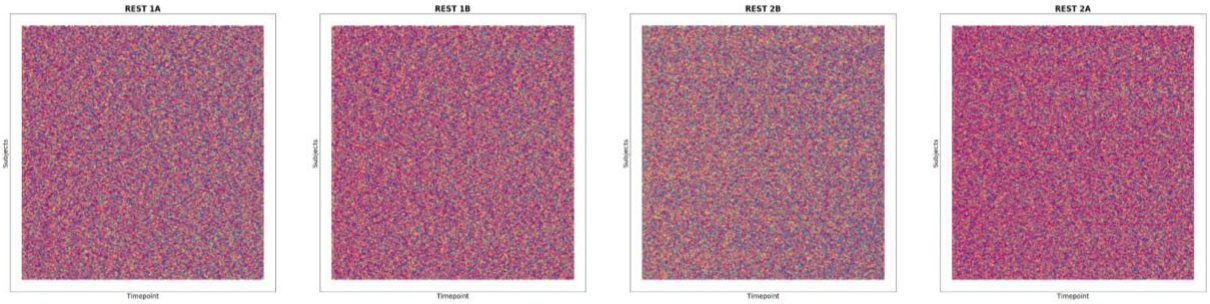

Figure 5.6. Temporal decomposition of resting state fMRI data with respect to states discovered by the CAP framework across four resting state scanning sessions.
As expected, there are no clear temporal patterns within or between subjects at rest, and due to the pointwise nature of the CAP analysis, state durations (i.e. dwell times) are short.

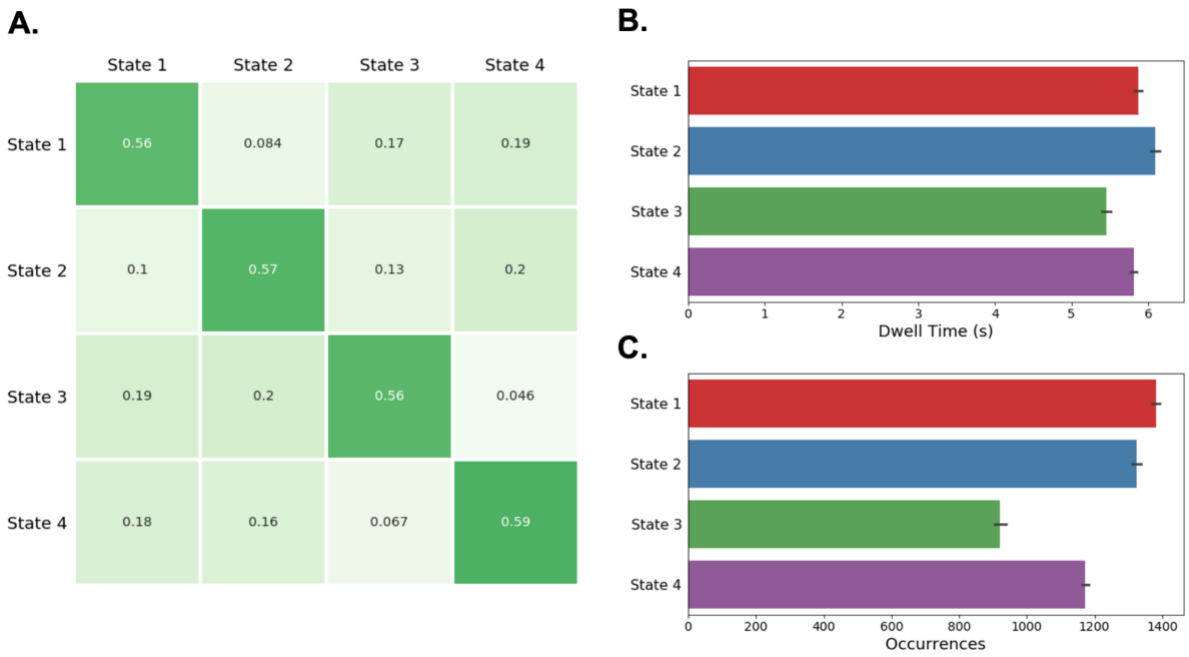

Figure 5.7. TVFC features extracted from resting states discovered by the CAP framework.
Average A) transition probabilities of moving from State X (along rows) to State Y (along columns), B) dwell times, and C) number of occurrences, computed across all 922 subjects and four resting state fMRI sessions.

Baseline Time Series	CAP		HMM	
	WM1	WM2	WM1	WM2
Activation				
Homogeneity	0.122	0.121	0.038	0.029
Completeness	0.125	0.121	0.038	0.029
NMI	0.124	0.121	0.038	0.029
ECF				
Homogeneity	0.040	0.023	0.054	0.028
Completeness	0.075	0.044	0.054	0.028
NMI	0.055	0.032	0.054	0.028
MTD				
Homogeneity	0.013	0.006	0.019	0.013
Completeness	0.027	0.011	0.019	0.013
NMI	0.019	0.008	0.019	0.013
DCC				
Homogeneity	0.009	0.011	0.026	0.027
Completeness	0.011	0.013	0.032	0.033
NMI	0.010	0.012	0.028	0.030

Table 5.1 Clustering accuracy for CAP and HMM instantaneous state estimation approaches across all baseline time series applied in data from WM Session 1 (WM1) and Session 2 (WM2).

Feature	**β coefficient**	**p-value**
Dependent variable = G; Model p-value = 1.09e-06		
Gender	0.396	0.000
State 1 to State 3 Transition Probability	0.061	0.024
Dependent Variable = Processing Speed; Model p-value = 0.00054		
Gender	0.193	0.008
State 1 to State 3 Transition Probability	0.071	0.004
State 1 to State 4 Transition Probability	0.046	0.017
State 3 to State 1 Transition Probability	0.284	0.015
State 4 to State 3 Transition Probability	0.323	0.042
Dependent variable = Attention Problems; Model p-value = 0.00145		
Gender	0.251	0.001
State 2 to State 3 Transition Probability	0.063	0.024
Dependent variable = Externalization; Model p-value = 2.62e-06		
Gender	0.275	0.000
Age	-0.093	0.006
Occurrence of State 3	-0.212	0.010
Dependent variable = Agreeableness; Model p-value = 2.38e-07		
Gender	-0.297	0.000

State 1 Dwell Time	0.303	0.005
Occurrence of State 1	-0.299	0.002

Table 5.2. Ordinary least squares regression results for significantly predicted phenotypes (Bonferroni-corrected significance threshold at $\alpha = 0.005$).

5.7 Acknowledgments

This chapter has been revised from a manuscript that is in preparation. I would like to thank Parmida Davarmanesh, Aman Taxali, Saige Rutherford and Mike Angstadt for their support and valuable feedback throughout this work. I would also like to acknowledge the contributions of my co-authors of the manuscript, Danai Koutra and Chandra Sripada.

This work was supported by funding from the University of Michigan Precision Health Investigator Award and the National Science Foundation Graduate Research Fellowship Program grant DGE-1256260.

5.8 Supplementary Material

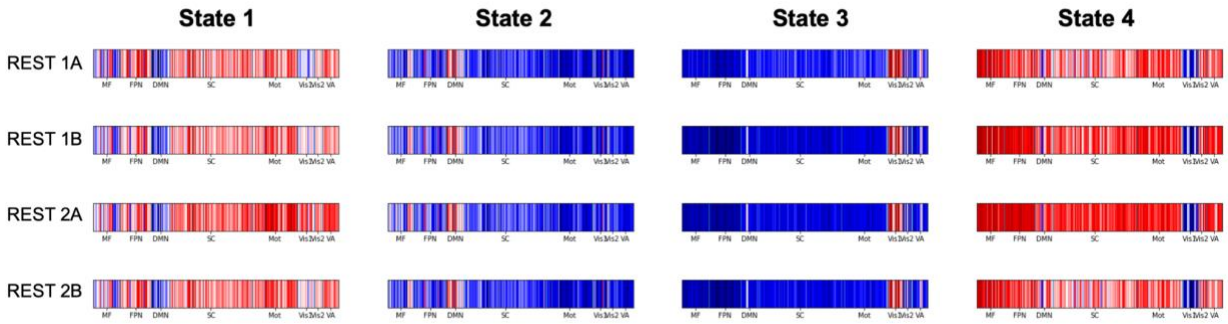

Supplementary Figure 5.1. Replication of resting states discovered by the CAP framework across four sessions of resting state fMRI.
For each of the four resting state experiments, the activation signature for each state is defined by the centroid of the corresponding *k*-means cluster. (Subnetwork Abbreviations—MF: Medial Frontal Network; FPN: Frontal Parietal Network; DMN: Default Mode Network; SC: Subcortical Cerebellum Network; Mot: Motor Network; Vis1: Visual 1 Network; Vis2: Visual 2 Network; VA: Visual Association Network).

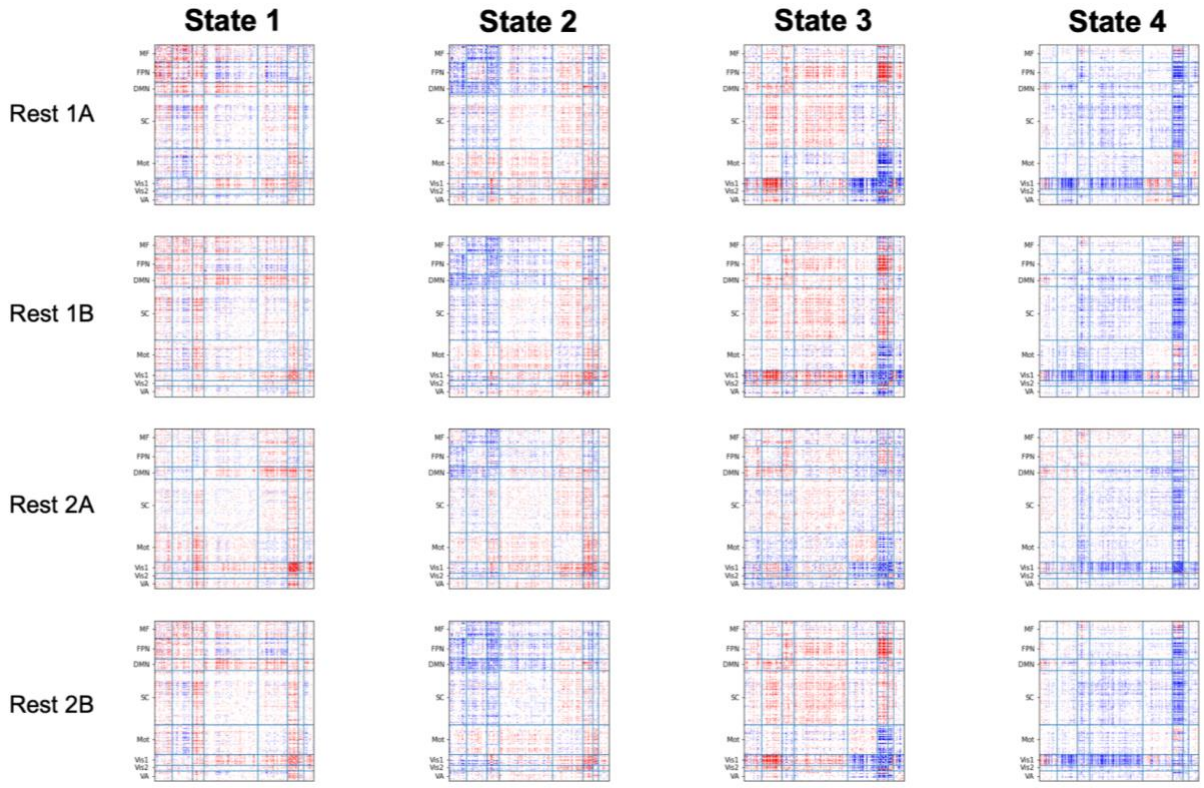

Supplementary Figure 5.2. Replication of connectivity signatures across resting states discovered by the CAP framework across four sessions of resting state fMRI.
For each of the four resting state experiments, connectomes are computed within consecutive runs of a given state (i.e. *k*-means cluster) and subsequently averaged across all subjects. Here, the plotted connectivity signatures for each state show the deviation of the mean state connectivity from the mean connectivity across all subjects, computed by subtracting the average session connectome from the average state connectome. (Subnetwork Abbreviations—MF: Medial Frontal Network; FPN: Frontal Parietal Network; DMN: Default Mode Network; SC: Subcortical Cerebellum Network; Mot: Motor Network; Vis1: Visual 1 Network; Vis2: Visual 2 Network; VA: Visual Association Network).

Chapter 6 - Exploration of Spatiotemporal Informed Segmentation with Deep Learning

6.1 Abstract

In Chapters 3 and 4, we have shown that data-driven informed segmentation approaches have significant utility for identifying time-varying changes in functional connectivity in both resting and task-evoked fMRI. Moreover, evidence presented across Chapters 3, 4, and 5 suggests that changes in the activation domain can accurately recover the boundaries between changing cognitive states, even more so than analogous changes in the connectivity domain. To date, most TVFC frameworks designed to operate in the activation domain rely mainly on linear relationships between regional activations and/or highly summarized measures of global activation change. Here, we propose a framework for spatiotemporal-informed segmentation. This proposed framework utilizes deep learning models, specifically recurrent neural networks, to generate future BOLD activation "snapshots" based on historical fMRI volumes and defines change points as predicted frames that deviate from the ground truth connectivity pattern significantly more than baseline. In this chapter, we describe the proposed method, include some preliminary proof-of-concept results, and present future directions for rigorous evaluation of this framework in line with that of our prior studies.

6.2 Introduction

Deep neural networks are a promising avenue of exploration for development of methods to objectively assess FC dynamics. The key advantage of deep learning in this context is its ability to automate extraction of complex, non-linear features from high-dimensional data. Currently, TVFC methods mainly consider linear correlations between ROIs over time, which could be a severe oversimplification of the actual functional integration of connected brain regions. Investigation of a neural network's learned FC patterns can provide insights into these potentially complex functional relationships. Furthermore, specialized recurrent neural network architectures enable the retention of long-range temporal patterns, something that is not often explored by other TVFC methodologies. Another advantage of deep neural networks is that they allow for the integration of spatial relationships between the ROIs in addition to their temporal BOLD activation signatures.

Recurrent neural networks (RNNs) are specialized deep learning architectures designed to handle sequential data, such as time series. RNNs perform the same task for every element of a sequence, where the output at each step is dependent on the "memory" from the previous steps. Long short-term memory (LSTM) networks are further specialized cases of RNNs that allow for long term dependencies, or in other words allow the "memory" of learned patterns at previous time points to persist across longer sequences, or likewise be methodically "forgotten" when they no longer serve predictions in the current instant (Hochreiter & Schmidhuber, 1997). Recently, an LSTM model (PredNet) was proposed for the computer vision task of predicting future video frames based on the current and previous frames (Lotter et al., 2017). Accurate automation of this prediction task is

especially relevant in the application of autonomous driving, in which the system must anticipate its surroundings in the next instant based on the current surroundings of the vehicle. Similarly, a system built to anticipate the next instant of FC over an fMRI time course can provide insights into neural dynamics.

The objective of this work is to assess TVFC using a novel application of this deep learning approach. We hypothesize that dynamic shifts in FC will correspond to significant drops in next-frame prediction accuracy, reflected as a rise in the framewise mean squared error (MSE). When next-frame prediction accuracy is stable, one can infer that the resting state activations in the brain are following a pattern that is predictable, i.e., a single connectivity state is maintained. However, if there are true underlying dynamics in FC patterns during rest, one would expect a sudden departure from the model's learned activation pattern when there is a distinct shift in connectivity states, resulting in a sudden increase in prediction error. Analyzing these patterns of volume-to-volume prediction errors will provide a robust approach for assessing TVFC with the highest possible temporal granularity. Specifically, we propose to integrate the resultant MSE series into our informed segmentation paradigm as an alternative approach for generating data-driven segments of stable connectivity in the spatiotemporal domain. Further, the convolutional layers of our RNN model can fully leverage the spatial resolution uniquely offered by fMRI, in contrast to the "spatially unaware" connectivity matrices that are classically used to study FC dynamics.

6.3 Methods

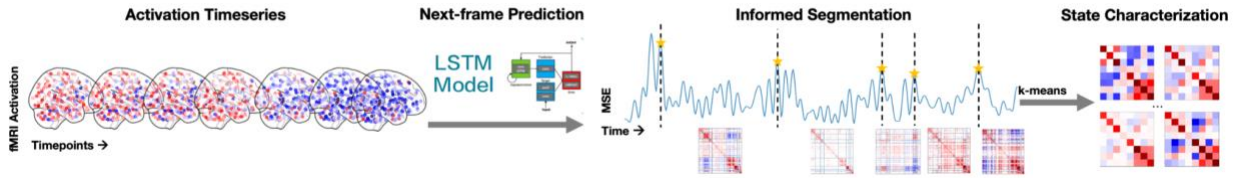

Figure 6.1. Proposed experimental pipeline.
Next-frame predictions will be generated across the fMRI activation time series using a variant of the PredNet LSTM model. The error series (MSE) associated with these predictions will be used for informed time series segmentation.

PredNet was originally designed to handle natural videos, i.e., series of two-dimensional (2D) frames over time. Though theoretically fMRI time series can be thought of as 3D-analogs of these video data, several important considerations separate fMRI from natural image sequences. Videos are dominated by smooth transitions between frames whereas the time-evolving synchronization between brain regions, combined with the significantly increased framerate of fMRI acquisition (TR = 0.72), may cause these framewise transitions to be less smooth in fMRI. Furthermore, the localization of information and relationships between data points differs considerably between fMRI and natural images—a car in one area of a video may have no relationship with a tree in a separate area, however spatially distinct brain regions may be highly related to one another.

With these considerations, we adapt the PredNet architecture to this domain-specific application. Namely, the architecture was adapted to not only handle 4D input (3D frames over time) but also expanded with 3D convolution, enabling the detection of functional activation patterns across all spatial axes of the fMRI volumes. We utilize the code base provided by the authors of

PredNet (https://github.com/coxlab/prednet) as the base architecture in this work, adjusting as necessary to fit our data and purposes. A full depiction of the proposed pipeline is provided in Figure 6.1.

6.4 Preliminary Results

The original PredNet model performed well on videos from dashboard-mounted car cameras (dash-cams), indicating the model is capable of learning complex temporal features. Following this example, the dynamic transition from FC state to FC state in fMRI is analogous to a concatenated series of distinct dash-cam videos. However, considering the fact that the hemodynamic response is intrinsically slow, state transitions may more closely resemble fading between unique videos in the sequence rather than an abrupt splicing. A preliminary analysis on both spliced (Figure 6.2a) and faded (Figure 6.2b) sequences of distinct dash-cam video clips indicates that PredNet prediction behaves as expected in both cases—the next-frame MSE spikes at the transition point and returns to baseline after exposure to 2-3 frames of the new scene. Across 83 pairs of randomly concatenated dash-cam videos, both the spliced and faded transitions had distributions of next-frame MSEs that significantly differed from that of stationary videos (Figure 6.2c).

As a preliminary examination of the performance of PredNet on real resting fMRI data, we trained and tested the out-of-the box 2D PredNet architecture on windowed connectomes (window size = 30 TR) derived from HCP data. The resultant patterns of next-frame MSEs are somewhat unstable, likely stemming from the fact that transitions between windowed connectomes are not

smooth (as they usually are between frames of a video), however, some evidence for connectivity state dynamics still exists in the form of MSE peaks (Figure 6.3). These results suggest TVFC transitions will be identifiable via patterns of PredNet next-frame prediction MSEs.

Finally, we utilized the extended 3D-PredNet model to perform a preliminary experiment using only 43s (60 volumes) of resting state fMRI data from a subset of 100 subjects and trained the model over only 50 epochs. Our results show that even this modest training intermediate of our model, learned from a small fraction of the available data, can capture temporal FC patterns in fMRI data (Figure 6.4).

6.5 Discussion and Future Directions

In this chapter, we present the intuition and preliminary results for a spatiotemporal-informed segmentation framework. This spatiotemporal-informed segmentation approach is analogous to our previously described activation- and connectivity-informed segmentation frameworks in that it leverages instantaneous data to identify connectivity change points, which ultimately define the boundaries of data-driven segments of the time series, but it has the additional benefit of leveraging information about the spatial orientation of the ROIs as well. LSTM architectures have been applied to fMRI time series for the purpose of change point detection in the past (Li and Fan, 2018), but these studies have not gone on to study the reliability or behavioral/cognitive significance of group-level states derived from this method. This previously demonstrated utility of LSTMs in this context, as well as the results from our preliminary experiments, suggest that the spatiotemporal-informed

segmentation approach will be useful for studying TVFC in rest and may generate new insights into the non-linear patterns of connectivity dynamics.

In future work, we plan to train models on the full set of HCP data, as outlined in the preceding chapters. Specifically, we plan to train a model on the WM Session 1 data and apply that model to both WM Session 1 and 2 data, as was done in the HMM approach described in Chapter 5. This serves as a sort of cross-validation method, enabling us to evaluate both the general performance of the model in identifying known state changes as well as its generalizability to new data. After evaluating model performance against the WM ground truth, we plan to similarly train a resting state model on the full set of subjects from Rest Session 1A and apply this model in all four resting state sessions. One major methodological challenge of this approach is the computational cost associated with training and testing of deep neural network models—even the preliminary model trained using only 100 subjects (~10% of all subjects) and 60 frames (5% of the entire resting state time series) required over 12 hours of training on a GPU-accelerated desktop (Nvidia GeForce GTX TITAN X). For this reason, we will use Amazon Web Services Cloud Computing to train the full models in a high-performance computing environment. Beyond this, we propose long-term future work in this space exploring the use of transformer models (Vaswani et al., 2017), which have been shown to model sequential data more effectively than RNN architectures with the added benefit of lower training time.

6.6 Figures and Tables

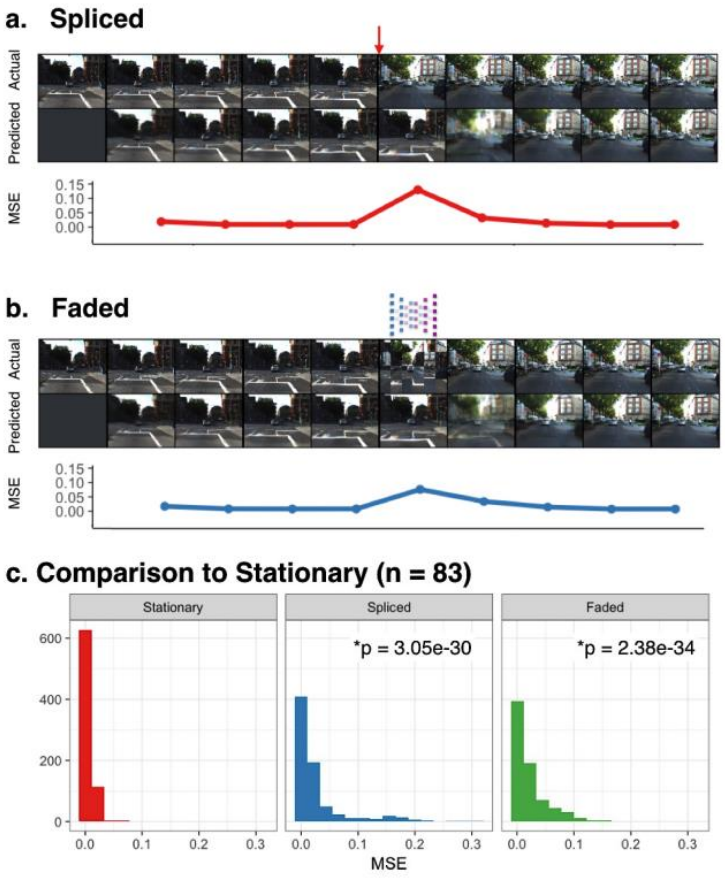

Figure 6.2. Patterns of next-frame prediction accuracies in dynamic video data.
Examples of next-frame predictions for spliced (a) and faded (b) video transitions show expected patterns of prediction MSEs. In samples of 83 videos the distribution of MSEs for both types of dynamic transitions were shown to significantly differ from that of stationary videos (KS test) (c).

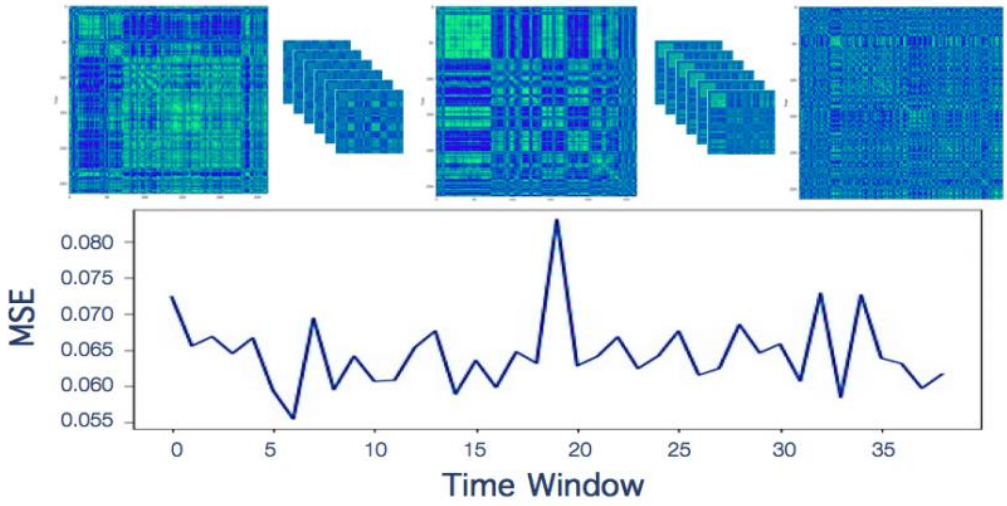

Figure 6.3. PredNet prediction accuracies on windowed connectome frames.
Predictions are relatively unstable as transitions between windowed connectomes are not smooth, however some evidence for connectivity state dynamics still exists (MSE peak).

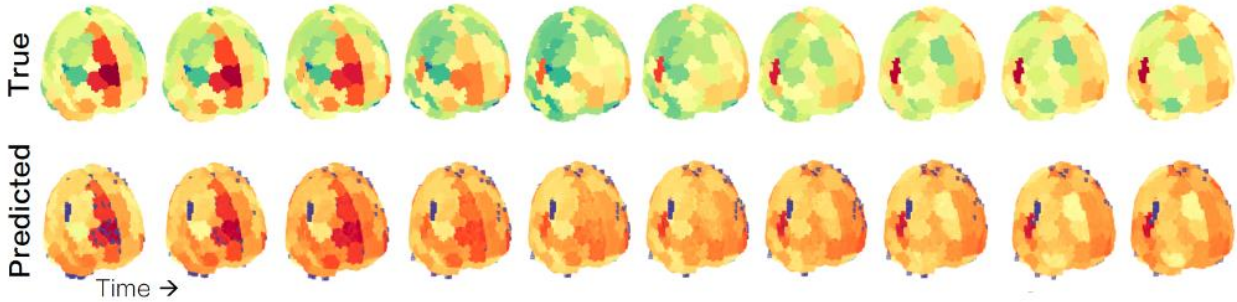

Figure 6.4. True and predicted brain activity.
Preliminary results from training the 3D extension of the PredNet architecture on only 43 seconds of resting fMRI data.

6.7 Acknowledgments

I would like to thank Parmida Davarmanesh, Aman Taxali, Saige Rutherford and Mike Angstadt for their support and valuable feedback throughout this work. I especially thank Yujun Yan

and Jiong Zhu for their technical support in relation to this work and valuable methodological feedback. I would also like to acknowledge the contributions of my co-authors of this work, Danai Koutra and Chandra Sripada.

This work was supported by funding from the University of Michigan Precision Health Investigator Award, the National Science Foundation Graduate Research Fellowship Program grant DGE-1256260, and the Nvidia Academic GPU grant.

Chapter 7 - Discussion

7.1 Summary of Main Findings

In this dissertation, we introduce the informed segmentation framework—a novel approach for uncovering time-varying changes in functional connectivity in resting state functional neuroimaging time series. Broadly, this newly proposed approach centers around tailored segmentation of fMRI time series at candidate FC state change points, which are informed by various instantaneous representations of functional activation and connectivity. The informed-segmentation framework serves as a data-driven alternative approach that bridges instantaneous and windowed methods for studying TVFC, in an attempt to mitigate the limitations of each while simultaneously leveraging the advantages of both.

This dissertation also serves as a compendium of instantaneous, windowed, and segmentation-based methodologies for assessing TVFC in resting state fMRI data. We apply rigorous evaluation of the accuracy of each TVFC approach against a standardized framework, which centers around the use of block-design task data as a naturalistic ground truth. As such, this work serves as the largest head-to-head comparative study of existing TVFC methodologies to date.

In Chapter 3, we present the activation-informed segmentation framework that is built upon FC state transition points estimated from changes in whole-brain functional activation. We found that

the activation-informed segmentation outperformed the conventional sliding window approach in accurately recovering time-varying connectivity structure evoked by changing cognitive task demands. When applied in resting state, the activation-informed segmentation method detected five brain states that exhibited distinct connectivity signatures, were highly reliable across experimental replicates, and were shown to be associated with individual variation in facets of cognition, behavior, and personality.

In Chapter 4, we conduct an extensive comparative analysis of three instantaneous FC estimators (ECF, MTD and DCC), and further combine each instantaneous FC method with state estimation approaches, including two distinct variants of our newly proposed connectivity-informed segmentation framework. Our results suggest that ECF-generated estimates of instantaneous FC captured changing connectivity evoked by known cognitive processes better than those of the MTD or DCC methods, and that combining the ECF with our novel connectivity-informed segmentation paradigm provided the best reconstruction of the underlying WM task structure overall. When applied in the resting state, this ECF + connectivity-informed segmentation framework detected five recurring brain states that largely recapitulated those identified via activation-informed segmentation. This convergence in resting brain states detected via parallel, yet distinct, methodologies underscores the utility of informed segmentation paradigms, and similarly points to these states as being cognitively meaningful.

In Chapter 5, we present a comparative analysis between data-driven and model-based approaches for instantaneous estimation of brain states, represented by the CAP and HMM approaches, in both the activation and connectivity domains. We observed that applying HMMs in

the connectivity (rather than activation) domain, specifically in conjunction with ECF-derived estimates of instantaneous FC, improved the prediction of underlying brain states. Conversely, we found that co-activation patterns outperformed co-connectivity patterns in discriminating between known cognitive states in the WM task, likely due to the nature of the increasing task difficulty, rather than cognitive task switching, in this specific task design. By applying CAP analysis in resting state, we identified four brain states that were characterized by short dwell times and fast oscillations, as well as similar connectivity motifs as states identified via informed segmentation approaches.

Finally, in Chapter 6, we introduce plans for a spatiotemporal-informed segmentation approach, which leverages recurrent neural network architectures to identify anomalous time points within the fMRI time series and generate tailored segments at these boundaries. We provide some initial proof-of-concept results supporting the future exploration of this framework.

7.2 Emerging Themes

7.2.1 Converging Evidence Across Diverse Methodologies Supports the Existence of TVFC During Rest

In this dissertation, we describe the results of three distinct TVFC pipelines, each with differing methodological considerations and baseline treatments of the fMRI data, that converge on a set of four to five recurring connectivity states within the resting condition. Across these methodologies, the resultant connectivity states exhibit several characteristic connectivity motifs. First, we find that most states are largely characterized by coherence or anti-coherence between the set of

medial frontal, frontoparietal or default mode networks and the visual/motor networks. This theme extended from the connectivity space (Chapter 3 and Chapter 4) to the activation space (Chapter 5). Second, we observed that many of these states were marked by a characteristic coupling in the patterns of default mode connectivity with motor/sensory networks and the medial frontal connectivity with motor/sensory networks, which appeared to oppose the connectivity patterns of the frontoparietal network with the motor/sensory networks. This motif was most evident in the ECF + connectivity-informed segmentation framework (Chapter 4) but was also evident to lesser extents in the results from the other two approaches. Finally, we observe that many of the discovered resting states are characterized by changing patterns of brain integration (i.e., within-network connectivity) and segregation (i.e., cross-network connectivity). This feature is predominantly observed in the connectivity states derived from the activation- and connectivity-informed segmentation frameworks, however, evidence for such patterns exists in the CAP-derived resting states as well.

Not only do we see a convergence across the methodologies tested within these collected works, but we also see convergence with states derived from sliding window approaches (Calhoun et al., 2014; Nomi et al., 2017) and HMM modeling (Shappell et al., 2021). The consequence of such divergent approaches resulting in such closely related states is multifaceted. First, it lends support to the informed segmentation paradigm as a whole. One of the main advantages of our proposed framework is its ability to significantly reduce the temporal dimensionality of the data compared to leading windowed and instantaneous approaches while still accurately localizing state change points in the fMRI time series. Demonstrating that the states derived by our informed segmentation approaches

mirror those generated by higher dimensional methods supports the claim that our proposed framework accurately and efficiently summarizes the data in a way that is relevant for uncovering changing connectivity states. Second, this convergence also suggests that the set of four to five resting states uncovered in this work, that are shown to be highly stable across fMRI sessions and TVFC methodologies, are meaningful and merit further study. This claim is underscored by the associations of our discovered states across a variety of behavioral and cognitive phenotypes. Finally, the convergence of results across divergent methodologies as well as across various domains of the fMRI time series provide compelling evidence for the existence of true time-varying functional states in the resting condition.

7.2.2 Block-Design Task Data Can Serve as a Natural Ground Truth for Testing TVFC Performance

Another main theme throughout this dissertation is the importance of the evaluation of TVFC methods in the context of ground truth. In true resting state fMRI, the timings of changing functional states or cognitive processes cannot be known as they are not tied to any exogenous stimulus, therefore evaluation of TVFC methodologies remains a challenge. Many works describing new TVFC frameworks choose to evaluate their proposed methodology against simulated data, where the underlying connectivity structure can be controlled across time. While simulation studies provide some evaluational utility, it is difficult to clearly understand how performance in simulations translates into the resting state, wherein many factors about the underlying functional dynamics are still unknown and therefore impossible to mimic in structured simulations. Beyond this, simulation

parameters (i.e., simulated TR, length of time series, temporal scale of dynamic changes, strength of state transitions, occupancy in multiple states, stark or blurred state boundaries, etc.) can vary drastically from study to study, making it difficult to evaluate the performance of comparable TVFC methodologies directly.

In this work, we suggest the adoption of structured, block-design task-evoked fMRI as a natural ground truth for evaluation of TVFC methods. Here, we utilized the WM task from the HCP dataset, as we found several design elements of that task structure to be advantageous for our purposes. First, the length of the task and rest blocks (27.5 and 15 seconds, respectively) were sufficiently long and resembled previously reported timescales of time-varying states in rest (Allen et al., 2014; Nomi et al., 2017). Moreover, the inclusion of both 0-back and 2-back working memory task blocks in addition to resting blocks enabled the evaluation of the specificity of each method for identification of certain types of state changes, such as fundamental changes in cognitive state (Task → Rest junctures), as well as more nuanced transitions that represent changing strength of underlying cognitive processes (Task 1 → Task 2 junctures). Specifically, we evaluated the accuracy of the final state predictions of each method considered throughout this work against the underlying ground truth task condition, and additionally evaluated the precision and recall of the change point analysis step of our activation- and connectivity-informed segmentation frameworks in identifying true junctures between known cognitive states. Finally, the entire HCP dataset is collected at a single site using a single scanner, preventing possible artifacts due to scanner calibration, and removing the need to control for site- or scanner-related variability.

Encouragingly, all methodologies tested throughout this work are shown to capture the changing connectivity structure of the WM task to some degree (Figures 3.3, 3.4, 4.2, 4.3, 4.4, 5.2, 5.3). This result suggests that 1) changes in underlying cognitive processes elicit substantial changes in activation and connectivity structure of the BOLD fMRI data, and 2) such changes are identifiable via a variety of parallel TVFC approaches.

A substantial contribution of this dissertation that we wish to highlight is the publication of standardized performance benchmarks for several of the top TVFC methodologies in one of the richest, publicly available neuroimaging datasets currently available. We encourage the use of such benchmarks for new methods proposed in the future to provide better contextualization of the proposed approach within the methodological landscape of TVFC, which is vast and continually evolving, as we've shown throughout this dissertation.

7.3.3 Data-Driven Informed Segmentation Approaches Outperform Purely Instantaneous and Rigid Windowing Approaches

In this dissertation, we have presented an extensive set of comparative analyses between several established classes of TVFC methods, namely instantaneous FC/state estimators and sliding window methodologies, and our newly proposed informed segmentation framework, which serves as a hybrid between noisy instantaneous methods and rigid windowing approaches. Across these extensive benchmarking studies, the informed segmentation consistently outperformed both instantaneous and sliding window-based methods. This held true across several metrics, ranging from the percent

variance explained by a fixed number of principal components to accuracy of state predictions and precision/recall of task condition onset points.

We found the activation-informed segmentation had the best performance overall, with an average precision of 0.72, average recall of 0.66, and average homogeneity/NMI between the resultant state predictions and ground truth labels of 0.280/0.195. The connectivity-informed segmentation framework exhibited slightly lowered performance compared to the activation-informed segmentation, with an average precision of 0.58, average recall of 0.66, and average homogeneity/NMI between the resultant state predictions and ground truth labels of 0.116/0.140. Interestingly, though the overall performance of the connectivity-informed segmentation method was lower compared to the activation-informed segmentation, we observed an increase in recall of Task 1 to Task 2 transitions from 0.57 in the activation-informed segmentation to 0.63 in the connectivity-informed segmentation framework. This result suggests that connectivity-informed segmentation approaches may be better suited than activation-informed segmentation approaches for identifying nuanced changes in cognitive processes. Further discussion on the difference in performance between activation- and connectivity- analyses is discussed in Section 7.3.4. In both cases, informed segmentation prevailed over the other comparable methods in their respective analyses.

7.3.4 Activation-Centric Methods Prevail Over Analogous Connectivity-Based Approaches

In a somewhat unexpected finding, we observed that activation-based methods outperformed the analogous connectivity-based approaches in two of three analyses. Specifically, we found that activation-informed connectivity outperformed connectivity-informed segmentation, and activation-based CAP clustering outperformed the analogous connectivity-based pointwise clustering. Only in the context of HMMs did the inclusion of instantaneous connectivity estimates improve the state prediction of the framework overall.

This result could potentially be attributed to the change in dimensionality when moving from the activation space (n = 268 ROIs) to the connectivity space (n = 35,778 edges). In the case of informed segmentation, summarizing global changes in moment-to-moment functional connectivity requires averaging over a much larger number of edge-specific values to generate the GCD series compared to the summarization over the ROI-specific activation changes to generate the analogous GTD. As such, strong changes across a small number of edges may not be as readily identifiable by our informed segmentation approach in the connectivity domain as a similar change in activations across a small number of ROIs would be in the activation domain.

Beyond the change point identification within the informed segmentation, this discrepancy in dimensionality has implications in the way the activation and connectivity time series are represented for the CAP and HMM approaches. We found the dimensionality of n=268 ROIs in the activation

space to be manageable for both *k*-means clustering and multivariate HMM fitting, so activation time series were not dimensionality reduced. Conversely, we utilized PCA-based dimensionality reduction to make clustering and HMM fitting in the connectivity domain computationally feasible. In Chapter 4, we report that the PCA-reduced feature set utilizing the top 100 PCs only captured ~30% of the total PVE across all instantaneous connectivity estimators. While initial experimentation did not show a significant decrease in performance in the clustering accuracy between the PCA-reduced data and the full vectorized connectome upper triangular, it is possible that this dimensionality reduction step had downstream effects that were not present in the unreduced activation data. Future work may consider testing other methodologies for reduced representations of connectivity matrices, including graph embedding approaches such as GraphWave.

7.3.4 ECF Shows Promise for Instantaneous FC Estimation

Though the activation-centric methods generally produced better reconstructions of underlying state structure in the WM evaluations, this is not to say that instantaneous connectivity time series are not useful as well. In fact, our evidence points to the contrary, especially in the context of HMMs. One clear theme that existed in the results from Chapters 4 & 5 was that ECF appeared to be the most promising methodology for estimating instantaneous FC. This assessment was not only based on the performance of the ECF across our studies, but also due to its computational simplicity, scalability to a large number of ROIs and direct connection to the popular and familiar metric of Pearson correlation. Taken together, the performance, efficiency, and interpretability of the ECF

suggests that future work aiming to localize instantaneous changes in functional connectivity should consider incorporation of this method.

7.3 Broader Limitations

In addition to the specific limitations discussed in each chapter, there exist several limitations that apply to the whole of this dissertation that we wish to address. First, all clustering analyses in this work rely on the standard implementation of *k*-means clustering based on Euclidean distances. Prior work has suggested the use of alternative methods, including hierarchical clustering (Ou et al., 2015, 2013) or *k*-means clustering paired with city-block distances (Allen et al., 2014). Early testing in our analyses did not point to increased accuracy in clustering when incorporating such methods and considering the number of moving parts already incorporated into our study designs, we chose not to introduce further degrees of freedom.

Furthermore, we were limited by the availability of public data, specifically for block-design task fMRI to serve as our evaluation set. For this reason, all our benchmarks are computed exclusively with respect to the WM task of the HCP data. While this task contained several design elements that were advantageous for our purposes (Section 7.2.2), our performance benchmarks are limited to interpretation within the context of this task only. Adding benchmarks in the context of other tasks in future studies would serve to bolster our results, as well as provide a more specific understanding of the kinds of cognitive transitions each method is capable of detecting. However, care must be taken in the kinds of tasks utilized for performance benchmarking, as task changes on a timescale much shorter

than that of the WM data may be 1) difficult to identify reliably with the currently available methodologies and 2) may not translate well to true FC states within rest.

Finally, all the analyses presented in this dissertation were computed with respect to the functional parcellation defined in (Finn et al., 2015). This had implications for the dimensionality of the data and the possible characterizations of the resultant states, which were limited by the subnetworks defined within this parcellation. Future work may explore how our results relate to those in similar pipelines that use other functionally derived parcellations, or data-driven alternatives such as spatial ICA (Calhoun et al., 2001).

7.3 Impacts

There are several important impacts of the work presented throughout this dissertation. Most consequentially, our work addresses several areas of need in the field of TVFC as presented in Section 2.6. We have proposed two distinct, yet related, approaches for assessing TVFC within the larger framework of informed segmentation, which operate in both the activation and connectivity domains. This method enables data-driven identification of change points in the time series and results in tailored, variably sized segments of stable FC, enabling the identification of temporally changing patterns of connectivity without imposing rigid and arbitrary time scale demands. We also conduct a systematic assessment of the major existing methodologies for studying TVFC, which provides performance benchmarks and examines the strengths and weaknesses of each approach, both methodologically and based on their observed performance. Finally, we provide recommendations for

standardized benchmarking practices that will enable clear and fair comparisons across methodologies. We hope that researchers in the field of TVFC will utilize our newly developed informed segmentation framework in their own analyses to continue the robust validation of our methods, as well as to extract novel insights about time-varying patterns of rsFC in typical and atypical cognition. We believe that the results of our comparative analysis may help inform design choices in future TVFC studies, and hope that the standardized benchmarking approaches, such as the block-design task data utilized here, will be widely adopted in future assessments of both new and existing TVFC methodologies.

7.4 Future Directions

There are several branching paths for future research stemming from the results presented within this dissertation. Many of these have been discussed within their relevant chapters, so here we focus on a few remaining "high-level" directions. Broadly, these remaining directions can be categorized into two branches: methodological directions and experimental directions.

7.4.1 Methodological Directions

In Chapter 6, we provide a brief introduction to preliminary work on an extension of our informed segmentation framework in the spatiotemporal domain of fMRI data. Specifically, we propose the use of a recurrent neural network to generate pointwise estimates of 3-dimensional fMRI frames at time *t*, using information extracted from time point *t-1* and prior. Informed segmentation can then be performed on the resultant prediction error series, under the assumption that peaks in the prediction error correspond to a sudden change in the connectivity structure governing the data from

the model's learned connectivity pattern to something new. While preliminary results suggest that 1) true changes in the connectivity structure of the data would elicit such behavior in the error series and that 2) the model can capture complex underlying connectivity patterns with some baseline degree of accuracy, more extensive applications of this framework are required to fully evaluate its performance. Immediate future directions in this space involve training and testing of deep learning models in WM data and evaluating the accuracy of change point detection with respect to ground truth changes in task condition. Beyond this, future work may also adapt and test more recent state-of-the-art deep learning models for handling sequence data, such as transformer architectures (Vaswani, 2017).

7.4.2 Experimental Directions

As mentioned above, one of the overarching limitations of this work is the singular use of the HCP WM task data as a ground truth for evaluation of the methodologies considered throughout. While we have reiterated why the design of this particular block-design task is especially suitable for our purposes, validation of our results across a variety of changing cognitive processes and contexts is required to gain a holistic understanding of the benefits and limitations of each approach. One promising avenue for continued evaluation of these methods is in the context of passive naturalistic stimuli, such as watching a movie or listening to an audio recording (Betzel et al., 2020). The use of these naturalistic stimuli provides the benefit of temporal alignment between subjects without imposing any explicit task demands, thereby more closely mimicking the kinds of cognitive variations (and associated connectivity changes) one might expect in a task-free resting state scan.

Thought probes provide another naturalistic framework that may be useful for testing the methodologies presented throughout this work. The thought probe framework can be implemented using experience sampling (Kucyi & Davis, 2014) or stream of thought narration (Sripada & Taxali, 2020) within the otherwise standard resting state setting. The benefit of these approaches is their ability to localize spontaneous thought in time, and though they may not exactly replicate the stream-of-consciousness progression that occurs in "pure" unprobed rest, they likely provide a closer approximation of resting state dynamics than other block-design tasks and would be worth exploring. The main caveat to the thought probe and passive movie watching frameworks is that these types of datasets are usually proprietary, and consist of only tens of subjects, compared to the almost 1000 subjects publicly available in the HCP.

Finally, another beneficial future direction of this work would be to apply the informed segmentation frameworks in resting state data from clinical populations. Such a study could examine the differences in the resultant states between patients and healthy controls, which we have shown through our HCP experiments exhibit highly reliable and replicable connectivity signatures. Not only would this provide further validation of our method, but it would also enable us to draw further insights into the clinical correlates of TVFC.

7.5 Conclusions

In this dissertation, we introduce a new data-driven approach for identifying time-varying functional connectivity in resting state fMRI data. This novel framework, termed the informed segmentation framework, bridges the existing instantaneous and windowed classes of methods, in an attempt to mitigate the limitations of each while also leveraging the advantages of both. We performed systematic and rigorous comparative analyses to evaluate the performance of our proposed framework against several existing TVFC frameworks and showed that our informed segmentation method outperformed existing methodologies in identifying known transitions between cognitive states in task. The activation- and connectivity-informed segmentation frameworks detected a convergent set of five time-varying connectivity states at rest that exhibited high reliability across experimental replicates and significant associations with various facets of human behavior and cognition. This work not only expands the methodological toolkit for the detection of TVFC in rest, but also provides valuable performance benchmarks across several popular classes of existing TVFC approaches that we anticipate will help shape the design of future TVFC studies.

Bibliography

Allen, E. A., Damaraju, E., Eichele, T., Wu, L., & Calhoun, V. D. (2018). EEG signatures of dynamic functional network connectivity states. *Brain Topography*, *31*(1), 101–116. https://doi.org/10.1007/s10548-017-0546-2

Allen, E. A., Damaraju, E., Plis, S. M., Erhardt, E. B., Eichele, T., & Calhoun, V. D. (2014). Tracking whole-brain connectivity dynamics in the resting state. *Cerebral Cortex (New York, N.Y.: 1991)*, *24*(3), 663–676. https://doi.org/10.1093/cercor/bhs352

Andrews-Hanna, J. R., Reidler, J. S., Huang, C., & Buckner, R. L. (2010). Evidence for the default network's role in spontaneous cognition. *Journal of Neurophysiology*, *104*(1), 322–335. https://doi.org/10.1152/jn.00830.2009

Baker, A. P., Brookes, M. J., Rezek, I. A., Smith, S. M., Behrens, T., Probert Smith, P. J., & Woolrich, M. (2014). Fast transient networks in spontaneous human brain activity. *ELife*, *3*, e01867. https://doi.org/10.7554/eLife.01867

Bassett, D. S., Wymbs, N. F., Porter, M. A., Mucha, P. J., Carlson, J. M., & Grafton, S. T. (2011). Dynamic reconfiguration of human brain networks during learning. *Proceedings of the National Academy of Sciences*, *108*(18), 7641–7646.

Baum, L. E., Petrie, T., Soules, G., & Weiss, N. (1970). A Maximization Technique Occurring in the Statistical Analysis of Probabilistic Functions of Markov Chains. *The Annals of Mathematical*

Statistics, *41*(1), 164–171. https://doi.org/10.1214/aoms/1177697196

Betzel, R. F., Byrge, L., Esfahlani, F. Z., & Kennedy, D. P. (2020). Temporal fluctuations in the brain's modular architecture during movie-watching. *NeuroImage*, *213*, 116687. https://doi.org/10.1016/j.neuroimage.2020.116687

Betzel, R. F., Fukushima, M., He, Y., Zuo, X.-N., & Sporns, O. (2016). Dynamic fluctuations coincide with periods of high and low modularity in resting-state functional brain networks. *NeuroImage*, *127*, 287–297. https://doi.org/10.1016/j.neuroimage.2015.12.001

Biswal, B., Yetkin, F. Z., Haughton, V. M., & Hyde, J. S. (1995). Functional connectivity in the motor cortex of resting human brain using echo-planar mri. *Magnetic Resonance in Medicine*, *34*(4), 537–541. https://doi.org/10.1002/mrm.1910340409

Bluhm, R. L., Miller, J., Lanius, R. A., Osuch, E. A., Boksman, K., Neufeld, R., Théberge, J., Schaefer, B., & Williamson, P. (2007). Spontaneous Low-Frequency Fluctuations in the BOLD Signal in Schizophrenic Patients: Anomalies in the Default Network. *Schizophrenia Bulletin*, *33*(4), 1004–1012. https://doi.org/10.1093/schbul/sbm052

Bluhm, R. L., Miller, J., Lanius, R. A., Osuch, E. A., Boksman, K., Neufeld, R. W. J., Théberge, J., Schaefer, B., & Williamson, P. C. (2009). Retrosplenial cortex connectivity in schizophrenia. *Psychiatry Research: Neuroimaging*, *174*(1), 17–23. https://doi.org/10.1016/j.pscychresns.2009.03.010

Bridgeford, E. W., Wang, S., Yang, Z., Wang, Z., Xu, T., Craddock, C., Dey, J., Kiar, G., Gray-Roncal, W., Coulantoni, C., Douville, C., Priebe, C. E., Caffo, B., Milham, M., Zuo, X.-N., &

Vogelstein, J. T. (2020). *Big Data Reproducibility: Applications in Brain Imaging and Genomics*. 29.

Buckner, R. L., Andrews-Hanna, J. R., & Schacter, D. L. (2008). The brain's default network: Anatomy, function, and relevance to disease. *Annals of the New York Academy of Sciences*, *1124*, 1–38. https://doi.org/10.1196/annals.1440.011

Cabeza, R., & Nyberg, L. (2000). Imaging cognition II: An empirical review of 275 PET and fMRI studies. *Journal of Cognitive Neuroscience*, *12*(1), 1–47. https://doi.org/10.1162/08989290051137585

Cabral, J., Vidaurre, D., Marques, P., Magalhães, R., Silva Moreira, P., Miguel Soares, J., Deco, G., Sousa, N., & Kringelbach, M. L. (2017). Cognitive performance in healthy older adults relates to spontaneous switching between states of functional connectivity during rest. *Scientific Reports*, *7*. https://doi.org/10.1038/s41598-017-05425-7

Cai, B., Zille, P., Stephen, J. M., Wilson, T. W., Calhoun, V. D., & Wang, Y. P. (2018). Estimation of Dynamic Sparse Connectivity Patterns From Resting State fMRI. *IEEE Transactions on Medical Imaging*, *37*(5), 1224–1234. https://doi.org/10.1109/TMI.2017.2786553

Calhoun, V. D., Adali, T., Pearlson, G. D., & Pekar, J. J. (2001). A method for making group inferences from functional MRI data using independent component analysis. *Human Brain Mapping*, *14*(3), 140–151. https://doi.org/10.1002/hbm.1048

Calhoun, V. D., Miller, R., Pearlson, G., & Adalı, T. (2014). The Chronnectome: Time-Varying Connectivity Networks as the Next Frontier in fMRI Data Discovery. *Neuron*, *84*(2), 262–

274. https://doi.org/10.1016/j.neuron.2014.10.015

Chang, C., & Glover, G. H. (2010). Time-frequency dynamics of resting-state brain connectivity measured with fMRI. *NeuroImage*, *50*(1), 81–98. https://doi.org/10.1016/j.neuroimage.2009.12.011

Chang, C., Liu, Z., Chen, M. C., Liu, X., & Duyn, J. H. (2013). EEG correlates of time-varying BOLD functional connectivity. *NeuroImage*, *72*, 227–236. https://doi.org/10.1016/j.neuroimage.2013.01.049

Chen, J. E., Chang, C., Greicius, M. D., & Glover, G. H. (2015). Introducing co-activation pattern metrics to quantify spontaneous brain network dynamics. *NeuroImage*, *111*, 476–488. https://doi.org/10.1016/j.neuroimage.2015.01.057

Chen, T., Cai, W., Ryali, S., Supekar, K., & Menon, V. (2016). Distinct Global Brain Dynamics and Spatiotemporal Organization of the Salience Network. *PLoS Biology*, *14*(6). https://doi.org/10.1371/journal.pbio.1002469

Choe, A. S., Jones, C. K., Joel, S. E., Muschelli, J., Belegu, V., Caffo, B. S., Lindquist, M. A., Zijl, P. C. M. van, & Pekar, J. J. (2015). Reproducibility and Temporal Structure in Weekly Resting-State fMRI over a Period of 3.5 Years. *PLOS ONE*, *10*(10), e0140134. https://doi.org/10.1371/journal.pone.0140134

Choe, A. S., Nebel, M. B., Barber, A. D., Cohen, J. R., Xu, Y., Pekar, J. J., Caffo, B., & Lindquist, M. A. (2017). Comparing Test-Retest Reliability of Dynamic Functional Connectivity Methods. *NeuroImage*, *158*, 155–175. https://doi.org/10.1016/j.neuroimage.2017.07.005

Cohen, J. R. (2018). The Behavioral and Cognitive Relevance of Time-Varying, Dynamic Changes in Functional Connectivity. *NeuroImage*, *180*(Pt B), 515–525. https://doi.org/10.1016/j.neuroimage.2017.09.036

Cole, M. W., & Schneider, W. (2007). The cognitive control network: Integrated cortical regions with dissociable functions. *NeuroImage*, *37*(1), 343–360. https://doi.org/10.1016/j.neuroimage.2007.03.071

Cole, M. W., Yarkoni, T., Repovš, G., Anticevic, A., & Braver, T. S. (2012). Global Connectivity of Prefrontal Cortex Predicts Cognitive Control and Intelligence. *Journal of Neuroscience*, *32*(26), 8988–8999. https://doi.org/10.1523/JNEUROSCI.0536-12.2012

Cordes, D., Haughton, V. M., Arfanakis, K., Carew, J. D., Turski, P. A., Moritz, C. H., Quigley, M. A., & Meyerand, M. E. (2001). Frequencies contributing to functional connectivity in the cerebral cortex in "resting-state" data. *American Journal of Neuroradiology*, *22*(7), 1326–1333. Scopus.

Cordes, D., Zhuang, X., Kaleem, M., Sreenivasan, K., Yang, Z., Mishra, V., Banks, S. J., Bluett, B., & Cummings, J. L. (2018). Advances in functional magnetic resonance imaging data analysis methods using Empirical Mode Decomposition to investigate temporal changes in early Parkinson's disease. *Alzheimer's & Dementia: Translational Research & Clinical Interventions*, *4*, 372–386. https://doi.org/10.1016/j.trci.2018.04.009

Damaraju, E., Allen, E. A., Belger, A., Ford, J. M., McEwen, S., Mathalon, D. H., Mueller, B. A., Pearlson, G. D., Potkin, S. G., Preda, A., Turner, J. A., Vaidya, J. G., van Erp, T. G., &

Calhoun, V. D. (2014). Dynamic functional connectivity analysis reveals transient states of dysconnectivity in schizophrenia. *NeuroImage. Clinical*, *5*, 298–308. https://doi.org/10.1016/j.nicl.2014.07.003

Davison, E. N., Schlesinger, K. J., Bassett, D. S., Lynall, M.-E., Miller, M. B., Grafton, S. T., & Carlson, J. M. (2015). Brain Network Adaptability across Task States. *PLOS Computational Biology*, *11*(1), e1004029. https://doi.org/10.1371/journal.pcbi.1004029

de Lacy, N., Doherty, D., King, B. H., Rachakonda, S., & Calhoun, V. D. (2017). Disruption to control network function correlates with altered dynamic connectivity in the wider autism spectrum. *NeuroImage: Clinical*, *15*, 513–524. https://doi.org/10.1016/j.nicl.2017.05.024

Díez-Cirarda, M., Strafella, A. P., Kim, J., Peña, J., Ojeda, N., Cabrera-Zubizarreta, A., & Ibarretxe-Bilbao, N. (2018). Dynamic functional connectivity in Parkinson's disease patients with mild cognitive impairment and normal cognition. *NeuroImage: Clinical*, *17*, 847–855. https://doi.org/10.1016/j.nicl.2017.12.013

Donnat, C., Zitnik, M., Hallac, D., & Leskovec, J. (2018). Learning Structural Node Embeddings via Diffusion Wavelets. *Proceedings of the 24th ACM SIGKDD International Conference on Knowledge Discovery & Data Mining*, 1320–1329. https://doi.org/10.1145/3219819.3220025

Du, Y., Pearlson, G. D., Yu, Q., He, H., Lin, D., Sui, J., Wu, L., & Calhoun, V. D. (2016). Interaction among subsystems within default mode network diminished in schizophrenia patients: A dynamic connectivity approach. *Schizophrenia Research*, *170*(1), 55–65.

https://doi.org/10.1016/j.schres.2015.11.021

Duda, M., Koutra, D., & Sripada, C. (2020). Validating Dynamicity in Resting State fMRI with Activation-Informed Temporal Segmentation. *BioRxiv*, 2020.10.12.335976. https://doi.org/10.1101/2020.10.12.335976

Engle, R. F. (2000). Dynamic Conditional Correlation—A Simple Class of Multivariate GARCH Models. *SSRN Electronic Journal*. https://doi.org/10.2139/ssrn.236998

Esfahlani, F. Z., Jo, Y., Faskowitz, J., Byrge, L., Kennedy, D. P., Sporns, O., & Betzel, R. F. (2020). High-amplitude cofluctuations in cortical activity drive functional connectivity. *Proceedings of the National Academy of Sciences*, *117*(45), 28393–28401. https://doi.org/10.1073/pnas.2005531117

Faghiri, A., Iraji, A., Damaraju, E., Belger, A., Ford, J., Mathalon, D., Mcewen, S., Mueller, B., Pearlson, G., Preda, A., Turner, J., Vaidya, J. G., Van Erp, T. G. M., & Calhoun, V. D. (2020). Weighted average of shared trajectory: A new estimator for dynamic functional connectivity efficiently estimates both rapid and slow changes over time. *Journal of Neuroscience Methods*, *334*, 108600. https://doi.org/10.1016/j.jneumeth.2020.108600

Faskowitz, J., Esfahlani, F. Z., Jo, Y., Sporns, O., & Betzel, R. F. (2020). Edge-centric functional network representations of human cerebral cortex reveal overlapping system-level architecture. *Nature Neuroscience*, *23*(12), 1644–1654. https://doi.org/10.1038/s41593-020-00719-y

Finn, E. S., Shen, X., Scheinost, D., Rosenberg, M. D., Huang, J., Chun, M. M., Papademetris, X., & Constable, R. T. (2015). Functional connectome fingerprinting: Identifying individuals using

patterns of brain connectivity. *Nature Neuroscience*, *18*(11), 1664–1671. https://doi.org/10.1038/nn.4135

Fisher, R. A. (1915). Frequency Distribution of the Values of the Correlation Coefficient in Samples from an Indefinitely Large Population. *Biometrika*, *10*(4), 507–521. JSTOR. https://doi.org/10.2307/2331838

Forney, G. D. (1973). The viterbi algorithm. *Proceedings of the IEEE*, *61*(3), 268–278. https://doi.org/10.1109/PROC.1973.9030

Fox, M. D., & Greicius, M. D. (2010). Clinical applications of resting state functional connectivity. *Frontiers in Systems Neuroscience*, *4*. https://doi.org/10.3389/fnsys.2010.00019

Fox, M. D., & Raichle, M. E. (2007). Spontaneous fluctuations in brain activity observed with functional magnetic resonance imaging. *Nature Reviews Neuroscience*, *8*(9), 700–711. https://doi.org/10.1038/nrn2201

Friston, K. J. (2003). Statistical Parametric Mapping. In R. Kötter (Ed.), *Neuroscience Databases: A Practical Guide* (pp. 237–250). Springer US. https://doi.org/10.1007/978-1-4615-1079-6_16

Fu, Z., Sui, J., Turner, J. A., Du, Y., Assaf, M., Pearlson, G. D., & Calhoun, V. D. (2021). Dynamic functional network reconfiguration underlying the pathophysiology of schizophrenia and autism spectrum disorder. *Human Brain Mapping*, *42*(1), 80–94. https://doi.org/10.1002/hbm.25205

Glasser, M. F., Sotiropoulos, S. N., Wilson, J. A., Coalson, T. S., Fischl, B., Andersson, J. L., Xu, J., Jbabdi, S., Webster, M., Polimeni, J. R., Van Essen, D. C., Jenkinson, M., & WU-Minn HCP

Consortium. (2013). The minimal preprocessing pipelines for the Human Connectome Project. *NeuroImage*, *80*, 105–124. https://doi.org/10.1016/j.neuroimage.2013.04.127

Gonzalez-Castillo, J., Hoy, C. W., Handwerker, D. A., Robinson, M. E., Buchanan, L. C., Saad, Z. S., & Bandettini, P. A. (2015). Tracking ongoing cognition in individuals using brief, whole-brain functional connectivity patterns. *Proceedings of the National Academy of Sciences*, *112*(28), 8762–8767. https://doi.org/10.1073/pnas.1501242112

Greicius, M. D. (2008). Resting-state functional connectivity in neuropsychiatric disorders. *Current Opinion in Neurology*, *21*(4), 424–430. https://doi.org/10.1097/WCO.0b013e328306f2c5

Greicius, M. D., Flores, B. H., Menon, V., Glover, G. H., Solvason, H. B., Kenna, H., Reiss, A. L., & Schatzberg, A. F. (2007). Resting-State Functional Connectivity in Major Depression: Abnormally Increased Contributions from Subgenual Cingulate Cortex and Thalamus. *Biological Psychiatry*, *62*(5), 429–437. https://doi.org/10.1016/j.biopsych.2006.09.020

Greicius, M. D., Krasnow, B., Reiss, A. L., & Menon, V. (2003). Functional connectivity in the resting brain: A network analysis of the default mode hypothesis. *Proceedings of the National Academy of Sciences*, *100*(1), 253–258. https://doi.org/10.1073/pnas.0135058100

Greicius, M. D., Srivastava, G., Reiss, A. L., & Menon, V. (2004). Default-mode network activity distinguishes Alzheimer's disease from healthy aging: Evidence from functional MRI. *Proceedings of the National Academy of Sciences*, *101*(13), 4637–4642. https://doi.org/10.1073/pnas.0308627101

Hafner, C. M., & Reznikova, O. (2012). On the estimation of dynamic conditional correlation

models. *Computational Statistics & Data Analysis*, *56*(11), 3533–3545. https://doi.org/10.1016/j.csda.2010.09.022

Hampson, M., Driesen, N. R., Skudlarski, P., Gore, J. C., & Constable, R. T. (2006). Brain Connectivity Related to Working Memory Performance. *Journal of Neuroscience*, *26*(51), 13338–13343. https://doi.org/10.1523/JNEUROSCI.3408-06.2006

Harlalka, V., Bapi, R. S., Vinod, P. K., & Roy, D. (2019). Atypical Flexibility in Dynamic Functional Connectivity Quantifies the Severity in Autism Spectrum Disorder. *Frontiers in Human Neuroscience*, *13*. https://doi.org/10.3389/fnhum.2019.00006

He, B. J., Snyder, A. Z., Vincent, J. L., Epstein, A., Shulman, G. L., & Corbetta, M. (2007). Breakdown of Functional Connectivity in Frontoparietal Networks Underlies Behavioral Deficits in Spatial Neglect. *Neuron*, *53*(6), 905–918. https://doi.org/10.1016/j.neuron.2007.02.013

He, C., Chen, Y., Jian, T., Chen, H., Guo, X., Wang, J., Wu, L., Chen, H., & Duan, X. (2018). Dynamic functional connectivity analysis reveals decreased variability of the default-mode network in developing autistic brain. *Autism Research*, *11*(11), 1479–1493. https://doi.org/10.1002/aur.2020

Hedden, T., Dijk, K. R. A. V., Becker, J. A., Mehta, A., Sperling, R. A., Johnson, K. A., & Buckner, R. L. (2009). Disruption of Functional Connectivity in Clinically Normal Older Adults Harboring Amyloid Burden. *Journal of Neuroscience*, *29*(40), 12686–12694. https://doi.org/10.1523/JNEUROSCI.3189-09.2009

Hindriks, R., Adhikari, M. H., Murayama, Y., Ganzetti, M., Mantini, D., Logothetis, N. K., & Deco, G. (2016). Can sliding-window correlations reveal dynamic functional connectivity in resting-state fMRI? *NeuroImage*, *127*, 242–256. https://doi.org/10.1016/j.neuroimage.2015.11.055

Hochreiter, S., & Schmidhuber, J. (1997). Long Short-Term Memory. *Neural Computation*, *9*(8), 1735–1780. https://doi.org/10.1162/neco.1997.9.8.1735

Hull, J. V., Dokovna, L. B., Jacokes, Z. J., Torgerson, C. M., Irimia, A., & Van Horn, J. D. (2017). Resting-State Functional Connectivity in Autism Spectrum Disorders: A Review. *Frontiers in Psychiatry*, *7*. https://doi.org/10.3389/fpsyt.2016.00205

Hutchison, R. M., & Morton, J. B. (2015). Tracking the Brain's Functional Coupling Dynamics over Development. *Journal of Neuroscience*, *35*(17), 6849–6859. https://doi.org/10.1523/JNEUROSCI.4638-14.2015

Hutchison, R. M., Womelsdorf, T., Allen, E. A., Bandettini, P. A., Calhoun, V. D., Corbetta, M., Penna, S. D., Duyn, J. H., Glover, G. H., Gonzalez-Castillo, J., Handwerker, D. A., Keilholz, S., Kiviniemi, V., Leopold, D. A., Pasquale, F. de, Sporns, O., Walter, M., & Chang, C. (2013). Dynamic functional connectivity: Promise, issues, and interpretations. *NeuroImage*, *80*. https://doi.org/10.1016/j.neuroimage.2013.05.079

Hutchison, R. M., Womelsdorf, T., Gati, J. S., Everling, S., & Menon, R. S. (2013). Resting-state networks show dynamic functional connectivity in awake humans and anesthetized macaques. *Human Brain Mapping*, *34*(9), 2154–2177. https://doi.org/10.1002/hbm.22058

Jafri, M. J., Pearlson, G. D., Stevens, M., & Calhoun, V. D. (2008). A method for functional network

connectivity among spatially independent resting-state components in schizophrenia. *NeuroImage*, *39*(4), 1666–1681. https://doi.org/10.1016/j.neuroimage.2007.11.001

Jia, H., Hu, X., & Deshpande, G. (2014). Behavioral Relevance of the Dynamics of the Functional Brain Connectome. *Brain Connectivity*, *4*(9), 741–759. https://doi.org/10.1089/brain.2014.0300

Jin, C., Jia, H., Lanka, P., Rangaprakash, D., Li, L., Liu, T., Hu, X., & Deshpande, G. (2017). Dynamic brain connectivity is a better predictor of PTSD than static connectivity. *Human Brain Mapping*, *38*(9), 4479–4496. https://doi.org/10.1002/hbm.23676

Jones, D. T., Vemuri, P., Murphy, M. C., Gunter, J. L., Senjem, M. L., Machulda, M. M., Przybelski, S. A., Gregg, B. E., Kantarci, K., Knopman, D. S., Boeve, B. F., Petersen, R. C., & Jr, C. R. J. (2012). Non-Stationarity in the "Resting Brain's" Modular Architecture. *PLOS ONE*, *7*(6), e39731. https://doi.org/10.1371/journal.pone.0039731

Kaiser, R. H., Whitfield-Gabrieli, S., Dillon, D. G., Goer, F., Beltzer, M., Minkel, J., Smoski, M., Dichter, G., & Pizzagalli, D. A. (2016). Dynamic Resting-State Functional Connectivity in Major Depression. *Neuropsychopharmacology*, *41*(7), 1822–1830. https://doi.org/10.1038/npp.2015.352

Karahanoğlu, F. I., & Van De Ville, D. (2015). Transient brain activity disentangles fMRI resting-state dynamics in terms of spatially and temporally overlapping networks. *Nature Communications*, *6*(1), 7751. https://doi.org/10.1038/ncomms8751

Keilholz, S. D., Magnuson, M. E., Pan, W.-J., Willis, M., & Thompson, G. J. (2013). Dynamic

Properties of Functional Connectivity in the Rodent. *Brain Connectivity*, *3*(1), 31–40. https://doi.org/10.1089/brain.2012.0115

Killingsworth, M. A., & Gilbert, D. T. (2010). A Wandering Mind Is an Unhappy Mind. *Science*, *330*(6006), 932–932. https://doi.org/10.1126/science.1192439

Kucyi, A., & Davis, K. D. (2014). Dynamic functional connectivity of the default mode network tracks daydreaming. *NeuroImage*, *100*, 471–480. https://doi.org/10.1016/j.neuroimage.2014.06.044

Kucyi, A., Esterman, M., Riley, C. S., & Valera, E. M. (2016). Spontaneous default network activity reflects behavioral variability independent of mind-wandering. *Proceedings of the National Academy of Sciences*, *113*(48), 13899–13904. https://doi.org/10.1073/pnas.1611743113

Kucyi, A., Salomons, T. V., & Davis, K. D. (2013). Mind wandering away from pain dynamically engages antinociceptive and default mode brain networks. *Proceedings of the National Academy of Sciences*, *110*(46), 18692–18697. https://doi.org/10.1073/pnas.1312902110

Laumann, T. O., Snyder, A. Z., Mitra, A., Gordon, E. M., Gratton, C., Adeyemo, B., Gilmore, A. W., Nelson, S. M., Berg, J. J., Greene, D. J., McCarthy, J. E., Tagliazucchi, E., Laufs, H., Schlaggar, B. L., Dosenbach, N. U. F., & Petersen, S. E. (2017). On the Stability of BOLD fMRI Correlations. *Cerebral Cortex (New York, NY)*, *27*(10), 4719–4732. https://doi.org/10.1093/cercor/bhw265

Li, H., & Fan, Y. (2018). Identification of temporal transition of functional states using recurrent neural networks from functional MRI. *ArXiv:1809.05560 [Cs, q-Bio]*.

http://arxiv.org/abs/1809.05560

Li, S.-J., Li, Z., Wu, G., Zhang, M.-J., Franczak, M., & Antuono, P. G. (2002). Alzheimer Disease: Evaluation of a Functional MR Imaging Index as a Marker. *Radiology*, *225*(1), 253–259. https://doi.org/10.1148/radiol.2251011301

Li, Y., Zhu, Y., Nguchu, B. A., Wang, Y., Wang, H., Qiu, B., & Wang, X. (2020). Dynamic Functional Connectivity Reveals Abnormal Variability and Hyper-connected Pattern in Autism Spectrum Disorder. *Autism Research*, *13*(2), 230–243. https://doi.org/10.1002/aur.2212

Liang, M., Zhou, Y., Jiang, T., Liu, Z., Tian, L., Liu, H., & Hao, Y. (2006). Widespread functional disconnectivity in schizophrenia with resting-state functional magnetic resonance imaging. *NeuroReport*, *17*(2), 209–213.

Liégeois, R., Laumann, T. O., Snyder, A. Z., Zhou, J., & Yeo, B. T. T. (2017). Interpreting temporal fluctuations in resting-state functional connectivity MRI. *NeuroImage*, *163*, 437–455. https://doi.org/10.1016/j.neuroimage.2017.09.012

Liégeois, R., Li, J., Kong, R., Orban, C., Van De Ville, D., Ge, T., Sabuncu, M. R., & Yeo, B. T. T. (2019). Resting brain dynamics at different timescales capture distinct aspects of human behavior. *Nature Communications*, *10*(1), 2317. https://doi.org/10.1038/s41467-019-10317-7

Lindquist, M. A., Xu, Y., Nebel, M. B., & Caffo, B. S. (2014a). Evaluating dynamic bivariate correlations in resting-state fMRI: A comparison study and a new approach. *NeuroImage*, *101*, 531–546. https://doi.org/10.1016/j.neuroimage.2014.06.052

Lindquist, M. A., Xu, Y., Nebel, M. B., & Caffo, B. S. (2014b). Evaluating dynamic bivariate correlations in resting-state fMRI: A comparison study and a new approach. *NeuroImage*, *101*, 531–546. https://doi.org/10.1016/j.neuroimage.2014.06.052

Liu, X., Chang, C., & Duyn, J. H. (2013). Decomposition of spontaneous brain activity into distinct fMRI co-activation patterns. *Frontiers in Systems Neuroscience*, *7*, 101. https://doi.org/10.3389/fnsys.2013.00101

Liu, X., & Duyn, J. H. (2013). Time-varying functional network information extracted from brief instances of spontaneous brain activity. *Proceedings of the National Academy of Sciences of the United States of America*, *110*(11), 4392–4397. https://doi.org/10.1073/pnas.1216856110

Liu, X., Zhang, N., Chang, C., & Duyn, J. H. (2018). Co-activation patterns in resting-state fMRI signals. *NeuroImage*, *180*, 485–494. https://doi.org/10.1016/j.neuroimage.2018.01.041

Lotter, W., Kreiman, G., & Cox, D. (2017). Deep Predictive Coding Networks for Video Prediction and Unsupervised Learning. *ArXiv:1605.08104 [Cs, q-Bio]*. http://arxiv.org/abs/1605.08104

Lurie, D. J., Kessler, D., Bassett, D. S., Betzel, R. F., Breakspear, M., Kheilholz, S., Kucyi, A., Liégeois, R., Lindquist, M. A., McIntosh, A. R., Poldrack, R. A., Shine, J. M., Thompson, W. H., Bielczyk, N. Z., Douw, L., Kraft, D., Miller, R. L., Muthuraman, M., Pasquini, L., … Calhoun, V. D. (2019). Questions and controversies in the study of time-varying functional connectivity in resting fMRI. *Network Neuroscience*, *4*(1), 30–69. https://doi.org/10.1162/netn_a_00116

Lurie, D. J., Kessler, D., Bassett, D. S., Betzel, R. F., Breakspear, M., Kheilholz, S., Kucyi, A., Liégeois,

R., Lindquist, M. A., McIntosh, A. R., Poldrack, R. A., Shine, J. M., Thompson, W. H., Bielczyk, N. Z., Douw, L., Kraft, D., Miller, R. L., Muthuraman, M., Pasquini, L., … Calhoun, V. D. (2020). Questions and controversies in the study of time-varying functional connectivity in resting fMRI. *Network Neuroscience*, *4*(1), 30–69. https://doi.org/10.1162/netn_a_00116

Lynall, M.-E., Bassett, D. S., Kerwin, R., McKenna, P. J., Kitzbichler, M., Muller, U., & Bullmore, E. (2010). Functional Connectivity and Brain Networks in Schizophrenia. *Journal of Neuroscience*, *30*(28), 9477–9487. https://doi.org/10.1523/JNEUROSCI.0333-10.2010

Madhyastha, T. M., Askren, M. K., Boord, P., & Grabowski, T. J. (2015). Dynamic Connectivity at Rest Predicts Attention Task Performance. *Brain Connectivity*, *5*(1), 45–59. https://doi.org/10.1089/brain.2014.0248

Madhyastha, T. M., & Grabowski, T. J. (2014). Age-Related Differences in the Dynamic Architecture of Intrinsic Networks. *Brain Connectivity*, *4*(4), 231–241. https://doi.org/10.1089/brain.2013.0205

Mao, N., Zheng, H., Long, Z., Yao, L., & Wu, X. (2017, July). *Gender differences in dynamic functional connectivity based on resting-state fMRI*. Annual International Conference of the IEEE Engineering in Medicine and Biology Society. IEEE Engineering in Medicine and Biology Society. Annual International Conference; Annu Int Conf IEEE Eng Med Biol Soc. https://doi.org/10.1109/EMBC.2017.8037473

Marshall, E., Nomi, J. S., Dirks, B., Romero, C., Kupis, L., Chang, C., & Uddin, L. Q. (2020).

Coactivation pattern analysis reveals altered salience network dynamics in children with autism spectrum disorder. *Network Neuroscience*, *4*(4), 1219–1234. https://doi.org/10.1162/netn_a_00163

Marusak, H. A., Calhoun, V. D., Brown, S., Crespo, L. M., Sala-Hamrick, K., Gotlib, I. H., & Thomason, M. E. (2016). Dynamic functional connectivity of neurocognitive networks in children. *Human Brain Mapping*, *38*(1), 97–108. https://doi.org/10.1002/hbm.23346

Marusak, H. A., Elrahal, F., Peters, C. A., Kundu, P., Lombardo, M. V., Calhoun, V. D., Goldberg, E. K., Cohen, C., Taub, J. W., & Rabinak, C. A. (2018). Mindfulness and dynamic functional neural connectivity in children and adolescents. *Behavioural Brain Research*, *336*, 211–218. https://doi.org/10.1016/j.bbr.2017.09.010

Mazoyer, B., Zago, L., Mellet, E., Bricogne, S., Etard, O., Houdé, O., Crivello, F., Joliot, M., Petit, L., & Tzourio-Mazoyer, N. (2001). Cortical networks for working memory and executive functions sustain the conscious resting state in man. *Brain Research Bulletin*, *54*(3), 287–298. https://doi.org/10.1016/s0361-9230(00)00437-8

McKiernan, K. A., Kaufman, J. N., Kucera-Thompson, J., & Binder, J. R. (2003). A parametric manipulation of factors affecting task-induced deactivation in functional neuroimaging. *Journal of Cognitive Neuroscience*, *15*(3), 394–408. https://doi.org/10.1162/089892903321593117

Medaglia, J. D., Lynall, M.-E., & Bassett, D. S. (2015). Cognitive Network Neuroscience. *Journal of Cognitive Neuroscience*, *27*(8), 1471–1491. https://doi.org/10.1162/jocn_a_00810

Miller, R. L., Abrol, A., Adali, T., Levin-Schwarz, Y., & Calhoun, V. D. (2018). Resting-State fMRI Dynamics and Null Models: Perspectives, Sampling Variability, and Simulations. *Frontiers in Neuroscience*, *12*. https://doi.org/10.3389/fnins.2018.00551

Miller, R. L., Yaesoubi, M., Turner, J. A., Mathalon, D., Preda, A., Pearlson, G., Adali, T., & Calhoun, V. D. (2016). Higher Dimensional Meta-State Analysis Reveals Reduced Resting fMRI Connectivity Dynamism in Schizophrenia Patients. *PLOS ONE*, *11*(3), e0149849. https://doi.org/10.1371/journal.pone.0149849

Mokhtari, F., Akhlaghi, M. I., Simpson, S. L., Wu, G., & Laurienti, P. J. (2019). Sliding window correlation analysis: Modulating window shape for dynamic brain connectivity in resting state. *NeuroImage*, *189*, 655–666. https://doi.org/10.1016/j.neuroimage.2019.02.001

Musall, S., Kaufman, M. T., Juavinett, A. L., Gluf, S., & Churchland, A. K. (2019). Single-trial neural dynamics are dominated by richly varied movements. *Nature Neuroscience*, *22*(10), 1677–1686. https://doi.org/10.1038/s41593-019-0502-4

Nguyen, V. T., Breakspear, M., Hu, X., & Guo, C. C. (2016). The integration of the internal and external milieu in the insula during dynamic emotional experiences. *NeuroImage*, *124*, 455–463. https://doi.org/10.1016/j.neuroimage.2015.08.078

Niendam, T. A., Laird, A. R., Ray, K. L., Dean, Y. M., Glahn, D. C., & Carter, C. S. (2012). Meta-analytic evidence for a superordinate cognitive control network subserving diverse executive functions. *Cognitive, Affective & Behavioral Neuroscience*, *12*(2), 241–268. https://doi.org/10.3758/s13415-011-0083-5

Nomi, J. S., Vij, S. G., Dajani, D. R., Steimke, R., Damaraju, E., Rachakonda, S., Calhoun, V. D., & Uddin, L. Q. (2017). Chronnectomic Patterns and Neural Flexibility Underlie Executive Function. *NeuroImage*, *147*, 861–871. https://doi.org/10.1016/j.neuroimage.2016.10.026

Ou, J., Xie, L., Jin, C., Li, X., Zhu, D., Jiang, R., Chen, Y., Zhang, J., Li, L., & Liu, T. (2015). Characterizing and Differentiating Brain State Dynamics via Hidden Markov Models. *Brain Topography*, *28*(5), 666–679. https://doi.org/10.1007/s10548-014-0406-2

Ou, J., Xie, L., Wang, P., Li, X., Zhu, D., Jiang, R., Wang, Y., Chen, Y., Zhang, J., & Liu, T. (2013). Modeling brain functional dynamics via hidden Markov models. *2013 6th International IEEE/EMBS Conference on Neural Engineering (NER)*, 569–572. https://doi.org/10.1109/NER.2013.6695998

Patanaik, A., Tandi, J., Ong, J. L., Wang, C., Zhou, J., & Chee, M. W. L. (2018). Dynamic functional connectivity and its behavioral correlates beyond vigilance. *NeuroImage*, *177*, 1–10. https://doi.org/10.1016/j.neuroimage.2018.04.049

Pedersen, M., Omidvarnia, A., Zalesky, A., & Jackson, G. D. (2018). On the relationship between instantaneous phase synchrony and correlation-based sliding windows for time-resolved fMRI connectivity analysis. *NeuroImage*, *181*, 85–94. https://doi.org/10.1016/j.neuroimage.2018.06.020

Poldrack, R. A. (2006). Can cognitive processes be inferred from neuroimaging data? *Trends in Cognitive Sciences*, *10*(2), 59–63. https://doi.org/10.1016/j.tics.2005.12.004

Poldrack, R. A. (2018). *The New Mind Readers*. Princeton University Press.

Poldrack, R. A., Laumann, T. O., Koyejo, O., Gregory, B., Hover, A., Chen, M.-Y., Gorgolewski, K. J., Luci, J., Joo, S. J., Boyd, R. L., Hunicke-Smith, S., Simpson, Z. B., Caven, T., Sochat, V., Shine, J. M., Gordon, E., Snyder, A. Z., Adeyemo, B., Petersen, S. E., … Mumford, J. A. (2015). Long-term neural and physiological phenotyping of a single human. *Nature Communications*, *6*(1), 8885. https://doi.org/10.1038/ncomms9885

Power, J. D., Barnes, K. A., Snyder, A. Z., Schlaggar, B. L., & Petersen, S. E. (2012). Spurious but systematic correlations in functional connectivity MRI networks arise from subject motion. *NeuroImage*, *59*(3), 2142–2154. https://doi.org/10.1016/j.neuroimage.2011.10.018

Power, J. D., Schlaggar, B. L., & Petersen, S. E. (2015). Recent progress and outstanding issues in motion correction in resting state fMRI. *NeuroImage*, *105*, 536–551. https://doi.org/10.1016/j.neuroimage.2014.10.044

Preti, M. G., Bolton, T. A., & Van De Ville, D. (2017). The dynamic functional connectome: State-of-the-art and perspectives. *NeuroImage*, *160*, 41–54. https://doi.org/10.1016/j.neuroimage.2016.12.061

Quinn, A. J., Vidaurre, D., Abeysuriya, R., Becker, R., Nobre, A. C., & Woolrich, M. W. (2018). Task-Evoked Dynamic Network Analysis Through Hidden Markov Modeling. *Frontiers in Neuroscience*, *12*. https://doi.org/10.3389/fnins.2018.00603

Rashid, B., Arbabshirani, M. R., Damaraju, E., Cetin, M. S., Miller, R., Pearlson, G. D., & Calhoun, V. D. (2016). Classification of schizophrenia and bipolar patients using static and dynamic resting-state fMRI brain connectivity. *NeuroImage*, *134*, 645–657.

https://doi.org/10.1016/j.neuroimage.2016.04.051

Rashid, B., Damaraju, E., Pearlson, G. D., & Calhoun, V. D. (2014). Dynamic connectivity states estimated from resting fMRI Identify differences among Schizophrenia, bipolar disorder, and healthy control subjects. *Frontiers in Human Neuroscience*, *8*. https://doi.org/10.3389/fnhum.2014.00897

Rosenberg, M. D., Finn, E. S., Scheinost, D., Papademetris, X., Shen, X., Constable, R. T., & Chun, M. M. (2016). A neuromarker of sustained attention from whole-brain functional connectivity. *Nature Neuroscience*, *19*(1), 165–171. https://doi.org/10.1038/nn.4179

Rossi, R. A., Jin, D., Kim, S., Ahmed, N. K., Koutra, D., & Lee, J. B. (2020). On Proximity and Structural Role-based Embeddings in Networks: Misconceptions, Techniques, and Applications. *ACM Transactions on Knowledge Discovery from Data*, *14*(5), 1–37. https://doi.org/10.1145/3397191

Sakoğlu, Ü., Pearlson, G. D., Kiehl, K. A., Wang, Y. M., Michael, A. M., & Calhoun, V. D. (2010). A method for evaluating dynamic functional network connectivity and task-modulation: Application to schizophrenia. *Magnetic Resonance Materials in Physics, Biology and Medicine*, *23*(5), 351–366. https://doi.org/10.1007/s10334-010-0197-8

Salimi-Khorshidi, G., Douaud, G., Beckmann, C. F., Glasser, M. F., Griffanti, L., & Smith, S. M. (2014). Automatic denoising of functional MRI data: Combining independent component analysis and hierarchical fusion of classifiers. *NeuroImage*, *90*, 449–468. https://doi.org/10.1016/j.neuroimage.2013.11.046

Sami, S., Robertson, E. M., & Chris Miall, R. (2014). The time course of task-specific memory consolidation effects in resting state networks. *Journal of Neuroscience*, *34*(11), 3982–3992. Scopus. https://doi.org/10.1523/JNEUROSCI.4341-13.2014

Satterthwaite, T. D., Wolf, D. H., Loughead, J., Ruparel, K., Elliott, M. A., Hakonarson, H., Gur, R. C., & Gur, R. E. (2012). Impact of in-scanner head motion on multiple measures of functional connectivity: Relevance for studies of neurodevelopment in youth. *NeuroImage*, *60*(1), 623–632. https://doi.org/10.1016/j.neuroimage.2011.12.063

Savva, A. D., Mitsis, G. D., & Matsopoulos, G. K. (2019). Assessment of dynamic functional connectivity in resting-state fMRI using the sliding window technique. *Brain and Behavior*, *9*(4), e01255. https://doi.org/10.1002/brb3.1255

Schaefer, A., Margulies, D. S., Lohmann, G., Gorgolewski, K. J., Smallwood, J., Kiebel, S. J., & Villringer, A. (2014). Dynamic network participation of functional connectivity hubs assessed by resting-state fMRI. *Frontiers in Human Neuroscience*, *8*, 195. https://doi.org/10.3389/fnhum.2014.00195

Schönbrodt, F. D., & Perugini, M. (2013). At what sample size do correlations stabilize? *Journal of Research in Personality*, *47*(5), 609–612. https://doi.org/10.1016/j.jrp.2013.05.009

Shakil, S., Billings, J. C., Keilholz, S. D., & Lee, C.-H. (2018). Parametric Dependencies of Sliding Window Correlation. *IEEE Transactions on Biomedical Engineering*, *65*(2), 254–263. https://doi.org/10.1109/TBME.2017.2762763

Shakil, S., Keilholz, S. D., & Lee, C.-H. (2015). On frequency dependencies of sliding window

correlation. *2015 IEEE International Conference on Bioinformatics and Biomedicine (BIBM)*, 363–368. https://doi.org/10.1109/BIBM.2015.7359708

Shakil, S., Lee, C.-H., & Keilholz, S. D. (2016). Evaluation of sliding window correlation performance for characterizing dynamic functional connectivity and brain states. *NeuroImage*, *133*, 111–128. https://doi.org/10.1016/j.neuroimage.2016.02.074

Shappell, H. M., Caffo, B. S., Pekar, J. J., & Lindquist, M. A. (2019). Improved state change estimation in dynamic functional connectivity using hidden semi-Markov models. *NeuroImage*, *191*, 243–257. https://doi.org/10.1016/j.neuroimage.2019.02.013

Shappell, H. M., Duffy, K. A., Rosch, K. S., Pekar, J. J., Mostofsky, S. H., Lindquist, M. A., & Cohen, J. R. (2021). Children with attention-deficit/hyperactivity disorder spend more time in hyperconnected network states and less time in segregated network states as revealed by dynamic connectivity analysis. *NeuroImage*, *229*, 117753. https://doi.org/10.1016/j.neuroimage.2021.117753

Shine, J. M., Koyejo, O., Bell, P. T., Gorgolewski, K. J., Gilat, M., & Poldrack, R. A. (2015). Estimation of dynamic functional connectivity using Multiplication of Temporal Derivatives. *NeuroImage*, *122*, 399–407. https://doi.org/10.1016/j.neuroimage.2015.07.064

Shine, J. M., & Poldrack, R. A. (2018). Principles of dynamic network reconfiguration across diverse brain states. *NeuroImage*, *180*(Pt B), 396–405. https://doi.org/10.1016/j.neuroimage.2017.08.010

Shou, H., Eloyan, A., Lee, S., Zipunnikov, V., Crainiceanu, A. N., Nebel, N. B., Caffo, B., Lindquist,

M. A., & Crainiceanu, C. M. (2013). Quantifying the reliability of image replication studies: The image intraclass correlation coefficient (I2C2). *Cognitive, Affective & Behavioral Neuroscience*, *13*(4), 714–724. https://doi.org/10.3758/s13415-013-0196-0

Siegel, J. S., Mitra, A., Laumann, T. O., Seitzman, B. A., Raichle, M., Corbetta, M., & Snyder, A. Z. (2017). Data Quality Influences Observed Links Between Functional Connectivity and Behavior. *Cerebral Cortex (New York, N.Y.: 1991)*, *27*(9), 4492–4502. https://doi.org/10.1093/cercor/bhw253

Smith, D. M., Zhao, Y., Keilholz, S. D., & Schumacher, E. H. (2018). Investigating the Intersession Reliability of Dynamic Brain-State Properties. *Brain Connectivity*, *8*(5), 255–267. https://doi.org/10.1089/brain.2017.0571

Smith, S. M., Miller, K. L., Moeller, S., Xu, J., Auerbach, E. J., Woolrich, M. W., Beckmann, C. F., Jenkinson, M., Andersson, J., Glasser, M. F., Essen, D. C. V., Feinberg, D. A., Yacoub, E. S., & Ugurbil, K. (2012). Temporally-independent functional modes of spontaneous brain activity. *Proceedings of the National Academy of Sciences*, *109*(8), 3131–3136. https://doi.org/10.1073/pnas.1121329109

Spielberg, J. M., Miller, G. A., Heller, W., & Banich, M. T. (2015). Flexible brain network reconfiguration supporting inhibitory control. *Proceedings of the National Academy of Sciences of the United States of America*, *112*(32), 10020–10025. https://doi.org/10.1073/pnas.1500048112

Sripada, C., Angstadt, M., Kessler, D., Phan, K. L., Liberzon, I., Evans, G. W., Welsh, R. C., Kim, P.,

& Swain, J. E. (2014). Volitional regulation of emotions produces distributed alterations in connectivity between visual, attention control, and default networks. *NeuroImage*, *89*, 110–121. https://doi.org/10.1016/j.neuroimage.2013.11.006

Sripada, C., Angstadt, M., Rutherford, S., Kessler, D., Kim, Y., Yee, M., & Levina, E. (2019). Basic Units of Inter-Individual Variation in Resting State Connectomes. *Scientific Reports*, *9*(1), 1900. https://doi.org/10.1038/s41598-018-38406-5

Sripada, C., Angstadt, M., Rutherford, S., Taxali, A., & Shedden, K. (2020). Toward a "treadmill test" for cognition: Improved prediction of general cognitive ability from the task activated brain. *Human Brain Mapping*, *41*(12), 3186–3197. https://doi.org/10.1002/hbm.25007

Sripada, C., & Taxali, A. (2020). Structure in the stream of consciousness: Evidence from a verbalized thought protocol and automated text analytic methods. *Consciousness and Cognition*, *85*, 103007. https://doi.org/10.1016/j.concog.2020.103007

Su, J., Shen, H., Zeng, L.-L., Qin, J., Liu, Z., & Hu, D. (2016). Heredity characteristics of schizophrenia shown by dynamic functional connectivity analysis of resting-state functional MRI scans of unaffected siblings. *NeuroReport*, *27*(11), 843–848. Scopus. https://doi.org/10.1097/WNR.0000000000000622

Syed, M. F., Lindquist, M. A., Pillai, J. J., Agarwal, S., Gujar, S. K., Choe, A. S., Caffo, B., & Sair, H. I. (2017). Dynamic Functional Connectivity States Between the Dorsal and Ventral Sensorimotor Networks Revealed by Dynamic Conditional Correlation Analysis of Resting-State Functional Magnetic Resonance Imaging. *Brain Connectivity*, *7*(10), 635–642.

https://doi.org/10.1089/brain.2017.0533

Tagliazucchi, E., von Wegner, F., Morzelewski, A., Brodbeck, V., & Laufs, H. (2012). Dynamic BOLD functional connectivity in humans and its electrophysiological correlates. *Frontiers in Human Neuroscience*, *6*, 339. https://doi.org/10.3389/fnhum.2012.00339

Telesford, Q. K., Lynall, M.-E., Vettel, J., Miller, M. B., Grafton, S. T., & Bassett, D. S. (2016). Detection of functional brain network reconfiguration during task-driven cognitive states. *NeuroImage*, *142*, 198–210. https://doi.org/10.1016/j.neuroimage.2016.05.078

Thirion, B., Pinel, P., Mériaux, S., Roche, A., Dehaene, S., & Poline, J.-B. (2007). Analysis of a large fMRI cohort: Statistical and methodological issues for group analyses. *NeuroImage*, *35*(1), 105–120. https://doi.org/10.1016/j.neuroimage.2006.11.054

Turner, B. O., Paul, E. J., Miller, M. B., & Barbey, A. K. (2018). Small sample sizes reduce the replicability of task-based fMRI studies. *Communications Biology*, *1*. https://doi.org/10.1038/s42003-018-0073-z

Van Dijk, K. R. A., Sabuncu, M. R., & Buckner, R. L. (2012). The influence of head motion on intrinsic functional connectivity MRI. *NeuroImage*, *59*(1), 431–438. https://doi.org/10.1016/j.neuroimage.2011.07.044

Van Essen, D. C., Smith, S. M., Barch, D. M., Behrens, T. E. J., Yacoub, E., & Ugurbil, K. (2013). The WU-Minn Human Connectome Project: An Overview. *NeuroImage*, *80*, 62–79. https://doi.org/10.1016/j.neuroimage.2013.05.041

Vaswani, A., Shazeer, N., Parmar, N., Uszkoreit, J., Jones, L., Gomez, A. N., Kaiser, Ł., & Polosukhin,

I. (2017). Attention is All you Need. *Advances in Neural Information Processing Systems*, *30*. https://papers.nips.cc/paper/2017/hash/3f5ee243547dee91fbd053c1c4a845aa-Abstract.html

Vidaurre, D., Abeysuriya, R., Becker, R., Quinn, A. J., Alfaro-Almagro, F., Smith, S. M., & Woolrich, M. W. (2018). Discovering dynamic brain networks from big data in rest and task. *NeuroImage*, *180*, 646–656. https://doi.org/10.1016/j.neuroimage.2017.06.077

Vidaurre, D., Llera, A., Smith, S. M., & Woolrich, M. W. (2021). Behavioural relevance of spontaneous, transient brain network interactions in fMRI. *NeuroImage*, *229*, 117713. https://doi.org/10.1016/j.neuroimage.2020.117713

Vidaurre, D., Quinn, A. J., Baker, A. P., Dupret, D., Tejero-Cantero, A., & Woolrich, M. W. (2016). Spectrally resolved fast transient brain states in electrophysiological data | Elsevier Enhanced Reader. *NeuroImage*, *126*, 81–95. https://doi.org/10.1016/j.neuroimage.2015.11.047

Vidaurre, D., Smith, S. M., & Woolrich, M. W. (2017). Brain network dynamics are hierarchically organized in time. *Proceedings of the National Academy of Sciences*, *114*(48), 12827–12832. https://doi.org/10.1073/pnas.1705120114

Wong, C. W., Olafsson, V., Tal, O., & Liu, T. T. (2013). The amplitude of the resting-state fMRI global signal is related to EEG vigilance measures. *Neuroimage*, *83*, 983–990. https://doi.org/10.1016/j.neuroimage.2013.07.057

Yaesoubi, M., Allen, E. A., Miller, R. L., & Calhoun, V. D. (2015). Dynamic coherence analysis of resting fMRI data to jointly capture state-based phase, frequency, and time-domain information. *NeuroImage*, *120*, 133–142. https://doi.org/10.1016/j.neuroimage.2015.07.002

Yaesoubi, M., Miller, R. L., & Calhoun, V. D. (2015). Mutually temporally independent connectivity patterns: A new framework to study the dynamics of brain connectivity at rest with application to explain group difference based on gender. *NeuroImage*, *107*, 85–94. https://doi.org/10.1016/j.neuroimage.2014.11.054

Yang, Z., Craddock, R. C., Margulies, D. S., Yan, C.-G., & Milham, M. P. (2014). Common intrinsic connectivity states among posteromedial cortex subdivisions: Insights from analysis of temporal dynamics. *NeuroImage*, *93*, 124–137. https://doi.org/10.1016/j.neuroimage.2014.02.014

Yu, Q., Erhardt, E. B., Sui, J., Du, Y., He, H., Hjelm, D., Cetin, M. S., Rachakonda, S., Miller, R. L., Pearlson, G., & Calhoun, V. D. (2015). Assessing dynamic brain graphs of time-varying connectivity in fMRI data: Application to healthy controls and patients with schizophrenia. *NeuroImage*, *107*, 345–355. https://doi.org/10.1016/j.neuroimage.2014.12.020

Zalesky, A., Fornito, A., Cocchi, L., Gollo, L. L., & Breakspear, M. (2014). Time-resolved resting-state brain networks. *Proceedings of the National Academy of Sciences*, *111*(28), 10341–10346. https://doi.org/10.1073/pnas.1400181111

Zeng, L.-L., Wang, H., Hu, P., Yang, B., Pu, W., Shen, H., Chen, X., Liu, Z., Yin, H., Tan, Q., Wang, K., & Hu, D. (2018). Multi-Site Diagnostic Classification of Schizophrenia Using Discriminant Deep Learning with Functional Connectivity MRI. *EBioMedicine*, *30*, 74–85. https://doi.org/10.1016/j.ebiom.2018.03.017

Zhang, D., & Raichle, M. E. (2010). Disease and the brain's dark energy. *Nature Reviews Neurology*,

6(1), 15–28. https://doi.org/10.1038/nrneurol.2009.198

Zhang, G., Cai, B., Zhang, A., Stephen, J. M., Wilson, T. W., Calhoun, V. D., & Wang, Y.-P. (2020). Estimating Dynamic Functional Brain Connectivity With a Sparse Hidden Markov Model. *IEEE Transactions on Medical Imaging*, *39*(2), 488–498. https://doi.org/10.1109/TMI.2019.2929959